G8651

LASER INDUCED PHOTOTHERMAL INVESTIGATIONS ON THERMAL AND TRANSPORT PROPERTIES OF CERTAIN SELECTED PHOTONIC MATERIALS

Sajan.D.George

International School of Photonics
Cochin University of Science and Technology
Cochin, India – 682 022

Laser Induced Photothermal Investigations on Thermal and Transport Properties of Certain Selected Photonic Materials
Ph. D thesis in the field of Photonics

Author :
Sajan D George
Research Fellow, International School of Photonics,
Cochin University of Science and Technology,
Cochin, India – 682 022
E mail: sajan@cusat.ac.in; sajanphotonics@yahoo.com
URL: www.geocities.com/sajandgeorge

Research Advisors:
Dr. C. P. Girijavallabhan,
Emeritus Professor, International School of Photonics,
Director, CELOS,
Dean, Faculty of Technology,
Cochin University of Science and Technology,
Cochin, India – 682 022
Email: vallabhan@vsnl.com

Dr. V. P. N. Nampoori,
Professor,
International School of Photonics,
Cochin University of Science and Technology,
Cochin, India – 682 022
E mail: vpnnampoori@cusat.ac.in

G 8651

International School of Photonics, Cochin University of Science and Technology,
Cochin, India – 682 022
URL: www.photonics.cusat.edu

November 2003

Front cover: *"Mirage in a desert"* Painting in the digital art medium.
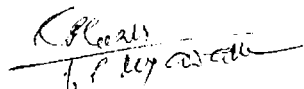**Back cover:** *A typical experimental setup to observe PTD phenomenon.*

Dedicated to

My loving parents
and
Dearest Brother

CERTIFICATE

Certified that the work presented in this thesis entitled **"LASER INDUCED PHOTOTHERMAL INVESTIGATIONS ON THERMAL AND TRANSPORT PROPERTIES OF CERTAIN SELECTED PHOTONIC MATERIALS"** is an authentic record of the bonafide research work done by Mr. Sajan D George, under my guidance and supervision in the International School of Photonics, Cochin University of Science and Technology, India – 682 022 and it has not been included in any other thesis submitted previously for the award of any degree.

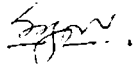Cochin – 22
18th November 2003

Dr. C. P. Girijavallabhan
(Supervising Guide)
International School of Photonics
CUSAT

DECLARATION

I hereby declare that the work presented in this thesis entitled "**LASER INDUCED PHOTOTHERMAL INVESTIGATIONS ON THERMAL AND TRANSPORT PROPERTIES OF CERTAIN SELECTED PHOTONIC MATERIALS**" is based on the original research work done by me under the guidance of Dr. C. P. Girijavallabhan, Emeritus Professor in International School of Photonics, and the co-guidance of Prof. V. P. N. Nampoori, Professor, International School of Photonics, Cochin University of Science and Technology, and it has not been included in any other thesis submitted previously for the award of any degree.

Cochin – 22
18th November 2003

Sajan D George

PREFACE

The last twenty five years have witnessed the emergence of nondestructive photothermal technique as an effective research and analytical tool for the characterization of matter in all its different states. Most of these photothermal methods depend upon the detection, by one means or other, of thermal waves generated in the specimen on illumination with a chopped or pulsed optical radiation. As the photothermal technique monitors the nonradiative path, it can throw light into several properties of the materials which are hard to measure using conventional spectroscopic techniques. The advancement in the detecting and measuring systems have made the photothermal techniques an effective tool for the in situ and in vivo studies on the thermal, transport and optical properties of materials, especially those of condensed matter. Among the variety of photothermal techniques employed, the laser induced nondestructive photoacoustic (PA) and photothermal deflection (PTD) techniques are the two popular techniques employed for the evaluation of material parameters due to its simplicity and versatility. The noncontact and nondestructive PTD technique allows point by point scanning on the sample surface as well as the characterization of anisotropy in thermophysical properties of specimen under investigation. Even though, the PA technique is an indirect technique, it allows the evaluation of material parameters with accuracy using a simple and elegant experimental setup.

In the present technological era emerging in the modern world, photonics replaces electronics due to several advantages of optical signal as compared to electronic signal. However, the progress in this field demands better understanding

of the fundamental properties of the materials used in this industry. The class of materials used here are the compound semiconductors, nanometal dispersed ceramics, composites of conducting polymer and liquid crystal mixtures. Compound semiconductors are widely used for the generation and detection of optical radiation whereas ceramics are considered to be the ideal material for many of the electronic and optoelectronic devices. In recent times, the fourth generation of polymers, viz., conducting polymers is widely used for the fabrication of plastic LED and many other optoelectronic sources. Liquid crystals are extensively used in the optical data storage devices. The performance and reliability of the device depends greatly on the thermal and transport properties of these materials. The work done here is focused on the evaluation of transport properties of some of these photonic materials using laser induced PTD and PA technique. The present thesis contains the details of the work done and it is organized into six separate chapters.

In chapter 1, an overview of various photothermal techniques are presented. The detailed account of the PA signal generation in condensed matter is given. A review of the work done by various researchers on the class of photonic materials using the experimental techniques employed in the present thesis is presented. Motivation of the present work is also well explained.

Chapter 2 is subdivided into two parts. In the first part, evaluation of the thermal diffusivity of intrinsic InP and InP doped with Sn, S and Fe using PTD technique is presented. The influence of doping as well as the nature of dopant on the thermal diffusivity value is investigated. The influence of plane of cleavage on the thermal diffusivity value of the semiconductor samples is also discussed. In the

second part of the chapter, results related to the heat transport through double GaAs epitaxial layer grown on GaAs substrate with varying concentration of Si and a particular concentration of Be are included. Analysis of the results shows that samples exhibit singnificant anisotropy in heat transport and hence show anisotropy in thermal diffusivity values along in-plane and cross plane direction.

Chapter 3 deals with the simultaneous measurement of thermal and transport properties viz. thermal diffusivity, diffusion coefficient, surface recombination velocity and nonradiative recombination time of some direct and indirect bandgap semiconductors. These thermal and transport properties of semiconductors are evaluated by fitting the experimentally obtained phase spectrum of the PA signal under heat transmission configuration to that of theoretical phase spectrum based on the thermal piston model of Rosencwaig and Gersho. This chapter is contains three sections. In the first section, evaluation of thermal and transport properties of some direct bandgap semiconductors namely InP, GaAs and InSb are presented. The second section deals with the measurement of the same in the case of intrinsic Si and Si doped with B and P. The latter section of this chapter discusses the measurement of thermal and transport properties of GaAs epitaxial layers. All these measurements are carried out using a home made Open Photoacoustic Cell.

In chapter 4, focus is made on the measurement of thermal diffusivity of nano Ag metal dispersed ceramic Alumina matrix and composites of conducting polymers, namely Camphor Sulphonic Acid doped Polyaniline with Cobalt Phthalocyanine. For the measurement of thermal diffusivity of ceramics, PA technique under Reflection Detection Configuration (RDC) is employed due to the

finite thickness of the specimen under investigation. The thermal diffusivity values are evaluated by knowing the transition frequency, at which sample changes from thermally thin to thermally thick region, from the amplitude spectrum of the PA signal. However, the thermal diffusivity values of the composites are measured using PA technique under heat transmission configuration. The thermoelastic bending of the specimen due to the finite temperature gradient existing within the specimen is also incorporated in the evaluation of thermal diffusivity. In this case the phase data of the PA signal as a function of modulation frequency is utilized for the evaluation of thermal diffusivity of the specimen.

Complete thermal characterization of liquid crystal mixtures namely, Cholesterol and 1 hexadecanol using PA technique is presented in chapter 5. The thermal diffusivity value of the specimen, by including the contribution from thermoelastic bending, is done using PA technique under heat transmission configuration. The phase data of the PA signal is used for the evaluation of thermal diffusivity of the specimen. The thermal effusivity values of the same are investigated using PA technique in RDC. In this case, the amplitude of the PA spectrum is utilized. By knowing these parameters, the thermal conductivity and thermal capacity of the samples as a function of the relative mass fraction of the constitutes is studied.

Conclusions based on the present work are presented in the Chapter 6. The future prospectus and possibility of the continuation of the present work are also included in this chapter.

LIST OF PUBLICATIONS

In International Journals

1. **Sajan D George**, Achamma Kurian, Martin Lase, V. P. N. Nampoori and C. P. G. Vallabhan, *Thermal characterisation of doped InP using photoacoustic technique* Proceedings of SPIE – International Society for Optical Engineering, Vol. 4595 pp 183-191 (2001).

2. **Sajan D George**, C. P. G. Vallabhan, M. Heck, P. Radhakrishnan, and V. P. N. Nampoori, *Photoacoustic Investigation of doped InP using open cell photoacoustic technique* Journal of Nondestructive Testing and Evaluation Vol.18, 2, pp75-82, (2002)

3. **Sajan D George**, Dilna. S, P. Radhakrishnan, V. P. N. Nampoori and C. P. G. Vallabhan, *Investigation of transport properties of doped GaAs epitaxial layers using an open photoacoustic cell* Proceedings of SPIE – International Society for Optical Engineering, Vol 4918 pp 267-273 (2002).

4. **Sajan D George**, Dilna. S, P. Radhakrishnan, C. P. G. Vallabhan and V. P. N. Nampoori, *Photoacoustic measurement of transport properties in doped GaAs epitaxial layers* Physica Status Solidi (a), 195 (2), 416-421 (2003)

5. **Sajan D George**, Saji Augustine, Elizabeth Mathai, P. Radhakrishnan, V. P. N. Nampoori and C. P. G. Vallabhan, *Effect of Te doping on the thermal diffusivity of Bi_2Se_3 crystals – A study using open cell photoacoustic technique* Physica Status Solidi (a), 196(2), 384-389 (2003).

6. **Sajan D George**, Dilna. S, Prasanth. R, P. Radhakrishnan, C. P. G. Vallabhan and V. P. N. Nampoori, *A photoacoustic study of the effect of doping concentration in the transport properties of GaAs epitaxial layers* Optical Engineering 42 (5), 1476-1480, (2003)

7. **Sajan D George**, Aji A Anappara, K. G. K. Warrier, P. Radhakrishnan, V. P. N. Nampoori and C. P. G. Vallabhan, *Laser induced thermal characterization of nanometal dispersed ceramic alumina matrix* Proceedings of SPIE – International Society for Optical Engineering, Vol. 5118 pp 207-212 (2003).

8. **Sajan D George**, P. Radhakrishnan, V. P. N. Nampoori and C. P. G. Vallabhan, *Thermal characterization of intrinsic and extrinsic InP using photoacoustic technique* Journal of Physics D: Applied Physics, 36 (8), 990-993 (2003).

9. **Sajan D George**, P. Radhakrishnan, V. P. N. Nampoori and C. P. G. Vallabhan, *Investigation of thermal and transport properties of doped Si using photoacoustic technique* Proceedings of SPIE, 5280 -119 (2003)

10. **Sajan D George**, P. Radhakrishnan, V. P. N. Nampoori and C. P. G. Vallabhan, *Photothermal deflection measurement on heat transport in GaAs epitaxial layers* Physical Review B 68 165319 (2003).

11. **Sajan. D. George**, P. Radhakrishnan, V. P. N. Nampoori and C. P. G. Vallabhan, *Photothermal deflection studies on heat transport in intrinsic and extrinsic InP* Applied Physics B: Lasers and Optics (Accepted)

12. **Sajan D George**, Rajesh Komban, K. G. K. Warrier, P. Radhakrishnan, V. P. N. Nampoori and C. P.G. Vallabhan *Thermal characterization of LaPO$_4$ ceramics using photoacoustic technique* (communicated)

13. **Sajan D George**, Aji A Annapara, P. R. S. Warrier, K. G. K. Warrier, P. Radhakrishnan, V. P. N. Nampoori and C. P. G. Vallabhan *Study of nano silver metal dispersed ceramic alumina matrix using photoacoustic technique* (communicated)

14. **Sajan D George**, A. K. George, P. Radhakrishnan, V. P. N. Nampoori and C. P. G. Vallabhan *Thermal characterisation of liquid crystal mixtures using photoacoustic technique* (communicated)

15. **Sajan D George**, A. K. George, P. Radhakrishnan, V. P. N. Nampoori and C. P. G. Vallabhan *Photoacoustic studies on thermal parameters of liquid crystal mixtures* (communicated)

16. **Sajan D George**, S. Saravanan, M. R. Anantharaman, S. Venketachalam, P. Radhakrishnan, V. P. N. Nampoori and C. P. G. Vallabhan, *Thermal characterization of doped polyaniline and its composites with CoPc* (communicated)

17. Achamma Kurian, Nibu A George, **Sajan D George**, K P Unnikrishnan, Binoy Paul, Pramod Gopinath, V P N Nampoori and C P G Vallabhan, *Effect of pH on the quantum yield of fluroscein using thermal lens technique* Journal of Optical Society of India 31(1) 29 (2002).

18. Achamma Kurian, Nibu A George, Thomas Lee. S, **D. Sajan George**, K. P. Unnikrishnan, V. P. N. Nmapoori and C. P. G. Vallabhan, *Realisation of logic gates using thermal lens technique* Laser Chemistry, 20,81(2002).

19. Achamma Kurian, K. P. Unnikrishnan, **D. Sajan George**, Pramod Gopinath, V. P. N Nampoori and C. P. G. Vallabhan, *Thermal lens spectrum of organic dyes using optical parametric oscillator* Spectrochimica Acta part A, 59, 487-491 (2003)

20. Achamma Kurian, K P Unnikrishnan, Thomas Lee S, **Sajan D George**, V P N Nampoori and C P G Vallabhan, *Studies of two photon absorption using thermal lens technique* Journal of Nonlinear Optical Physics & Materials, 12(1), 75-80 (2003)

Papers presented conference/seminars

1. **Sajan D George**, C. P. G. Vallabhan, Martin Leys and V. P. N. Nampoori Thermal diffusivity of doped InP using OPC Procedings of Second International Conference and XXVII Annual Convention of the Optical Society, August 27 – 29, Trivandrum, Kerala, India (2001)
2. **Sajan D George**, P. Radhakrishnan, V. P. N. Nampoori and C. P. G. Vallabhan Thermal diffusivity of substrate of two-layer system using photoacoustic technique Proccedings of National Laser Symposium December 19-21, CAT Indore, India (2001).
3. **Sajan D George**, Rajesh Komban, K.G. K Warrier, P. Radhakrishnan, V. P. N. Nampoori and C. P. G. Vallabhan Influence of porosity on thermal diffusivity of LaPO₄ cermics – A photoacoustic measurement Procedings of National Laser Symposium at Thiruvanathapuram India, November (2002).
4. **Sajan D George**, Dilna.S, A. K. George, P. Radhakrishnan, V. P. N. Nampoori and C. P. G. Vallabhan Use of Photoacoustic technique to measure the thermal diffusivity and phase transition in liquid crystals Procedings of Photonics 2002, TIFR, India (2002).
5. **Sajan D George**, P. Radhakrishnan, V. P. N. Nampoori and C. P. G. Vallabhan Laser induced nondestructive evaluation of transport properties of intrinsic and extrinsic Si, International Conference on Laser Applications ICLAOM Optical Metrology, IIT Delhi (2003) (Accepted)
6. **Sajan D George**, A. K. George, P. Radhakrishnan, V. P. N. Nampoori and C. P. G. Vallabhan, Thermal characterization of liquid crystal mixtures using photoacoustic technique – NLS 2003 (Accepted)

WORDS OF GRATITUDE

providing me the samples as well as for intellectual discussions. The ongoing fruitful collaboration of the department with **Dr. A. K. George**, Sultan Quoboos University, Oman has given me a chance to work on liquid crystals, which have wide application in photonic industry. I thank him for that. I also thank **Dr. Elizabeth Mathai** and **Dr. Saji Augustine** of Department of Physics, Cochin University of Science and Technology, India for a collaborative work. I extend my sincere thanks to **nonteaching staff of ISP, USIC** and **staffs of various libraries** for their timely help and assistance. The most important and essential part of this research is provided by **Council of Scientific and Industrial Research, India** in the form of Junior and Senior Research Fellowship. I also thank **NUFFIC** for the financial assistance through ISP-MHO program.

The fruitful discussion with our "Young Scientist" **Dr. Deepthy Menon** has always been an asset both in professional and personal front of my life. Her enthusiasm and attitude towards research always encourages me.

I am extremely thankful to **P. Suresh Kumar, Ms. Viji, Paru** and **Appu** for considering me as one among them. The love, care and the wonderful moments that they provided me will always be cherished in my memories.

It is beyond words to express my gratitude to **Dilna** and **her parents**, whose house was a home away from home, for all the care and love that they shown towards for me. The help and support, both intellectually and personally, given by Dilna during the preparation of all my manuscripts and thesis is unique.

Last but not the least, I would like to express my sincere gratitude to **my loving parents** and **dearest brother**, the greatest gift that god has given me on this earth, for their constant support, encouragement and prayers. Their appreciation and support for even in my small achievements, has always been a source of motivation for me. I thank them for being with me in all crests and troughs of my life. I am sure that I would not have been able to achieve anything without their support, help and prayers.

Above all, my gratitude towards the power that controls everything, without his blessings and mercy we cannot accomplish anything in this world. Thank **God**.

<div align="right">

SAJAN D GEORGE

</div>

Contents

Imagination is more important than knowledge

— Albert Einstein

Chapter 1

Photothermal methods and their applications to photonic materials

Abstract

This chapter which is of an introductory nature, presents a short description of various phenomena arising due to light matter interaction with special emphasis on the nonradiative processes and that lead to photothermal phenomena. An overview of various photothermal methods and their applicability for the characterisation of photonic materials are explained in detail. A comprehensive account of the various techniques used for the detection of photothermal signal is also given here. The experimental techniques employed in the present thesis and their significance and uniqueness are well addressed. A review of the work done by various researchers on the applicability of photothermal deflection and photoacoustic technique for the characterisation of photonic materials is also included. The motivation behind the present work is highlighted in this chapter.

1.1. Light Matter Interaction

Interaction of light with matter gives a better understanding of microscopic as well as macroscopic properties of matter in all its different states. The advent of coherent, monochromatic and highly directional light source, namely, laser has lead to a major renaissance in this field. Depending on the strength of the interacting electric field of the electromagnetic radiation, materials exhibit several linear and nonlinear phenomena [1-2]. When the strength of interacting electric field is of the order of atomic field, materials show different nonlinear optical properties such as harmonic generation, hyper polarisability, higher order susceptibility, etc. [3]. The interactions of matter with intense short optical pulses give rise to more interesting phenomena such as laser ablation, plasma generation, etc [4-5]. However, the light-matter interaction at low levels of optical power results in various thermo-optical and photo chemical reactions [6]. Irradiation of a specimen with an optical radiation results in the excitation of the atoms in the sample to higher energy levels from which they release their energy either in the form of light or heat so as to return to the ground state energy level. These processes can takes place either in a radiative way or through nonradiative way. The emission of light by a substance due to any processes other than due to temperature rise is called luminescence [7]. If the deexcitation is taking place from a metastable state, it is called phosphorescence so that the luminescence persists significantly even after the exciting source is removed. However, in the case of fluorescence, the emission of radiation occurs instantaneously [8-9]. The excitation of specimen can also results in the transfer of energy through chemical reaction [6]. During the last two decades, many researchers has explored the nonradiative path of deexcitation of specimen after excitation with a chopped optical radiation to investigate the thermal, optical, transport and structural properties of material in all its different states [10-21]. Various experimental techniques such as 3ω method, Laser calorimetry and Photothermal methods are used for studying these thermal waves generated due to nonradiative deexcitation of samples [15-20]. The present thesis deals with the use of two photothermal methods,

namely, photoacoustic and photothermal deflection technique to investigate the thermal and transport properties of certain selected photonic materials.

1.2. Photothermal methods

In recent years, thermal wave physics has emerged as an effective research and analytical tool for the characterisation of materials [22-25]. The nondestructive and nonintrusive photothermal methods are based on the detection by one means or the other, of a transient temperature change that characterizes the thermal waves generated in the sample after illumination with a pulsed or chopped optical radiation [26-40]. The detected photothermal signal depends on the optical absorption coefficient at the incident wavelength as well on how heat diffuses through the sample [41-45]. Dependence of photothermal signal on how heat diffuses through the specimen allows the investigation of transport and structural properties such as thermal diffusivity, thermal effusivity, thermal conductivity, voids, etc [46-55]. Photothermal methods can be effectively used for the optical characterisation of the sample due to its dependence on optical absorption coefficient [56-60]. The unique feature of photothermal methods is that the detected photothermal signal depends only on the absorbed light and it is independent of transmitted or scattered light. The two features that make photothermal methods superior to conventional methods is that it can directly monitor the nonradiative path of deexcitation in addition to being sensitive to very small optical absorption coefficient [59-60]. Apart from this, photothermal effects can amplify the measured optical signal which is referred to as enhancement factor and it is the ratio of the signal obtained using photothermal spectroscopy to that obtained using conventional transmission spectroscopy. Enhancement factors depend on thermal and optical properties of the sample, the power or energy of the light source used to excite the sample and the optical geometry used to excite the sample [61]. As these parameters can vary externally, photothermal methods can be used even for specimens having relatively poor thermal and optical properties. The merit of these methods also lies in the extremely sensitive

detection technique used here in comparison to conventional transmission methods. The various photothermal methods are depicted in figure 1. The magnitude of photothermal signal depends on the specific method used to detect the photothermal effect and on the type of the sample analyzed.
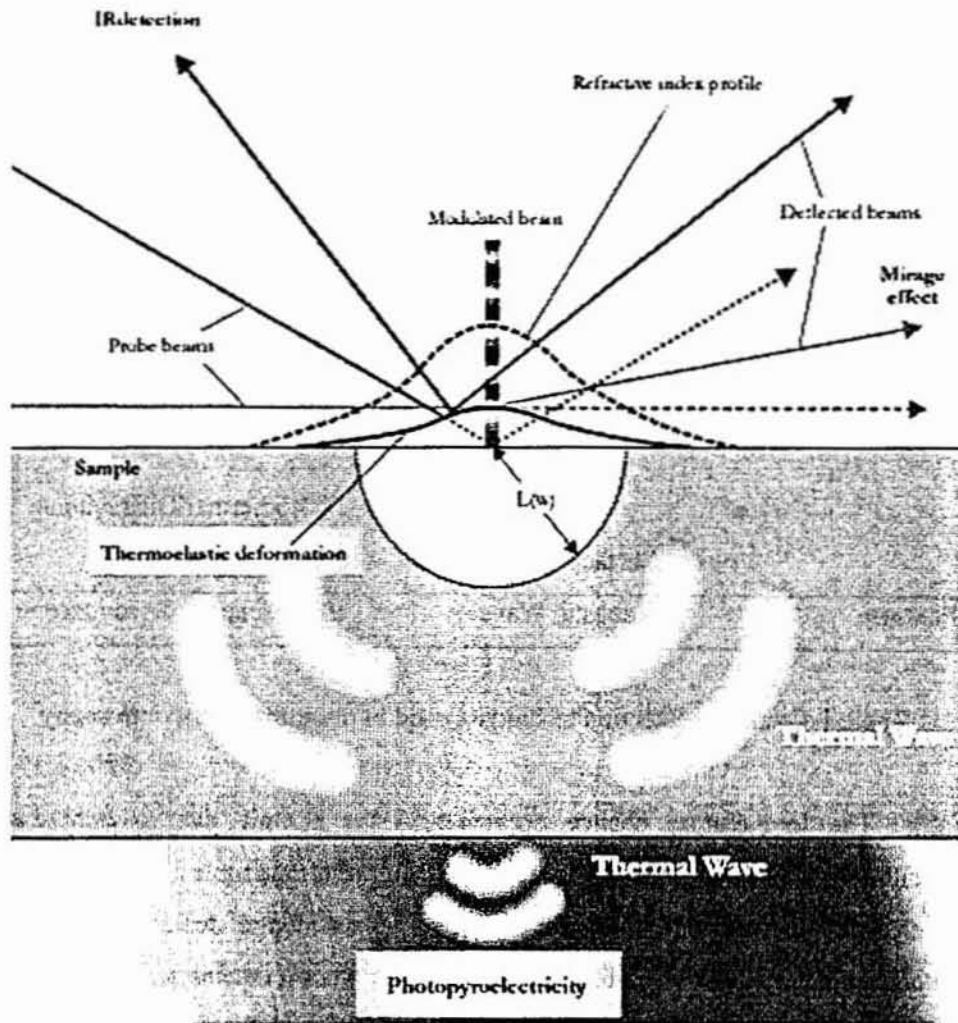
Figure 1. Different types of photothermal signal generation

1.3. A brief account of the different photothermal methods

The common techniques that are employed in photothermal methods are shown in the table I. Eventhough all these techniques are based on the same principle, the detecting parameter changes from one technique to other.

Thermodynamic Parameter	Measured Property	Detection Technique
Temperature	Temperature	Calorimetry
	Infrared Radiation	Photothermal Radiometry
Density	Refractive Index	Photothermal Lens
		Photothermal Interferometry
		Photothermal Deflection
		Photothermal Refraction
		Photothermal Diffraction
	Surface Deformation	Surface Deflection
Pressure	Acoustic Wave	Photoacoustic Spectroscopy

Table I. Common detection techniques used in photothermal spectroscopy

The temperature change occurring in the sample due to nonradiative deexcitation can be directly measured using thermocouples, thermistors or pyroelectric devices and the corresponding experimental technique is called *photothermal calorimetry* [62-65]. In the *photopyroelectric technique* [66-68], which can be used for the simultaneous measurement of different thermal parameters such as thermal diffusivity, effusivity etc., a thermally thick pyroelectric film (thickness of the film is greater than thermal diffusion length of the film) is attached to one side of the thermally thick sample and the combination is mounted on a thermally thick backing medium. The other side of the specimen is illuminated by an intensity

6

modulated optical radiation. When thermal waves reache the pyroelectric sensor-sample interface, the pyroelectric sensor detects an electric current, which contains information about the structure and thermal and optical properties of the sample. In general, a PVDF film coated with Ni-Cr is used as the pyroelectric detector [69]. However, this method demands accurate calibration of the detector and it suffers from thermal impedance mismatch between sample and the mountings. A variant configuration of the standard photopyroelectric method, well suited for thermal effusivity measurements, is the so-called inverse photopyroelectric technique (IPPE). In the inverse configuration introduced by Chirotic and co-workers [70], light is incident directly on the surface of pyroelectric transducer and the substrate is substituted by the sample. The thermal effusivity of binary liquid mixtures are measured using this technique [70]. Application of the IPPE technique for the measurement of thermal effusivity of margarines, cultured milk and pastry materials is a typical example of the potential application of this technique for the quality control of the foodstuff [71-72]. Direct determination of thermal conductivity of solids and liquids was recently discussed by Thoen and co-workers [73].

In the case of *photothermal radiometry* [74], the temperature change is measured indirectly by monitoring the infrared emission and it can be used in situations where a large temperature change has occurred. Although not very sensitive, this method has potential for application in nondestructive materials analysis and testing. Using sensitive infrared cameras, it can be used for imaging the thermal properties of large samples. However, in photothermal radiometry, a more careful analysis of the spectral detectivity of detector, spectral absorption of the sample and the geometry of the optical equipment are essential [75]. The inherent advantage of this technique is that signal can be obtained remotely [76]. The shape of the objects can be arbitrary. Nevertheless, it is better to make sure that the quality for imaging a sample spot on the detector is constantly good. Signal evaluation may be complicated if the sample is transparent or reflective in the infrared spectral range.

In steady state and isobaric conditions, the temperature change due to nonradiative deexcitation can result in a variation in volume expansion coefficient and a consequent change in density of the specimen. Direct measurement of this temperature dependent density is very difficult. In the case of solids, these density changes can alter the physical dimension of the surface of specimen under investigation. Depending on the spatial homogeneity and the deformation of the specimen, two photothermal technique namely *photothermal interferometry* [77-80] and *photothermal surface deflection method* [81-82] are employed for the evaluation of material parameters. The major difference between these methods and earlier mentioned photothermal methods is that, in this case a pump laser is used to produce photothermal effects and a probe laser is used to monitor the refractive index change. Photothermal interferometric technique is effectively employed for samples having homogenous deformation (expansion or contraction) of the surface due to temperature change. Using this technique, a small displacement of the order of parts-per million of the wavelength of the probe beam is accurately measured, which in turn helps in the sensitive measurement of solid sample absorption. In this technique, both the pump and probe beam passes through the sample, which is optically transparent at the probe beam wavelength. The optical path length change that occurs due to photothermally induced refractive index variation can be measured using photothermal interferometric technique. This method is effectively employed in the case of liquids also. A spatially heterogeneous expansion (or contraction) can cause change in surface angle and a probe beam reflected from the surface of specimen can be used to monitor this change in angle. This method is referred to as photothermal surface deflection spectroscopy.

The spatially varying refractive index profile arising due to photothermal effect as a result of irradiation with pump beam can cause focusing or defocusing of the probe beam, provided the refractive index profile is curved. Thus the thermally perturbed sample and the consequent spatially varying refractive index can act as a

lens. Depending on the sign of $\dfrac{dn}{dT}$, it can act either as a converging or diverging lens.

Light transmitted through an aperture placed beyond the photothermal lens will vary with the strength of the lens. Photothermal methods based on the measurement of the strength of the lens are called *thermal lens spectroscopy* [6, 83-84]. This technique has proven to be a valuable tool to study the thermophysical properties of transparent materials such as, glasses, liquid crystals and polymers. It allows the determination of thermal diffusivity, thermal conductivity, the temperature coefficient of the optical path length, optical absorption coefficient and fluorescence quantum efficiency [6]. Since this is a remote sensing technique, measurement of samples in inaccessible environment presents no extra difficulties. This is an important aspect if one wants to carry out thermo-optical measurements on samples placed inside a high temperature furnace. Extensive use of this technique for investigation of the thermal and optical properties of different materials has been made by Baesso and co-workers [85-88].

In the case of opaque solid samples, illumination with focused optical radiation heats the specimen locally and shares its energy to the coupling medium, where a refractive index gradient is generated due to temperature dependent index of refraction. A probe laser beam passing parallel to the sample surface and through the coupling medium gets deflected from its normal path. The technique that makes use of this bending to study properties of materials is commonly called *photothermal deflection spectroscopy* [89-92]. An overview of different configurations of this technique is given in the next section. In *photothermal refraction spectroscopy*, the detected signal is due to the combined effects of both deflection and lensing. *Photothermal diffraction technique* is based on the probe-beam diffraction due to a periodic index of refraction (grating) generated when two pump-beams cross each other inside or at the surface of a sample [93]. The grating will diffract light at an angle according to Bragg's law. This method is widely used for studies in ultra-short time scales.

Another important parameter that is exploited in photothermal methods is the pressure change associated with the transient temperature change in the specimen. Pressure transducers such as microphones and piezoelectric crystals are commonly used for the measurement of pressure waves associated with a rapid sample heating. The branch of photothermal method based on the detection of these pressure waves is known as *optoacoustic* or *photoacoustic (PA) technique* [94-96]. A detailed description of this technique is given in the ensuing sections.

Two types of pumping mechanism are commonly employed in photothermal experiments, namely, pulsed optical excitation or modulated continuous wave optical radiation. Choice of detecting instruments depends greatly on the mode of excitation. Optical excitation through pulsed radiation results in a transient signal of large amplitude immediately after the optical radiation and it decays as the sample approaches thermal equilibrium through thermal diffusion processes. These transient signals last for a few microseconds in gaseous state and for few milliseconds in condensed media. Excitation through intensity modulated optical radiation results in periodic thermal waves and the amplitude and phase of the generated photothermal signal is a function of the frequency of modulation of incident radiation. These thermal waves carry information about the thermal, transport and optical properties of the specimen under investigation.

1.4. Photothermal deflection technique.

In spite of a variety of photothermal methods used for the characterisation of materials, the noncontact photothermal deflection (PTD) technique possesses some unique characteristics and advantages compared to other photothermal methods [97-98]. Ever since the theory of transverse photothermal deflection technique was put forward by Fournier et.al in early eighties [89], this technique is effectively employed in spectroscopic measurements due to its extremely high sensitivity to a very low absorption coefficient. The absorption of optical radiation (pump beam) causes a corresponding change in the index of refraction in the optically heated region as well

as in a thin layer adjacent to the sample surface. By probing the gradient of the varying index of refraction with a second beam (probe beam), one can relate its deflection to the optical absorption as well as to thermal parameters of the samples [99-104]. Depending on the relative positions of the pump and the probe beam, two choices of PTD techniques are possible viz, transverse PTD technique and collinear PTD technique. A schematic representation of these two configurations is given in figure 2 and figure 3, respectively. In the transverse PTD technique, probing is done on the gradient of index of refraction in the thin layer adjacent to the sample whereas in the collinear PTD technique, a gradient of index of refraction is created and probed within the sample itself.
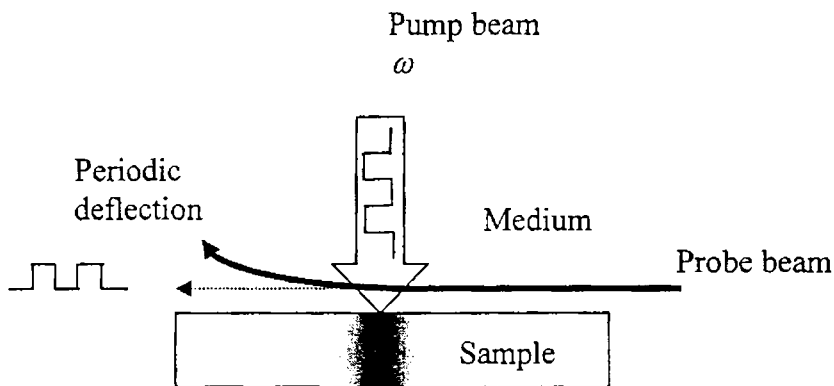
Figure 2. Schematic representation of transverse photothermal deflection technique
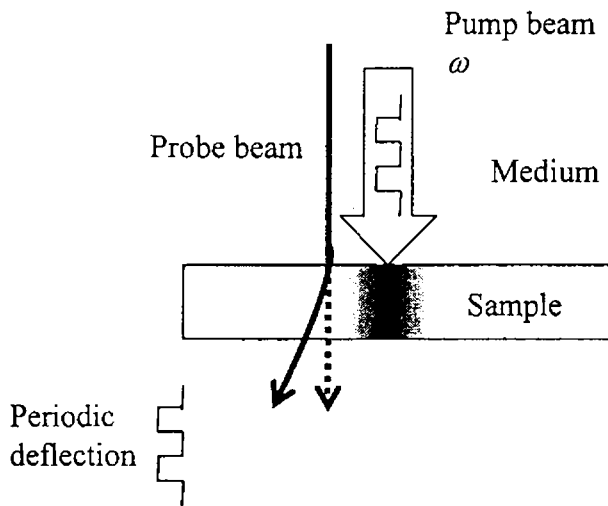
Figure 3. Schematic representation of collinear photothermal deflection technique.

The two configurations of PTD technique allow, in principle, a local testing of the absorption of a given sample. The collinear method, however, can only be used for samples which neither absorb nor scatter the probe beam. Spatial resolution in the surface plane [(x,y) plane] is, for both methods, determined by the width of the pump beam. In the z-direction, the resolution of the transverse PTD method depends strongly on the thermal diffusion length in the sample. In the case of thermally thin sample, the transverse PTD technique, measures the total (surface and bulk) accumulated absorption over the whole thickness of the sample. A theoretical background of the transverse PTD is given in next chapter. For the collinear method, the resolution and the locality of the measurement are determined by the cross-sectional area of the pump and probe beam. However, for thin samples and small angles between pump and probe beam, the collinear PTD technique also measures the accumulated absorption over the whole thickness of the sample. It is already been reported that transverse PTD technique is more effective in evaluating the material parameters of opaque and solid samples, especially for samples having poor optical

quality [105-106]. The potential of PTD technique in imaging and scanning microscopy is well demonstrated in earlier reports [104-105]. Using this technique a temperature change of the order of few mK can be easily detected.

1.5. Photoacoustic technique

The photoacoustic (PA) effect is the generation of acoustic waves in the specimen after illumination with a chopped or pulsed optical radiation. Graham Bell discovered the PA effect in 1880, when he noticed that the incidence of modulated light on a diaphragm connected to a tube produced sound [107-108]. Thereafter, Bell studied the photoacoustic effect in liquids and gases, showing that the intensity of acoustic signal depends on the absorption of light by the material. In the nineteenth century, it was known that the heat of a gas in a closed chamber produces pressure and volume change in this gas. In the subsequent years many theories were developed by different researchers to explain the PA effect [109-116]. According to Rayleigh [117], this effect was due to the movement of the solid diaphragm. Bell believed that the incidence of light on a porous sample expanded its particles, producing a cycle of air expulsion and reabsorption in the sample pores. Both were contested by Preece [117], who pointed out that the expansion/contraction of the gas layer inside the photoacoustic cell is the cause of the phenomenon. Mercadier [117] explained the effect conceiving what we call today the thermal diffusion mechanism: the periodic heating of the sample is transferred to the surrounding gas layer, generating pressure fluctuations. The lack of a suitable detector for the photoacoustic signal made the interest in this area to decline until the invention of the sensitive and compact microphone. Even then, research in this field was restricted to applications in gas analysis up to 1973, when Rosencwaig started to use the PA technique for spectroscopic studies of solids and, together with Gersho, developed a theory for the PA effect in solids [109-116]. Ever since the theory of PA effect in solids was developed by Rosencwaig and Gersho, this technique has been effectively used in diverse areas of physics, chemistry and medicine [34, 117-118]. With the advent of

sophisticated data acquisition systems and tunable light sources, the versatility of PA technique paved way to several innovative experiments.

The PA generation can be classified as direct and indirect. In the direct PA signal generation, the acoustic wave is produced in the sample whereas in the indirect PA generation the acoustic wave is generated in the coupling medium adjacent to the sample.

In the direct PA signal generation in solids or liquids, the acoustic wave generated due to transient temperature change is measured using a piezoelectric transducer [usually lead zirconate titanate (PZT) ceramic] placed in intimate contact with specimen. These detectors can detect temperature changes of $10^{-7}\,°C$ to $10^{-6}\,°C$, which for a particular solid or liquid corresponds to thermal inputs of the order of 10^{-6} cal/cm^3-sec. Since the volume expansion of solids or liquids is 10 to 100 times less than that of gases, this technique is more sensitive than the microphone version of PA technique. Depending on the optical transparency at the incident wavelength, different configurations of piezoelectric PA technique can be employed as shown in figure 4. In the case of optically opaque samples, it is better to attach PZT on the rear side of the specimen (Figure 4.a) whereas in the case of optically transparent samples, the transducer is placed on either side of sample in the form of an annulus (Figure 4.b). In the case of liquids, the PZT is mounted on one of the walls of the liquid container [119-124].
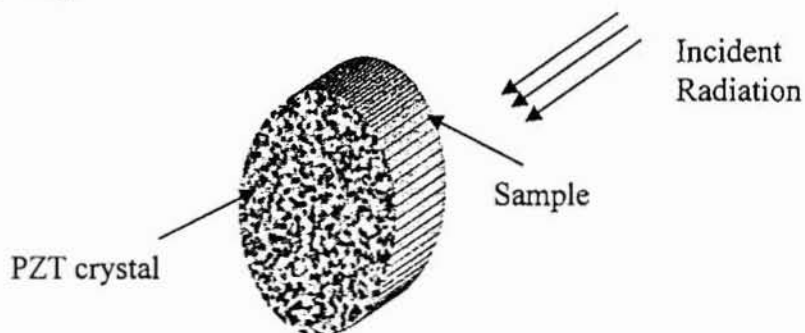
Figure 4.a) PZT configuration for opaque samples
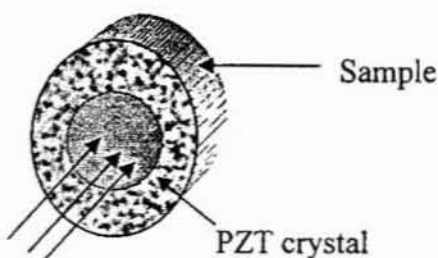
Figure 4.b) PZT configuration for transparent samples

However, in the case of powdered samples or gels, the PZT version of PA technique is not applicable. In such cases, the microphone version of PA technique is extensively used. The simple and elegant microphone version of PA technique, though indirect, can measure a temperature rise of 10^{-6} to 10^{-5} °C or a thermal input of about 10^{-6} to 10^{-5} cal/cm^{-3} –sec. In the past, different versions of microphone based PA technique, viz., closed PA technique, Open Cell Photoacoustic (OCP) technique etc are effectively employed for the characterisation of condensed matter [125-127]. Depending on the position of microphone in the PA cell cavity, the PA technique can be employed in two configurations viz., either in reflection configuration mode (Figure 5.a) or in transmission detection configuration (Figure 5.b). The transmission detection configuration, which is the basis of minimal volume Open Photoacoustic Cell (OPC) technique, is found to be more useful in evaluating the thermal and transport properties, especially for semiconductors. Perondi and Miranda described the OPC as "an inexpensive detector sensitive to any radiation, ranging from microwave to x-ray" [128-129]. The disadvantage of microphone version of PA technique is that the response time of the detector is limited by the transient time of acoustic waves in the PA cell cavity and low frequency response of the microphone.
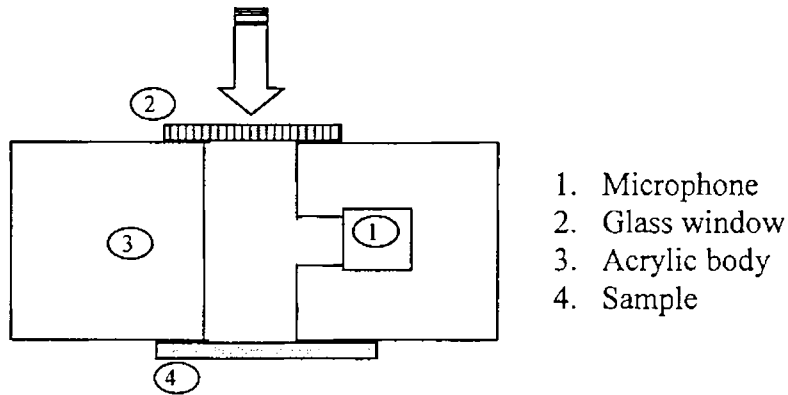
Figure 5.a) Reflection detection configuration of PA technique

1. Microphone
2. Glass window
3. Acrylic body
4. Sample
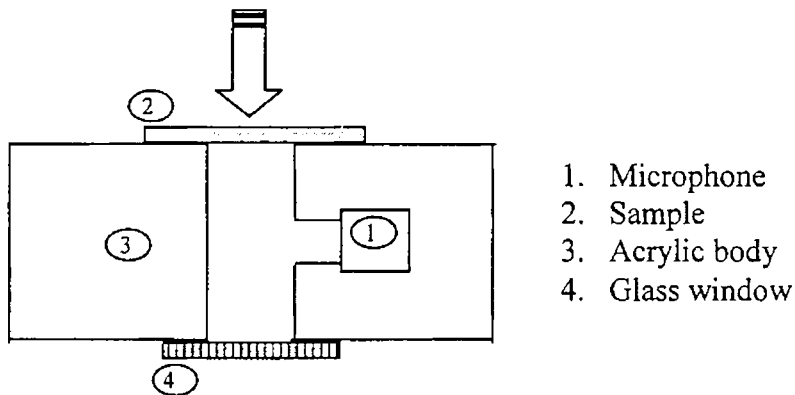
Figure 5.b) Transmission detection configuration of PA technique

1. Microphone
2. Sample
3. Acrylic body
4. Glass window

1.6. Rosencwaig and Gersho Theory

According to R-G theory, which is based on the one dimensional heat flow model, the pressure fluctuation detected by the microphone depends on the acoustic pressure disturbance at the sample-gas interface. The generation of surface pressure disturbance, in turn, depends on the periodic temperature fluctuations at the sample-gas interface. Rosencwaig and Gersho developed and exact expression for the temperature fluctuations by treating the acoustic disturbance in the gas in an approximate heuristic manner.

The theoretical formulation of the R-G model is based on the light absorption and the thermal wave propagation in an experimental configuration as shown in figure 6. Here, the sample, which is in the form a disc having a thickness l is in contact with backing material of low thermal conductivity and of thickness l_b. The front surface of the sample is in contact with a gas column of length l_g. The backing and the gas are considered to be nonabsorbing at the incident wavelength. Following are the parameters used in the theoretical explanation of R-G model.

k, the thermal conductivity ρ, the density

C, the specific heat capacity $\alpha = {k}/{\rho C}$, the thermal diffusivity

$a = \sqrt{{\omega}/{2\alpha}}$, the thermal diffusion coefficient   and

$\mu = {1}/{a}$, the thermal diffusion length
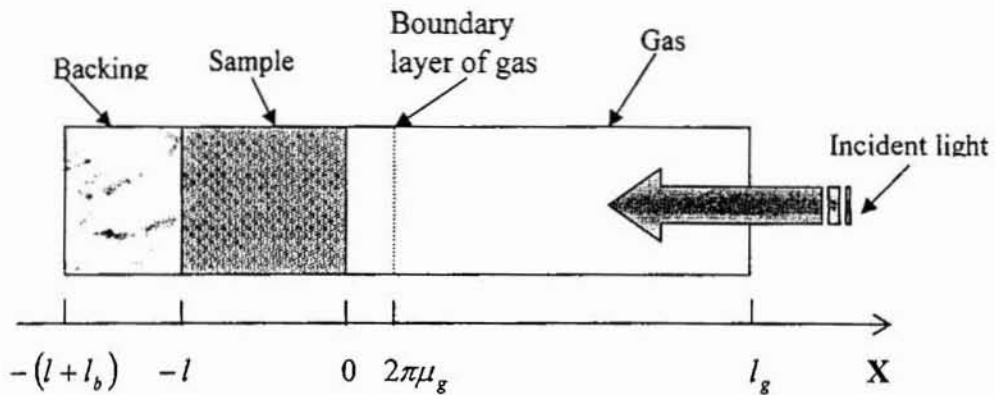
Figure 6: Schematic representation of photoacoustic experimental configuration.

When a sinusoidally modulated light beam of intensity I_0 is incident on a solid sample having an absorption coefficient β, the heat density generated at any point due to the light absorbed at this point can be represented by

$$\frac{1}{2}\beta I_0 e^{\beta x}(1+\cos \omega t)$$
(1)

The thermal diffusion equation in the three regions by taking into account of the heat diffusion equation can be written as

$$\frac{\partial^2 \theta}{\partial x^2} = \frac{1}{\alpha}\frac{\partial \theta}{\partial t} - \frac{\beta I_0 \eta}{2k}e^{\beta x}\left(1+e^{\beta x}\right) \qquad \text{for } -l \leq x \leq 0$$
(2)

$$\frac{\partial^2 \theta}{\partial x^2} = \frac{1}{\alpha_b}\frac{\partial \theta}{\partial t} \qquad \text{for } -(l+l_b) \leq x \leq -l$$
(3)

$$\frac{\partial^2 \theta}{\partial x^2} = \frac{1}{\alpha_g}\frac{\partial \theta}{\partial t} \qquad \text{for } 0 \leq x \leq l_g$$
(4)

Where θ and η are the temperature and light to heat conversion efficiency respectively. Here the subscripts b and g represent the backing medium and gas respectively. The real part of the complex valued solution of these equations has physical significance and it represents the temperature fluctuations in the gas cell as a function of position and time.

After applying proper boundary conditions for temperature and heat flow continuity, and by neglecting the convective heat flow, the period temperature fluctuations at the sample-gas interface can be obtained as

$$\theta_0 = \frac{\beta I_0}{2k(\beta^2-\sigma^2)}\left[\frac{(r-1)(b+1)e^{\sigma l}-(r+1)(b-1)e^{-\sigma l}+2(b-r)e^{\beta l}}{(g+1)(b+1)e^{\sigma l}-(g-1)(b-1)e^{-\sigma l}}\right]$$
(5)

where

$$b = \frac{k_b a_b}{ka}, \qquad g = \frac{k_g a_g}{ka}, \qquad r = (1-i)\frac{\beta}{2a}, \qquad \sigma = (1+i)a$$
(6)

The periodic thermal waves, which are rapidly attenuating, damp completely as it travels a distance equal to $2\pi\mu_g$. Thus the gas column within this distance expands and contracts periodically so that it acts as an acoustic piston for the

18

remaining gas in the PA cell. Assuming that the rest of the gas responds adiabatically to the action of acoustic piston, the adiabatic gas law can be used to derive an expression for the complex envelope of the sinusoidal for the pressure variation Q as

$$Q = \frac{\gamma P_0 \theta_0}{\sqrt{2} T_0 l_g a_g} \tag{7}$$

Where γ, P_0 and T_0 are the ratio of heat capacities of air, ambient pressure and temperature respectively. Equation (7) can be used to evaluate the magnitude and phase of the acoustic pressure wave in the cell due to photoacoustic effect. This expression takes a simple form in special cases.

1. Optically transparent solids $\left(l_\beta > l\right)$

Case 1(a): Thermally thin solids $\left(\mu \gg l; \mu > l_\beta\right)$

We can set $e^{-\beta l} \cong 1 - \beta l, e^{\pm \sigma l} \cong 1$ and $|r| > 1$ in equation (7) and we obtain

$$Q \cong \frac{(1-i)\beta l}{2a_g}\left(\frac{\mu_b}{k_b}\right)Y \tag{8}$$

with $Y = \frac{\gamma P_0 I_0}{2\sqrt{2} T_0 l_g} \tag{9}$

Now the acoustic signal is proportional to βl and varies as f^{-1}. Moreover, the signal is now determined by thermal properties of the backing material.

Case 1(b): Thermally thin solids $\left(\mu > l; \mu < l_\beta\right)$

We can set $e^{-\beta l} \cong 1 - \beta l, e^{\pm \sigma l} \cong \left(1 \pm \sigma l\right)$ and $|r| < 1$ in equation (7) and we obtain

$$Q \cong \frac{(1-i)\beta l}{2a_g}\left(\frac{\mu_b}{k_b}\right)Y \tag{10}$$

The acoustic signal now behaves in the same fashion as in the previous case.

Case 1(c): Thermally thick solids $\left(\mu < l; \mu << l_\beta\right)$

We can set $e^{-\beta l} \cong 1 - \beta l, e^{-\sigma l} \cong 0$ and $|r| << 1$ in equation (7) and we obtain

$$Q \cong -i \frac{\beta\mu}{2a_g}\left(\frac{\mu}{k}\right)Y \qquad (11)$$

Now, only the light absorbed within the first thermal diffusion length contributes to the signal inspite of the fact that light is being absorbed throughout the length of the sample. Also since $(\mu < l)$, the backing material does not have any contribution to the signal. Interestingly, the signal now varies as $f^{-1.5}$.

2. Optically opaque solids $\left(l_\beta << l\right)$

Case 2(a): Thermally thin solids $\left(\mu >> l; \mu >> l_\beta\right)$

We can set $e^{-\beta l} \cong 0, e^{\pm\sigma l} \cong 1$ and $|r| >> 1$ in equation (7) and we obtain

$$Q \cong \frac{(1-i)}{2a_g}\left(\frac{\mu_b}{k_b}\right)Y \qquad (12)$$

Now the signal is independent of β, which is valid for a perfect black absorber such as carbon black. The signal will be much stronger compared to the case 1 (a) and varies as f^{-1}, but still depends on the properties of backing material.

Case 2 (b): Thermally thick solids ($\mu < l$; $\mu > l_\beta$)

We can set $e^{-\beta l} \cong 0$, $e^{-\sigma l} \cong 0$ and $|r| > 1$ in equation (7) and we obtain

$$Q \cong \frac{(1-i)}{2a_g}\left(\frac{\mu}{k}\right)Y \qquad (13)$$

Equation (13) is analogous to (12), but the thermal properties of backing material are now replaced with those of the sample. Again the signal is independent of β and varies as f^{-1}.

Case 2 (c): Thermally thick solids ($\mu << l$; $\mu < l_\beta$)

We can set $e^{-\beta l} \cong 0$, $e^{-\sigma l} \cong 0$ and $|r| < 1$ in equation (7) and we obtain

$$Q = -i \frac{\beta \mu}{2a_g} \left(\frac{\mu}{k} \right) Y \tag{14}$$

This is very interesting and important case. Eventhough the solid is optically opaque, the photoacoustic signal is proportional to β as long as $\beta\mu < 1$. As in case 1 (c), the signal is independent of the thermal properties of the backing material and varies as $f^{-1.5}$. The R-G theory also predicts the linear dependence of PA signal to light intensity.

1.7. Photonic Materials

The area of photonics reflects the synergy between optics and electronics and also shows the tie between optical materials, devices and systems [130-131]. Electronics involves the control of electron-charge flow in vacuum or in matter, whereas photonics deals with the control of photons in free space or in matter. However, photonics is replacing electronics due to fast data transmission capability of photon as well as its other advantages. The development of photonics is multidirectional. It can be broadly classified into three categories (a) sources such as lasers, (b) optical functional devices and (c) operational optical components. Now a days, photonics find applications in all realms of life extending from communication to medical sciences. However, the effective use and progress of this modern technology demands a better understanding of the materials used for the fabrication of photonic devices and components. Hence, a branch of photonics is completely devoted to the preparation and characterisation of photonic materials.

Semiconductors, liquid crystals, ceramics etc are the commonly used materials in photonics industry.

Semiconductors play a vital role in the advancement of photonics as they are extensively used for the generation, detection and modulation of electromagnetic radiation as well as in the fabrication of monolithic optoelectronic devices. In the last decade significant improvements in epitaxial growth techniques resulted in the fabrication of high quality layered structures such as superlattices and quantum wells. These layered structures show several novel properties, which are not possible by conventional materials. The recent development in the fabrication of compound semiconductors holds promises for achieving visible and ultraviolet semiconductor lasers useful for optical storage, printing, display devices and many more new applications [132-134].

Ceramics are considered to be a key material for the fabrication of various electronic and optoelectronic devices. Its applications extend from semiconductor device fabrication to spacecraft industry. These materials find wide applications in photonics industry due to their special properties such as tunable electrical properties, toughness, high temperature tolerance, light weight and excellent resistance to corrosion and wear. These materials are also used as thermal barrier resistances. However, the performance of devices made from ceramics is limited greatly by the thermal behavior of these materials [135-136].

Liquid crystals are another class of materials, which are considered to be ideal candidates as photonic materials due to their extensive use in display devices as well as in optical data storage materials. These materials are called smart materials as the properties of these materials can be altered by changing the external parameters such as pressure, temperature, pH and even moisture. In addition to it, liquid crystals can be switched with very low voltage, which has an enormous impact on display technology and photonics industry. The optical and thermal behaviour of these liquid crystals greatly affects the performance of devices based on these materials [137-138].

1.8. Photothermal deflection studies on semiconductors

In 1979 Boccara *et.al* proposed and demonstrated the usefulness of photothermal beam deflection (mirage effect) method for monitoring the temperature gradient field close to a sample surface or within the bulk of a sample [89]. Ever since, this method is used with much effectiveness in the thermal and optical characterisation of semiconductors. In 1981 Jackson et.al used this technique for the investigation of sub gap and band edge optical absorption in Si:H [99]. Penna et.al measured the optical absorption in single quantum wells using this method in 1985 [139]. Thereafter, it has been used for measurement of parameters of thin films [140-145], passivation effect in amorphous silicon [146], thermal diffusivity of compound semiconductors [147-148], heterojunctions [149-150] etc. Sheih et.al utilized this technique for studying the impurity induced disordering in multiple quantum well structures [151]. A large number of investigations using photothermal deflection are devoted for studying multiple quantum well heterostructures [151-152], quantum dots [153-154]. In 1991, Zammit etal used this technique for investigating the influence of defects in the absorption spectra of semiinsulating GaAs [155]. A theoretical investigation of three dimensional photothermal phenomena was put forward by Cheng J C et.al in 1991[156]. A different version of photothermal deflection technique called differential photothermal deflection spectroscopy [157], is also used for the investigation of thermal and optical characterisation of semiconductors. A modified version of photothermal deflection technique is applied for direct determination of energy levels and the effective correlation energy of dangling-bond defects in a Si:H [158-159]. The quantum confinement effect and time dependent optically induced degradation in CdS and CdSe semiconductor doped glasses were observed using photothermal deflection technique. The average radius of the semiconductor microcrystals is also measured using this method [153]. Ambacher et.al, in 1996, observed the sub-bandgap absorption in GaN using this technique [160]. The bouncing configuration of photothermal deflection technique is also

effectively used for the evaluation of thermal properties of compound semiconductors [161]. Thermal characterisation of semiconductors is carried out using a new photothermal deflection method by Bertlotti etal in 1997 [147]. It has been reported that the PTD technique is more than sufficient to measure the optical absorption for a thickness of few atomic layers and it is an effective method to study nanostructures [154]. This technique is also used for the absorption studies in GaN/InGaN/GaN single quantum wells as well as InGaN/GaN heterostructure [162]. Recently this technique has been utilized for thermal characterisation of layered structures [163] as well as for the optical characterisation of amorphous silicon based alloys [164].

1.9. Photoacoustic investigation of simultaneous measurement on thermal and transport properties of semiconductors

The laser induced nondestructive PA technique find wide applicability in the evaluation of thermal and transport properties of semiconductors. An early investigation in this regard has been carried out by V A Sabilikov etal [126]. Numerical evaluation of thermal and transport properties of semiconductors are done by Pinto Neto etal by taking account of the various heat generation mechanisms in semiconductors [165-166] which is followed by further investigations of influence of doping on thermal and transport properties in epitaxial layers [167-168]. An analytical solution of the various heat generation mechanisms in semiconductors is done by Dramicanin etal. in 1995 [169]. The minimal volume open cell photoacoustic technique along with analytical solution forwarded by Dramicanin et.al [169] is effectively used for the investigation of thermal and transport properties of large number of semiconductors such as CdTe, Ge, GaAs, GeSe etc [170-174]. In 1997, Todorovic etal proved that heat transmission configuration is more useful in evaluating the thermal and transport properties of semiconductors [175]. The simultaneous measurement of thermal and transport properties of semiconductor thin films, which is difficult to be evaluated by conventional methods, can be performed accurately using PA effect [172, 176]. They also studied, both theoretically and

experimentally, about the influence of thermo elastic and electronic strain on the PA signal generation in semiconductors. In 1998, E Marin etal, used this technique for the evaluation of nonradiative recombination time and hence to study the nonradiative recombination mechanisms in semiconductors [177]. They also used this technique for the evaluation of surface recombination velocity at the interface. Qingshen etal carried out studies on the thermal and electronic properties of $CdInGaS_4$ using the heat transmission configuration technique [178-179]. In recent years, this technique is also being used for the photoacoustic characterisation of semiconductor pellets, thin films and also to study the influence of doping on thermal diffusivity value of semiconductors [55, 176, 180]. PA technique is employed with much effectiveness in studying the heat diffusion in two layer structures [181]. It has been well established that, eventhough the pulsed PA technique is more useful for the optical characterisation of semiconductors, the microphone version of PA technique under heat transmission configuration is more useful in evaluating its the thermal and transport properties.

1.10. Photoacoustic studies on ceramics

The versatility of PA technique is well established for the insitu and invivo measurements of the thermal properties of ceramics. A major part of the work done on ceramics using PA technique is focused on the thermal characterisation of ceramics and its correlation with microstructural properties. This technique allows us to investigate some defects occurring in ceramics such as cracks, subsurface cracks, and residual stresses etc [11, 15-17, 182-183]. This technique is also being employed for the evaluation of specific heat, phase transitions etc [184-185] as well as for the detection of water vapour permeability in ZrO_2-TiO_2 ceramics [186]. As the macroscopic thermal properties such as thermal diffusivity, thermal conductivity etc are greatly affected by microstructural variations, these methods can be effectively utilized for the study of the influence of microstrutural variation arising due to sintering temperature, incorporation of foreign atom etc. on the macroscopic

properties. This technique has been used for the measurement of thermal diffusivity of γ alumina and the influence of hydroxyl ion on its thermal diffusivity value [135]. Currently, the measurement of thermal parameters and its correlation with porosity of ceramics are in progress [187].

1.11. Photoacoustic Studies on conducting polymers

Conducting polymers are the most recent generation of polymers. In 1976, Alan J Hegger and his co-workers discovered conducting polymers and observed that when doped, its electrical conductivity can vary from that of an insulator to that of a conductor [188-189]. The discovery of this material is particularly interesting because it created a new field of research on the boundary between chemistry and condensed matter physics. Eventhough the last two decade have witnessed great expansion of photoacoustic and photothermal techniques for the nondestructive and nonintrusive characterisation of thermal, optical and structural properties of different materials, work related to conducting polymers is limited. Recently, the photothermal technique has been used for the measurement of thermal parameters of polyaniline and doped polyaniline [190].

1.12. Photoacoustics and liquid crystals

In recent times considerable efforts have been made on the evaluation of thermal parameters of liquid crystals in all its phases, as the performance of the devices based on these materials depends greatly on the thermophysical properties of materials. Measurement on the static thermophysical quantities is carried out using the steady state adiabatic or ac calorimetric techniques [191]. In a limited number of cases, the low resolution steady gradient or transient techniques are employed for the evaluation of thermophysical properties [192]. However, the discovery of PA effect and related photothermal techniques have revolutionalised the scenario of thermal characterization of liquid crystals. Photoacoustic and photothermal techniques have proven to be capable of high-resolution measurement of the temperature dependence

of several static and dynamic parameters of liquid crystals, especially across the region of phase transitions [193-197]. An important advantage of this technique is that it allow simultaneous determination of the heat capacity and thermal conductivity of very small liquid crystal samples, given a properly chosen measuring configuration. The early reports on the application of PA effect for the characterisation of liquid crystals is mainly focused on the phase transition studies. The microphone version of PA technique is used to investigate both first order and second order phase transitions in 8CB liquid crystal [198-199]. In 1989, Jan Thoen and his co-workers described a completely automated personal-computer controlled photoacoustic set up for the thermal characterisation of small liquid crystal samples [194].

A pulsed PA technique is employed for the investigation of thermal and optical properties, light absorption and light scattering properties of liquid crystals by using the excitation/detection configuration [200]. Results of the investigations show that light scattering can strongly influence the pulsed PA response signal through the light absorption profile, especially at phase transition, subjected to small changes in thermal properties, such as the nematic/isotropic phase transitions [201]. However, the minimal volume open cell photoacoustic technique is explored new applicability of PA technique for the thermal characterisation of liquid crystals [202]. Recent reports point to the use of the OPC technique for measuring the thermal effusivity of transparent liquid crystals as well as optically absorbing liquid crystals with great effecitveness [203, 204].

1.13. Motivation of the present work

In the present modern world, where photonics replaces electronics, there are countless devices fabricated using semiconductors. Any further progress in this domain demands a better understanding of the fundamental properties of materials used in the microelectronic and optoelectronic industry. Both direct and indirect bandgap semiconductors find wide applicability in these areas especially for the

fabrication of semiconductor lasers, detectors, LEDs etc. The electrical and electrooptical properties of devices based on these materials depend greatly on the thermal and transport properties of carriers. Recent measurements on heat transport in semiconductors show that doping can affect heat transport in semiconductors. In this context, a systematic study of the influence of doping on thermal diffusivity value of compound semiconductors using the nondestructive and noncontact PTD technique has great importance. As the plane of cleaveage has extreme importance in the growth of heterostructures, a study of influence of the plane of cleavage on the propagation of phonons bear great practical applications. The point-by-point scanning made use of in the PTD technique can offer some additional information about these effects on heat transport and hence thermal diffusivity value. Layered structures are reported to exhibit different thermal properties as compared to bulk sample [205]. A detailed investigation of the propagation of phonons in the in plane and cross plane directions and hence the evaluation of thermal diffusivity value along these directions have been attempted here [206]. Thus the PTD technique allows us to measure the thermal anisotropy in the effective thermal parameters of layered structures.

It is well established that the PA technique is an effective tool for the evaluation of thermal and transport properties of semiconductors [165-175]. However, no systematic studies have been reported on the influence of doping on these parameters. As the doping can engineer the optical and thermal properties of semiconductors, detailed investigations of the optical and thermal properties of intrinsic as well as doped semiconductors have wide practical applications. This also gives a better insight into the physical processes occurring in semiconductors. In the present work, we used the phase of PA signal obtained under heat transmission configuration to evaluate the thermal and transport properties viz., thermal diffusivity, diffusion coefficient, surface recombination velocity and nonradiative recombination time of both direct and indirect band gap semiconductors.

Thermal and transport properties of polycrystalline dielectric materials are directly influenced by its microstructure. In dielectric materials, phonon propagation

determines the transport of thermal energy. In recent years, porous materials have attracted much attention due to its enhanced properties as compared to bulk sample. Pores in the dielectric lattice can act as effective scattering centers for phonons. It is reported that the sintering temperature can affect the porosity of the ceramic specimen. Incorporation of foreign atoms also affects the heat transport in ceramics. In this context, a systematic study on the heat transport and hence the thermal diffusivity and the study of influence of sintering temperature as well as incorporation of foreign atoms on the thermal diffusivity value of ceramic alumina will provide a better understanding of heat transport in porous materials.

Conducing polymers are considered to be the materials of the present century due to its tunable electrical and optical properties. The utility of conducting polymers in wide variety of applications depends on the unique combination of properties, not observed much in other class of materials. This fourth generation polymeric materials can exhibit semiconducting properties and even metallic properties depending on the ease of charge transport. The doped conjugated conducting polymers are good conductors for two reasons. Firstly, doping introduces carriers into their electronic structure. Secondly, the attraction of an electron in one repeat unit to the nuclei in the neighboring units leads to carrier delocalisation along the polymer chain and to charge carrier mobility, which is extended into three dimensions through interchain electron transfer. As the composites can tune the dynamical thermal properties of the materials, the present evaluation of thermal diffusivity of Camphor Sulphonic Acid doped polyaniline and its composites with Cobalt Phthalocyanine has great practical applications.

Eventhough, the applicability of PA technique in liquid crystals are well established, only in recent years, the open cell photoacoustic technique is employed for the measurement of thermal diffusivity and thermal effusivity [203-204]. The versatility of PA technique is established by measuring the thermal effusivity of liquid crystals and polymers. In the present thesis focus is made on the dependence of different thermal properties such as thermal diffusivity, thermal effusivity, thermal

conductivity and heat capacity on the composition of the reactants used for the synthesis of liquid crystal mixtures.

1.14. Conclusion

In conclusion, this opening chapter gives an account of the various photothermal signal generation and the detection schemes with special emphasis on photothermal deflection technique and photoacoustic technique. A review on the applicability of these techniques, namely PA and PTD technique, on the class of materials under investigation is also presented. The motivation of the work presented in this thesis is also presented.

1.15. References

1. P. Sathy, Studies on two photon absorption in certain dyes using photoacoustic and fluroscence technique (Ph.D Thesis, Cochin University of Science and Technology) 1994.

2. Geetha. K . Varier, Investigations on nonlinear and radiative properties of certain photonic materials (Ph.D Thesis, Cochin University of Science and Technology), 1998.

3. K. P. Unnikrishnan, Z scan and degenerate four wave mixing studies in certain photonic materials (Ph.D Thesis, Cochin University of Science and Technology), 2003.

4. Riju C Issac, Evolution and dynamics of plasma generated from solid targets by strong laser field (Ph.D Thesis, Cochin University of Science and Technology), 1998.

5. S. S. Harilal, Optical emission diagonostics of laser produced plasma from carbon and $YBa_2Cu_3O_7$ (Ph.D Thesis, Cochin University of Science and Technology), 1998.

6. Achamma Kurian, Characterisation of photonic materials using thermal lens technique (Ph.D Thesis, Cochin University of Science and Technology), 2002.

7. J. D. Winefordner, S. G. Schulman and T. C. O'Haver, Luminescence spectroscopy in analytical chemistry, (Wiley Interscience, New York), 1972.

8. G. G. Guilbault, Practical fluorescence: theory, methods and technique, (Marcel Dekker, New York) 1973.

9. E. L. Wehry, Modern fluorescence spectroscopy, Vols. I-II (Plenum, New York) 1976.

10. P. Hess (Edit.), Photoacoustic, photothermal and photochemical processes in Gases,(Springer-Verlag, Berlin) 1989.

11. P. Hess and J. Pelzl (Eds.), Photoacoustic and photothermal phenomena, (Springer-Verlag,Berlin) 1988.

12. S. E. Bialkoswski, Photothermal Spectroscopy Method Chemical Analysis (Wiley New York) 1996.

13. G. Chen Phys. Rev. B 57, 14958 (1998)

14. E. Luscher, P. Korpiun, H. Coufal and R. Tilgner, Photoacoustic effect: principles and applications, (Friedr.Vieweg & Sohn, Braunschweig) 1984.

15. A. Rosencwaig, Photoacoustics and photoacoustic spectroscopy, (John Wiley & Sons,New York) 1980.

16. J. A. Sell (Edit), Photothermal investigations of solids and fluids, (Academic Press, Boston) 1989.

17. P. Hess (Edit.) Photoacoustic and photothermal processes at surfaces and thin films, (Springer-Verlag, Berlin) 1989.

18. A. Mandelis (Edit.) Photoacoustic and thermal wave phenomena in semiconductors,(North Holland, New York) 1987.

19. Y. H. Pao (Edit.), Optoacoustic spectroscopy and detection, (Academic press, New York)1977.

20. D. Bicanic (Edit.), Proceedings of seventh international topical meeting on photoacousticand photothermal phenomena, 1991.

21. J. Badoz and D. Fournier (Eds.) Photoacoustic and photothermal spectroscopy, J.de Phys.,Colloque C6 (Les Editions de Physique, Les Ulis) 1983.

22. Yu. G. Gurevich, G. Gonzalez de la Cruz, G. Logvinov and M. N. Kasyanchuk, Semiconductors, 32(11), 1179 (1998).

23. A. Mandelis Physics Today, August, 29-34 (2000).

24. George Biranbaum and Bert A Auld (Ed.) Sensing for materials characterisation, processing and manufacturing, (The American Society for Nondestructive Testing, Inc., Columbus) 1998.

25. A. Mandelis (Edit.) Principles and Perspectives of Photothermal and Photoacoustic Phenomena (Elsevier, Oxford) 1992.

26. H. Vargas and L. C. M. Miranda, Phys. Rep. 161 (2), 43-101 (1988).

27. D. Fournier, A. C. Boccara, A. Skumanich and N. M. Amer, J. Appl. Phys. 59 (3), 787 (1986).

28. I. A. Vitkin, C. Christofields and A. Mandelis, Appl. Phys. Lett., 54, 2392 (1989).

29. A. Mandelis and M. M. Zver, J. Appl. Phys., 57, 4421 (1985).

30. H. Coufal, Appl. Phys. Lettt.,45, 516 (1984).

31. A. Mandelis, Nondestructive Evaluation (PTR Prentice Hall, Englewood Cliffs, New Jersy) 1994.

32. R. L. Thomas, Anal. Sciences, 17, April, (2001).

33. H. Shinoda, T. Nakajima, K. Ueno and N. Koshida, Nature, 400, August (1999).

34. H. Vargas and L. C. M. Miranda, Review of Scientific Instruments, 74 (1), 794, (2003).

35. P. Helander, J. Phtooacoust 1, 103 (1982).

36. Achamma kurian, K. P. Unnikrishnan, Sajan. D. George, Pramod Gopinath, V. P. N Nampoori and C. P. G. Vallabhan Spectrochimica Acta part A, 59, 487-491 (2003).

37. P. R. Bajra, Revista Phsyicae, I, 1 (2000).

38. J. C. Krapez, J. of Appl. Phys. 87 (9), (2000).

39. J. R. D. Pereira, A. M. Mansanares, E. C. de Silva, J. Palangana, m. L. Baesso, Molecular Crystals and Liquid Crystals, 332, 569 (1999).

40. F. Scudieri and M. Bertolotti, Proce. 10th Conference of Phtooacoustic and Photothermal Phenomena (AIP, New York) 1999.

41. A. Fukuyama, Y. Akashi, K. Yoshino. K. Madea and T. Ikari, Phys. Rev. B, 58 (19), 12868 (1998).

42. J. A. Balderas Lopez, A. Mandelis and J. A. Gracia, J. Appl. Phys., 92 (6), (2002).

43. W. Y. Zhou, S. S. Xie , S. F. Qian , G. Wang, L. X. Qian, D. S. Tang and Z. Q. Liu, J. of Phys. Chem. of Solids 61 (7) 1165 (2000).

44. B. X. Shi, C. W. Ong. and K. L. Tam, Journal of Material Science 34 (21) 5169 (1999).

45. Q. E. Khuen, W. Faubel, H. J. Ache Journal de Physique 4 (C7), 361 (1994).

46. M. Bertolotti, G. L. Liakhou, A. Ferrari, V. Ralchenko, A. A. Smolin E. Obraztsova, K. G. Korotoushenko, S. M. Pimenov and V. I. Konov J. of Appl Phys 75 (12) 7795 (1994).

47. Sajan D George, C. P. G. Vallabhan, M. Heck, P. Radhakrishnan, and V. P. N. Nampoori Journal of Nondestructive Testing and Evaluation Vol.18 ,2, 75, (2002).

48. R Castro-Rodriguez, M Zapata-Torres, V Rejon Moo, P Bartolo-Perez and J.L.Pena, J. Phys. D: Appl. Phys., 32, 1194 (1999).

49. N. F. Leite and L. C. M. Miranda, Rev. Sci. Instru. 63, 4398 (1992).

50. P. Charpentier, F. Lepoutre and L. Bertrand, J. Appl. Phys., 53, 608 (1982).

51. X. Quelin, B. Perrin, G. Louis and P. Peretti, Phys. Rev. B, 48, 3677 (1993).

52. J A Balderas-Lopez and A. Mandelis, J. Appl Phys. 88 (11) 6815 (2000).

53. B. C Li, R. Gupta, J. Appl Phys 89 (2) 859 (2001).

54. M. Bertolotti, A Falabella, R Li Voti, S Paoloni, C. Sibilia, G. L. Liakhou, High Temperatures – High Pressures 31 (2), 235 (1999).

55. Sajan D George, P. Radhakrishnan, V. P. N. Nampoori and C. P. G. Vallabhan, J. of Phys. D: Appl. Phys. 36 (8), 990 (2003).

56. Z. Bozoki, J. Sneider A. Mikols, Acoustica 82 (1) 118 (1996).

57. Achamma kurian, K. P. Unnikrishnan, Sajan D George, Pramod Gopinath, V. P. N Nampoori and C. P. G. Vallabhan Spectrochimica Acta part A, 59, 487-491 (2003).

58. Ristovski Z D and M. D. Dramicanin, Appl. Opt. 36 (3) 648 (1997).

59. A. Fukuyama, T. Ikari, K. Miyazaki, K. Maeda and K. Futagami, Jpn. J. Appl. Phys. Suppl. 31, 20 (1992).

60. A. Fukuyama, T. Ikari, K. Maeda and K. Futagami, Jpn. J. Appl. Phys. Part 1, 32, 2567 (1993).

61. S. E. Bialkowski Photothermal spectroscopy Methods for Chemical Analysis (John Wiley and Sons, New York) 1996.

62. C. W. Garland Thermochemica Acta, 88, 127 (1985).

63. I. Hatta, Y. Sasuga, R. Kato and A. Maesono, Rev. Sci. Instrum. 56, 1643 (1985).

64. I. Hatta Pure and Applied Chem., 64, 79 (1992).

65. R. Geer, T. Stobe, T. Pitchford and C. C. Huang, Rev. Sci. Instrum., 62, 415 (1991).

66. Christofides, A. Mandelis, A. Engel, M. Bisson and G. Harling, Can. J. Phys. 69, 317 (1991).

67. A. Mandelis, J. Vanniasinkam, S. Budhudhu, A. Orthonos and Kokta M, Phys. Rev. B, 48, 6808 (1993).

68. J. Shen and A. Mandelis, Rev. Sci. Instrum., 66, 4999 (1995).

69. Jacob Philip, Ravindran Rajesh and Preethy C Menon, Anal. Sci.,17, April (2001).

70. D. Dadarlat, M. Chirtoc, C. Nematu, R. M. Ca^ndea, and D. Bicanic, Phys.Status Solidi (a), 23, 121 (1990).

71. D. Bicanic, M. Chirtoc, V. Tosa and P. Torfs, Ber Bunsenges, Phys. Chem. 95, 766 (1991).

72. J. R. D. Pereira, E. C. da Silva, A. M. Manasanares, and L. C. M. Miranda, Anal. Sci.,17, April S 172 (2001).

73. S. Pittois, M. Chirtoc, C. Glorieux, Van den Brill and J. Thoen, Anal. Sci, 17, April S 110 (2001).

74. P. E. Nordal and S. O. Kanstad, Pysica Scripta 20, 59 (1979).

75. S. O. Kanstad and P. E. Nordal, Can. Phys. 64, 1155 (1986).

76. P. E. Nordal and S. O. Kanstad, Appl. Phys. Lett., 38, 486 (1981).

77. J. Stone, Appl. Opt., 12, 1828 (1973).

78. A. Hordvik, Appl Opt., 16, 2827 (1977).

79. Y. Othsuka and K. Itoh., Appl. Opt., 18, 219 (1979).

80. S. Ameri, E. A. Ash, V. Neuman and C. R. Petts, Electron. Lett., 17, 357 (1981).

81. L. C. M. Miranda, Appl. Opt., 22, 2882 (1983).

82. M. A. Olmstead, N. M. Amer, S. Kohn, D. Fournier and A. C. Boccara, Appl. Phys. A., 32, 141 (1983).

83. Bindhu.C.V, Studies on laser induced photothermal phenomena in selected organiccompounds and fullerenes, (Ph.D. thesis, Cochin University of Science and Technology) 1998.

84. J. P. Gordon, R. C. C. Leite, R. S. Moore, S. P. S. Porto and j. R. Whinery, J. Appl. Phys., 36, 3 (1965).

85. M. L. Baesso, J. Shen, and R. D. Snook, Chem. Phys. Lett. 197,255 (1992).

86. M. L. Baesso, A. C. Bento, A. A. Andrade, T. Catunda, E. Pecoraro, L. A. O. Nunes, J. A. Sampaio, and S. Gama, Phys. Rev. B 57, 10545 (1998).

87. S. M. Lima, T. Catunda, R. Lebullenger, A. C. Hernandes, M. L. Baesso, A. C. Bento, and L. C. M. Miranda, Phys. Rev. B 60, 15173 (1999).

88. J. H. Rohling, A. M. F. Caldeira, J. R. D. Pereira, A. F. Rubira, A. N. Medina, A. C. Bento, M. L. Baesso, and L. C. M. Miranda, J. Appl. Phys. 89, 2220 (2001).

89. A. C. Boccara, D. Fournier, and J. Baldoz, Appl. Phys. Lett. 36, 130 (1980).

90. J. C. Murphy and L. C. Aamodt, J. Appl. Phys. 51, 4580 (1980).

91. L. C. Aamodt and J. C. Murphy, J. Appl. Phys. 522, 4903 (1981).

92. W. B. Jackson, N. M. Amer, A. C. Boccara, and D. Fournier, Opt. Lett. 5, 377 (1980).

93. P. Charpentier, F. Lepoutre, and L. Bertrand, J. Appl. Phys. 53,608 (1982).

94. N. F. Leite and L. C. M. Miranda, Rev. Sci. Instrum. 63, 4398 (1992).

95. K. Song, H. Cha, J. Lee and I. A. Veselovskii, Appl Phys. B, 61, 547 –552 (1995).

96. K. Yoshino, A. Fukuyama, H. Yokoyama, K. Meada, P. J. Fones, A. Yamada, S. Niki and T. Ikari, Thin solid films 33-334, 591 (1995).

97. A. C. Boccara, D. Fournier, and J. Badoz, Appl. Phys.Lett. 36, 130–132 (1980).

98. N. A. George, C. P. G. Vallabhan, V. P. N. Nampoori and P. Radhakrishnan, Appl. Opt. 41 (24), 5179 (2002).

99. A. C. Boccara, D. Fournier, W. B. Jackson, and N. M. Amer, Appl. Opt. 20, 4580 (1981).

100. A. Salazar, A. Sa´nchez-Lavega, and J. Ferna´ndez, J. Appl. Phys. 65, 4150 (1989).

101. A. Salazar, A. Sa´nchez-Lavega and J. Ferna´ndez, J. Appl. Phys. 74, 1539 (1993).

102. A. Salazar, M. Gateshki, G. Gutie´rez-Jua´rez, A. Sa´nchez-Lavega, and W. T. Ang,Anal. Sci. 17,S95 (2001).

103. D. Fournier, J. P. Roger, C. Boue, H. Stamm, and F. Lakestani, Anal. Sci. 17, S158 (2001).

104. W. B Jackson and N. M. Amer, Phys. Rev. B, 25, 5559 (1982).

105. G. Grillo and L. De Angelis, J. Non Crystalline Solids 114, 750 (1989).

106. Salazar.A and Lavega.A.S. Rev.Sci.Instrum. 65, 2896 (1994).

107. A. G. Bell, Am. J Sci., 20, 385 (1880).

108. A. G. Bell Philoss. Mag., 11, 510 (1881).

109. A. Rosencwaig, Science, 181, 657 (1973).

110. A Rosencwaig, Phys. Today, 29, 9, 23 (1975).

111. A. Rosencwaig and A. Gersho, J. Appl. Phys., 47, 64 (1975).

112. A. Rosencwaig, Anal Chem. 47 (6), 502 (1975).

113. A. Rosencwaig, Rev. Sci. Instrum. 48, 1133 (1977).

114. A. Rosencwaig, Opt. Commun., 7, 305 (1973).

115. A. Rosencwaig, Anal. Chem. 47, 592 (1975).

116. A. Rosencwaig, Advances in Electronics and Electron Physics, 46 (1978).

117. R. L . Thomas, Anal. Sci. 17, April s1, (2001) and the references therein.

118. Werner Faubel, Stefan Heissler, Ute Pyell and Natalia Ragozina, Rev. Sci. Instrum. 74 (1), 491 (2003).

119. J. B. Callis, J. Res. Natul. Bur. Stand. A. 80, 413 (1976).

120. A. Hordvik and H. Scholssberg, Appl. Opt. 16, 101 (1977).

121. A. Hordvik and H. Scholssberg, Appl. Opt. 16, 2919 (1977).

122. W. Lahmann, J. J. Ludewig and H. welling, Chem. Phys. Lett., 45, 177 (1977).

123. S. Oda, T. Sawada and K. Kamada, Anal. Chem., 50, 865 (1978).

124. M. M. Farrow, R. K. Burnham, M. Auzaneau, S. L. Olsen, N. Pudie and E. M. Eyring, Appl. Opt., 17, 1093 (1998).

125. S. Sankara Raman, V. P. N. Nampoori , C. P. G. Vallabhan, G. Ambada and S. Sugunan, Appl. Phys. Lett., 67, 2939 (1995).

126. V. A. Aablikov and V. B. Sandomirski, Phys. Stat. Solidi (a), 120, 471 (1983).

127. N. A. George, V. P. N. Nampoori, P. Radhakrishnan, C. P. G. Vallabhan, Opt. Eng. 41(1), 251 (2002).

128. L. F. Perondi, and L. C. M. Miranda, J. Appl. Phys., 62, 2955 (1987).

129. M. D. da Silva, I. N. Bandeira and L. C. M. Miranda, J. Phys. E 20, 1476 (1987)

130. Mool. C. Gupta, Handbook of Photonics (CRC Press, New York) 1997.

131. Chai Yeh, Applied Photonics (Academic Press, London) 1994.

132. Jasprit Singh, Semiconductor Optoelectronics, Physics and Technology (Mc-Graw Hill, Singapore) 1995.

133. Ben G Streetmann and Sanjay Banerjee, Solid State Electronic Devices, (Prentice Hall, India) 2001.

134. Charles M Wolfe, Nick Holonyak and Gregory E. Stillmann, Physical Properties of Semiconductors (Prentice – Hall, New York) 1989.

135. Sankara Raman. S, Investigation of thermal diffusivity of some selected materials using laser induced photoacoustic effect (Ph.D Thesis, Cochin University of Science and Technology) 1999.

136. Mel Schwartz, Hand book of Structural Ceramics(Mc. Graw Hill, New York) 1992.

137. Steve Elston and Roy Sambles, The Optics of Thermotropic Liquid Crystals (Taylor and Francis, U K) 1998.

138. Satyen Kumar (Ed.) Liquid Cystals – In the Nineties and Beyond (World Scientific, Singapore) 1995.

139. A. F. S. Penna, J. Shah, A. E. Digiovanni, A. Y. Chao and A. C. Gossard Appl. Phys. Lett. 47 (6) 591 (1985).

140. J. G. Mendozaalvarez, B. S. H. Royce, F. Sanchezsinencio, O. Zelayaangel, C. Menezes, R. Triboulet, Thin Solid Films, 102 (3), 259 (1983).

141. D. Dadarlat, M. Chirtoc, R. M. Candea, Phys. Stat. Solidi (a) 98 (1), 279 (1986).

142. H. Fujimori, Y. Asakura, K. Suzuki, S. Uchida, Jpn. J. Appl. Phys. I 18 (3), 277 (1987).

143. S. K. So, M. H. Chan and L. M. Leung, Appl. Phys. A – Materials Science and Processing 61 (2), 159 (1995).

144. B. C Li, Y. Z. Deng, J. Cheng, J. of Modern Optics 42 (5), 1093 (1995).

145. S. Hasegwa, T. Nishiwaki, H, Habuchi, S. Nitta and S. Nonomura, Fullerene Science and Technology 3)3), 313 (1995).

146. M. Fatallah, J. of Non-Cystalline Solids, 166, 909 (1993).

147. M. Bertolotti, V. Dorogon, G. Liakhou, R. L. Voti, S. Paoloni and C. Sibilia, Rev. Sci. Instrum. 68 (3) (1997).

148. A. S. Kumar, K. L. Narasimhan, R. Rajalekshmi, S. S. Chandavankar and B. M. Arora, App. Phys. Lett. 55 (24), 2512 (1989).

149. A. Asano, T. Ichimura, M. Ohsawa, H. Sakai and Y. Uchida, J. of Non. Crystalline Solids, 97 (8), 971 (1987).

150. W. A Mcghan and K. D. Cole, J. Appl. Phys. 72 (4), 1362 (1992).

151. C. Shieh, H, J. Mantz, C. Colvarad, K. Alavi, R. Engelmann, Z. Smith and S. Wagner, Superlattices and Microstructures 4 (4-5), 597 (1988).

152. C. Wetzel, V. Petrovakoch, M. Zachau, F. Koch and D. Grutzmacher, Superlattices and Microstructures 6 (1) 99 (1989).

153. Y. S. Yuang, Y. F. Chen, Y. Y. Lee and L. C. Liu, J. Appl. Phys. 76 (5), 3041 (1994).

154. Y. T. Dai, Y. T. Liu, R. M. Lin, M. C. H. Lio, Y. F. Chen, S. C. Lee and H. H. Lin Jpn.J. App. Phys. II 36 (6B), L811 (1997).

155. U. Zammit, F. Gasparrini, M. Marinelli, R. Pizzoferrato, F. Scudieri and S. Martellucci, Appl.Phys. A – Materials Science and Processing 52 (2) 112 (1991).

156. J. C. Cheng, and S. Y. Zhang J. Appl. Phys. 70(11) 7007 (1991).

157. S. E. Bialkowski, X. Y. Gu, P. E. Poston, and L. S. Powers, Appl. Spect. 46 (2), 1335 (1992).

158. G. Amato and F. Giorgis, J.Appl. Phys. 74 (6), 3956 (1993).

159. Y. F. Chen, Y. T. Dai, H. P. Chou, I. and M. Chang, Chinese Journal of Physics, 31 (6), 767 (1993).

160. O. Ambacher, W. Riegerm P. Ansmann, H. Angerer, T. D. Moutakas andd M. Stutuzmann, Solid State Communications, 97 (5), 365 (1996).

161. M. Bertolotti, A. Falabella, R. L. Voti, S. Paoloni, C. Sibila and G. L. Liakhou, Progress in Natural Science 6, S665 (1996).

162. J. W. Kim, Y. K. Part, Y. T. Kim and I. H. Choi, Journal of Korean Physical Society, 35, s1033 (1999).

163. O. Ambacher, D. Brunner and R. Dimitrov, Jpn. J. Appl. Phys –I 37 (3A) 745 (1998).

164. A. K. Sinha and S.C. Agarwal, Pholos. Mag.B 77 (4) 945 (1998).

165. A. Pinto Neto, H. Vargas, N. Leite and L. C. M. Miranda, Phys. Rev. B 40, 3924 (1989).

166. A. Pinto Neto, H. Vargas, N. Leite and L. C. M. Miranda, Phys. Rev. B, 41, 9971 (1990).

167. Sajan D George, Dilna. S, P. Radhakrishnan, C. P. G. Vallabhan and V. P. N. Nampoori ,Physica Status Solidi (a), 195 (2), 416-421 (2003).

168. Sajan D George, Dilna. S, R. Prasanth, P. Radhakrishnan, C. P. G. Vallabhan and V. P. N. Nampoori, Opt. Eng. ,42 (5), 1476 (2003)

169. M. D. Dramicanin, Z. D. Ristovski, P. M. Nikolic, D. G. Vasiljevic and D. M. Todorovic, Phys. Rev. B., 51 (20), 14226 (1995).

170. D. M. Todorovic, P. M.. Nikolic, M. D. Dramicanin, D. G. Vasiljevic and Z. D. Ristovski, J. Appl. Phys. 78(8), 5750 (1995).

171. D. M. Todorovic, P. M. Nikolic, D. G. Vasiljevic and M. D. Dramicanin, J. Appl. Phys. 76 (7), 4012 (1994).

172. P. M. Nikolic, D. M. Todorovic, A. I. Bojicic, K. T. Radulovic, D. Urosevic, J. Elzar, V. Balgojevic, P. Mihajlovic and M. Miletic, J. Phys. Condens. Matter. 8, 5673 (1996).

173. P. M. Nikolic, D. M. Todorovic, D. G. Vasiljevic, P. Mihajlovic, Z. D. Rsitovski, J. Elzar, V. Blagojevic and M. D. Dramicanin, J. Microelcton., 27, 459 (1996).

174. I. Delgadillo, M. Vargas, A. Cruz-Orea, J. J. Alvarado-Gil, R. Baquero, F. Sanchez Sinencio and H. Vargas, Appl. Phys. B, 64, 97 (1997).

175. D. M. Todorovic and P. M. Nikolic, Opt. Eng. 36 (2), 432- 445 (1997).

176. J. B. Alavrado, M. Vargas, J. J. Alavarado-Gil, I. Delgadillo, A. Cruz-Orea, H. Vargas, M. Tufino Velazquez, M. L. Albor-Aguilera and M. A. Gonzalez-Trujillo, J. Appl. Phys. 83 (7), 3807 (1998).

177. E. Marin, I. Riech, P. Diaz, J. J. Alvarado-Gil, R. Baquero, J. G. Mendoza-Alvarez, H. Vargas, A. Cruz-Orea and M. Vargas, J. Appl. Phys. 83 (5), 2604 (1998).

178. Qing Shen and Taro Toyoda, Jpn. J. Appl. Phys., 39, 511 (2000).

179. Qing Shen and Taro Toyoda, Jpn. J. Appl. Phys., 39, 3164 (2000).

180. J. B. Alvarado, M. Vargas Luna, O. Solorza Feria, R. Mondrogon and N. Alonso Vante, J. Appl. Phys. 88 (6). 3771 (2000).

181. E. Marin, J. L. Pichardo, A. Cruz-Orea, P. Diaz, G. Torres-Delgado, I. Delgadillo, J. J. Alvarado Gil, J. G. Menoza Alvarez and H. Vargas, J. Phys.D. Appl. Phys. 29, 981 (1996).

182. Taro Toyoda and Kazuki Shinoyama, Jpn. J. Appl Phys. 36 (5B), 3300 (1997).

183. Qing Shen, Y. Kato and T. Toyoda, Jpn. J. Appl. Phys. 36 (5B), 3297 (1997).

184. M. Hangyo, S. Nakashima, Y, Oohara and S. Kimura, J. Appl. Phys. 63 (2), 295 (1987).

185. R. Castaneda-Guzman, M. Villagaran-Muniz, J. M. Sanger-Blesa and S. J. Perez-Ruiz, App. Phys. Lett. 77 (19), 3087, (2000).

186. S. A. Tomas, R. E. Sammiguel, A Cruz-Orea, M. Gomas da Silve, M. S. Sthel, H. Vargas and L. C. M. Miranda, Meas. Sci. Technol. 9, 803 (1998).

187. A. Sanchez-Lavega, A. Salzar, A. Ocariz, L. Pottier, E. Gomez, L. Mn. Villar and E. Macho, Appl. Phys. A, 65, 15 (1997).

188. E. R. Holland, S. J. Pomfret, P. N. Adams and A. P. Monkman, J. Phys. Condes. Matter, 8, 1991 (1996).

189. Alan. J Hegger, Current Applied Physics, I, 247-267 (2001).

190. V. Pilla, D. T. Balogh, R. M. Faria, and T. Catunda, Rev. Sci. Instrum. 74 91), 866 (2003).

191. J. Thoen and C. Glorieux, Thermochemica acta, 304/305, 137 (1997).

192. T. Akhane, M. Kondok, K. Hashimoto and N. Nagakawa, Jpn. J. Appl. Phys. 26, L 100 (1987).

193. M. Marinelli, U. Zammit, F. Scudieri and S. Martelluci, Nuovo Cimento, 9D, 855 (1987).

194. C. Glorieux, E. Schoubs, ang J. Thoen, Mater. Sci. Eng., A122, 87 (1989).

195. J. Thoen, C. Glorieux, E. Schoubs and W. Lauriks, Mol. Cryst. Liq. Cryst., 191, 29 (1990).

196. U. Zammit, M. Marinelli, R. Pizzoferrato, F. Scudieri and S. Martellucci, Phys. Rev. A, 41, 1153 (1990).

197. J. Thoen, E. Schoubs, V. Fagard in O. Leroy and M.A. Breazeale (Eds.), Physical Acoustics: Fundamentals and Applications, (Plenum Press, New York), 1992.

198. M. Marinelli, U. Zammit, F. Scudieri and S. Martellucci, High Temperature – High Pressures, 18, 1 (1986).

199. F. Scudieri, M. Marinelli, U. Zammit and S. Martellucci, J. Phys. D: Appl. Phys., 20, 1045 (1987).

200. G. Pucceti and R. M. Leblanc, J. Chem. Phys., 108 (17), 7258 (1998).

201. J. Thoen, Intl. J. Mod. Phys. B, 9 (18 & 19), 2157 (1995).

202. N.A. George, C.P.G. Vallabhan, V.P.N. Nampoori, A.K.George and P. Radhakrishnan, Appl. Phys. B 73, 145 (2001).

203. N.A. George, Smart Mater. Struct. 11, 561 (2002).

204. N.A. George, C.P.G. Vallabhan, V.P.N. Nampoori, A.K.George and P. Radhakrishnan, Opt. Eng., 40(7) 1343, (2001).

205. Sajan D George, P. Radhakrishnan, V. P. N. Nampoori and C. P. G. Vallabhan, Appl. Phys. B: Lasers and Optics (In print)

206. Sajan D George, P. Radhakrishnan, V. P. N. Nampoori and C. P. G. Vallabhan, Phys. Rev. B, 68 (16), 165319 (2003)

Chapter 2

Photothermal deflection studies on heat transport in InP and GaAs layered structures

Abstract

In this chapter, the necessary theoretical background for the evaluation of thermal diffusivity using transverse photothermal deflection technique is described. The thermal diffusivity values are evaluated from the slope of PTD spectrum with pump-probe offset. Evaluation of thermal diffusivity of intrinsic InP and InP doped with Sn, S and Fe has been carried out using transverse photothermal deflection technique. The in plane and cross plane measurement of thermal diffusivity of double epitaxial layers of n-type GaAs doped with various concentration of Si and Be doped p-type GaAs layers grown GaAs substrate have been studied. The results are interpreted in terms of phonon assisted heat transfer mechanism and the various scattering processes which are operative during the propagation of phonons.

2.1. Introduction

In recent years, thermal wave physics has emerged as an effective research and analytical tool in all branches of science and technology covering diverse fields such as medicine, agriculture, photonics etc. [1]. Invention of Photoacoustic (PA) effect and the subsequent emergence of various photothermal methods have revolutionized the applicability of thermal waves for the detection and evaluation of material properties and processes [2]. All the photothermal methods are based on the detection of thermal waves generated in the specimen after illumination with a chopped or pulsed optical radiation. In 1979, Boccara et.al proposed and demonstrated the usefulness of a new photothermal technique, namely photothermal deflection technique (PTD) for the evaluation of thermal and optical properties of materials [3]. These authors explained both theoretically and experimentally, the effectiveness of transverse PTD (mirage effect) in monitoring the temperature field gradient close to a sample surface or within the bulk of the specimen. Thereafter, many theoretical and experimental developments on the applicability of this method have been reported [4-7]. The PTD technique is essentially based on the detection of refractive index gradient associated with the temperature gradient generated in the sample following an optical excitation. The physical mechanism behind the PTD signal generation and the various configurations of PTD technique are already explained in chapter I. The thermal waves generated as a results of absorption of chopped pump beam heats up the sample periodically. The temperature gradient thus generated produces refractive index gradient in both sample as well as in the coupling medium. A low power laser beam (probe beam) propagating through this varying refractive index gets deflected from its normal path. The amount of deflection, which can be measured using a position sensitive quadrant detector, is determined by the thermophysical parameters of the material under investigation. An outline of the theoretical background of PTD technique is given in the following section of this chapter.
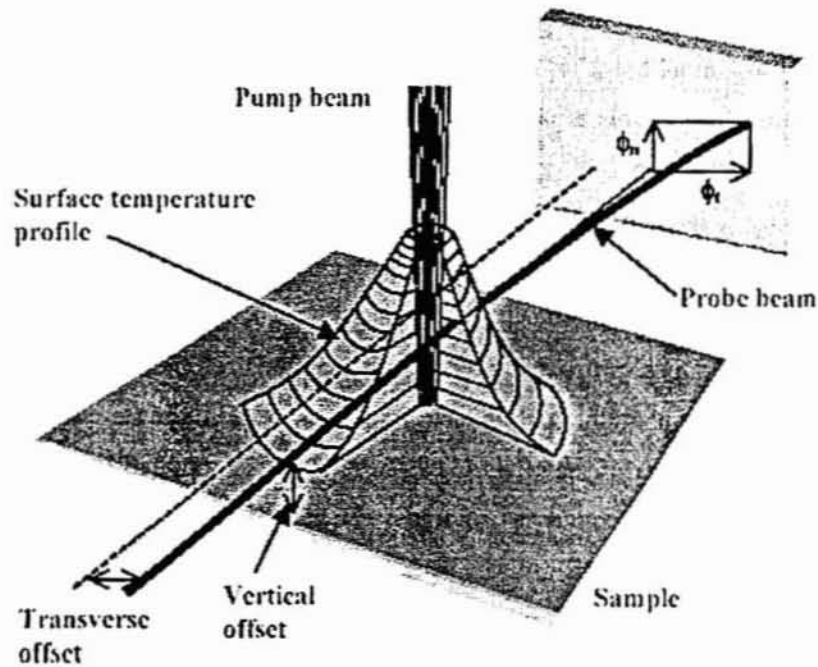
Figure 1. A schematic diagram of the passage of probe beam passing through
a refractive index profile and the resulting normal and transverse
components of PTD signal

2.2. Theoretical background: Mirage Effect

Figure 1 depicts the diagrammatic representation of PTD technique. The beam parameters of a guassian beam propagating through an inhomogeneous medium can be deduced from the analysis given by Casperson [8]. The propagation of light beam through a spatially varying index of refraction is governed by the equation [9]

$$\frac{d}{ds}\left(n_0 \frac{dr_0}{ds}\right) = \nabla_\perp n(r,t) \tag{1}$$

where r_0 is the perpendicular displacement of the probe beam from its original direction, n_0 is the uniform index of refraction, and $\nabla_\perp n(r,t)$ is the gradient of index of refraction perpendicular to the ray path. The above relation can be integrated over ray path :

$$\frac{dr_0}{ds} = \frac{1}{n_0} \int_{path} \nabla_\perp n(r,t) ds \tag{2}$$

where s is the optical path length. Since the deviation is small, one can get the expression for the deflection $\theta(t)$ as

$$\frac{dr_0}{ds} = \theta(t) = \frac{1}{n_0} \frac{\partial n}{\partial T} \int_{path} \nabla_\perp T(r,t) ds \tag{3}$$

where $\nabla_\perp T(r,t)$ is the temperature gradient perpendicular to the ray path. The deflection $\theta(t)$ can be resolved into two components θ_n and θ_t, which are respectively, the deflections normal and parallel to the sample surface and are given by

$$\theta_n = \frac{1}{n_0} \frac{dn}{dT} \int_{-\infty}^{+\infty} \frac{\partial T_f}{\partial z} dx \tag{4}$$

and
$$\theta_t = \frac{1}{n_0} \frac{dn}{dT} \int \sin\alpha \frac{\partial T_f}{\partial r} dx \tag{5}$$

In the one-dimensional heat flow model, which is usually employed in the photoacoustic effect, is found to be inadequate to evaluate the temperature field in the sample and in the surrounding fluid during a PTD experiment. In order to get a complete solution for the temperature field in the sample and in the coupling medium and three-dimensional analysis is needed. Consider an experimental configuration as shown in

figure 2. In this case, thermal conduction in both the solid as well as in the coupling fluid has to be taken into account which results in a complicated model when compared to photoacoustic effect.
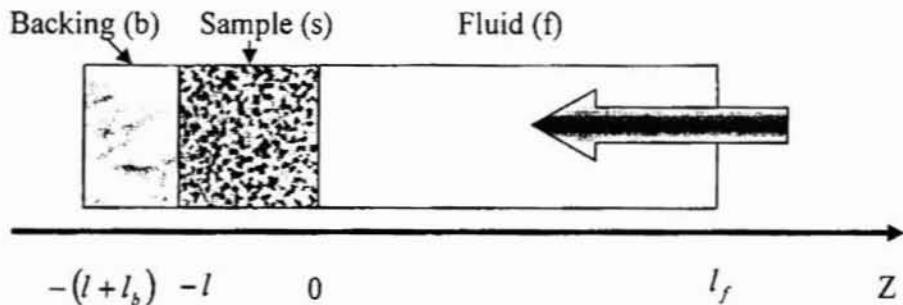
Figure 2. Schematic representation of the experimental geometry used in the 3-D model.

It may be assumed that the homogeneous sample is the only absorbing medium whereas the coupling fluid and backing material are transparent. It is also assumed that the sample extend infinitely in the radial direction, with the irradiated area usually being limited and small compared to the radial size of the specimen under investigation. The heat diffusion equations in the three regions are

$$\frac{\partial^2 T_f}{\partial r^2} + \frac{1}{r}\frac{\partial T_f}{\partial r} + \frac{\partial^2 T_f}{\partial z^2} = \frac{1}{D_f}\frac{\partial T_f}{\partial t} \qquad \text{for } 0 \le z \le l_f \quad (6)$$

$$\frac{\partial^2 T_s}{\partial r^2} + \frac{1}{r}\frac{\partial T_s}{\partial r} + \frac{\partial^2 T_s}{\partial z^2} = \frac{1}{D_s}\frac{\partial T_s}{\partial t} - A(r,t)e^{\alpha z}\left(1+e^{j\alpha t}\right) \quad \text{for } -l \le z \le 0 \quad (7)$$

44

$$\frac{\partial^2 T_b}{\partial z^2} + \frac{1}{r}\frac{\partial T_b}{\partial r} + \frac{\partial^2 T_b}{\partial z^2} = \frac{1}{D_b}\frac{\partial T_b}{\partial t} \qquad \text{for } -(l + l_b) \le z \le -l \qquad (8)$$

Here, the suffixes f, s and b stands for fluid, sample and backing material respectively. D is the thermal diffusivity and α is the optical absorption coefficient of the specimen at the incident wavelength.

After introducing appropriate boundary conditions and making use of Henkel transform, one can arrive at the expressions for the modulated temperature field in the three regions as

$$T_f(r,z,t) = \int_0^\infty T_s(\lambda)\exp(-\beta_f z)\exp(j\omega t)J_0(\lambda_r)\lambda d\lambda \qquad (9)$$

$$T_b(r,z,t) = \int_0^\infty W(\lambda)\exp(\beta_b(z+l) + j\omega t)J_0(\lambda_r)\lambda d\lambda \qquad (10)$$

$$T_s(r,z,t) = \int_0^\infty [U(\lambda)\exp(\beta_s z) + V(\lambda)\exp(\beta_s z) - E(\lambda)\exp(\alpha z)]$$

$$\times \exp(j\omega t)J_0(\lambda_r)\lambda d\lambda \qquad (11)$$

where

$$E(\lambda) = \frac{P\eta}{\pi k_s}\frac{\exp\left(-\frac{\lambda^2 a^2}{8}\right)}{\left[-\lambda^2 - j\left(\frac{\omega}{D_s}\right) - \alpha^2\right]} \qquad (12)$$

with $\quad a^2\exp\left(-\frac{\lambda^2 a^2}{8}\right) = \int_0^\infty \exp\left(-\frac{2r^2}{a^2}\right)J_0(r\lambda)r dr \qquad (13)$

45

$$\beta_i^2 = \lambda^2 + \frac{j\omega}{D_i} \qquad (14)$$

$$T_s(\lambda) = -E(\lambda) + U(\lambda) + V(\lambda) \qquad (15)$$

$$W(\lambda) = -E(\lambda)\exp(-\alpha l) + U(\lambda)\exp(-\beta s l) + V(\lambda)\exp(\beta_s l) \qquad (16)$$

$$U(\lambda) = [(1-g)(b-r)\exp(-\alpha l) + (g+r)(1+b)\exp(\beta_s l)]\frac{E(\lambda)}{H(\lambda)} \qquad (17)$$

$$V(\lambda) = [(1+g)(b-r)\exp(-\alpha l) + (g+r)(1-b)\exp(-\beta_s l)]\frac{E(\lambda)}{H(\lambda)} \qquad (18)$$

with $\quad g = \dfrac{\beta_f k_f}{\beta_s k_s}, \qquad b = \dfrac{\beta_b k_b}{\beta_s k_s} \quad$ and $\quad r = \dfrac{\alpha}{\beta_s} \qquad (19)$

$$H(\lambda) = (1+g)(1+b)\exp(\beta_s l) - (1-g)(1-b)\exp(-\beta_s l) \qquad (20)$$

In photothermal deflection technique, measurements are carried out using a probe beam propagating through a transparent fluid in contact with the sample surface. The temperature field along the probe beam path is a function of both the surface temperature and the distance between the probe beam and the sample surface.

The complex temperature of the sample surface can be obtained as

$$T_s(0,t) = \int E(\lambda)\left[\frac{-(1+b)(1-r)\exp(\beta_s l) + (1-b)(1+r)\exp(-\beta_s l) - 2(r-b)\exp(-\alpha l)}{(1+g)(1+b)\exp(\beta_s l) - (1-g)(1-b)\exp(-\beta_s l)}\right]$$

$$\times J_0(\lambda r)\lambda d\lambda \exp(j\omega t) \qquad (21)$$

In the above expression, terms in the bracket describes the thermal response of the three media namely, the sample, backing and the coupling fluid. If the sample under investigation is thermally thick, the surface temperature of the sample can be evaluated easily by replacing the expression in the bracket by

$$\frac{(r-1)}{(g+1)} \tag{22}$$

and for thermally thin sample, the term in the bracket becomes

$$\frac{(r-b)(1-\exp(-\alpha l))+\sigma_s l(rb-1)}{(b+g)} \tag{23}$$

Based on the expression (21), many researchers have carried out photothermal deflection measurements on thermal and optical properties of solids [10-13]. Thermal diffusivity is one of the most important thermophysical parameter that is studied extensively using this technique. Salzar et.al analysed the various experimental and theoretical conditions and arrived at certain expressions which describes a linear relationship of PTD signal phase with various parameters such as pump-probe offset, height of the pump beam above the sample surface etc [10]. For $a = b = z = 0$, where a, b and z are the pump-beam spot size, probe-beam spot size and the probe-beam height above the sample surface, there exists a linear relationship between the phase of the PTD signal and pump-probe offset. Slope of the plot connecting the phase of the PTD signal and the pump-probe offset is given by

$$m = \frac{1}{\mu_s} = \sqrt{\frac{\pi f}{\alpha_s}} \tag{24}$$

where α_s is the thermal diffusivity value of the sample under investigation. All the measurements presented on this chapter are based on the above expression. The importance and popularity of PTD technique lies in the fact that it can probe surfaces irrespective of the size of the sample [14]. Furthermore, the signal amplitude is proportional to absorbance, specimens of ultra low absorption can be studied using this technique.

2.3. Heat conduction in semiconductors

In general, the electrical conductivity of a material is determined by the movement of free charge carriers in the specimen, whereas, thermal conductivity is determined by the movement of both the carriers and phonons. Thus the thermal conductivity arising out of the temperature gradient existing within the specimen is determined by the contribution from electrons with electronic thermal conductivity $\left(k_e\right)$ and from phonons giving lattice thermal conductivity $\left(k_{ph}\right)$ The total thermal conductivity $\left(k\right)$ of any specimen thus must be expressed as

$$k = k_e + k_{ph} \qquad (25)$$

However, the relative contributions of these components differ from metal to dielectrics. In the case of metals, $k_e \gg k_{ph}$ whereas for dielectrics $k_{ph} \gg k_e$. In the case of semiconductors, electronic contribution to thermal conductivity depends strongly on the composition as well as on the temperature [15]. In addition to the heat transport mechanism described above, the photoexcited carriers also contributed to the transport of thermal energy in semiconductors. In a semiconductor which is excited by an optical energy greater than bandgap energy, the heat is generated mainly due to three processes viz., thermalisation, nonradiative bulk recombination and nonradiative surface recombination [16-17] Deexcitation of electrons from the excited level to the bottom of the conduction band results in the liberation of thermal energy to lattice and this process is known as thermalisation. This phonon assisted intraband transition is very fast and takes place in time scale of picoseconds. The nonradiative recombination of electrons and holes within the bulk and surface of the specimen also results in the generation of thermal energy. The interband transitions in semiconductors are called nonradiative bulk recombination, which take place within the bulk of the semiconductor specimen while the surface recombination, takes place at the surface of the specimen. The nonradiative

band-to-band transition recombination rate is essentially determined by the minority carrier concentration and the rate is proportional to photoexcited carrier concentration in semiconductors. The bulk recombination rate is mainly determined by the carrier concentration and the scattering processes occurring during the propagation of these carriers. Surfaces and interfaces of the semiconductors contain large number impurities to which they are exposed to during the growth of the material. In addition to this, surfaces and interfaces contain large number of dangling bonds due to the abrupt termination of the crystal. These impurities can act as recombination centers for photoexcited carriers. Thus the surface recombination rate depends greatly on the growth mechanism of the semiconductors. However, in modulated photothermal experiments the thermalisation component dominates in the photothermal signal generation, especially in the low chopping frequency range. The effect of bulk and surface recombination processes are visible only at much higher frequencies.

2.4. Importance of thermal diffusivity

As is well known, there are three common mechanisms for transferring heat from one place to another. The first is radiation, in which heat is transferred by electromagnetic waves. The second is convection, where heat is transferred directly by the flow of a hot (or cold) fluid thermal carrier. The third is conduction, in which heat, in the form of random microscopic motions of atoms and molecules in a gas, or by electrons and phonons in a solid (carriers), is transferred from one location to another in a material by the random movement and collision between these carriers [18]. The rate of heat conduction in a solid material is determined by several material parameters as well as by the temperature difference in the material. The heat flow inhomogeneous solid is governed by the Fourier's law [19-21]

$$\frac{\partial Q}{\partial t} = -kA\frac{\partial T}{\partial x} \tag{26}$$

The above equation (Fourier equation) implies that the quantity of heat dQ conducted in the x direction of a uniform solid material in a time interval dt is equal to the product of conducting area A normal to the flow path, the thermal conductivity k and the temperature gradient $\frac{dT}{dx}$ along this path.

The thermal diffusivity comes into picture during the derivation of a transient temperature field in a conducting material from Fourier equation. For a homogenous material with no internal heat sources, the thermal diffusion is given by Carslaw and Jaeger as

$$\nabla^2 T(r,t) = \frac{1}{\alpha}\frac{\partial T(r,t)}{\partial t} \tag{27}$$

where α is the thermal diffusivity of the material which conducts heat. Thermal diffusivity is an important thermophysical parameter, which measures the ability of the specimen of the material to absorb heat on a transient basis, and hence it is extremely important in time dependent heat diffusion conditions. Thermal diffusivity essentially determines the temperature distribution in systems where a heat flow occurs. Thermal diffusivity value is usually expressed in cm^2 s^{-1}. The inverse of thermal diffusivity is a measure of the time required to heat a conducting material to a specific temperature. For specimens having same thickness, heating is determined by the thermal diffusivity value. Obviously, thermal diffusivity is an important parameter from device fabrication point of view. Very recently, Fournier etal correlated thermal diffusivity with hardness of the specimen, which has tremendous impact on the industry.

2.5. III-V Semiconductors and Layered Structures

The majority of research activities related to optoelectronics are mainly focused on the characterisation and application of compound semiconductors and other photonic materials. Compound semiconductors are considered to be the most suitable material for the fabrication of semiconductor laser, LEDs, solar cells, detectors etc due to certain characteristics such as direct band, tunability in thermal, electronic and optical properties [22-24]. Eventhough most of the III-V semiconductors have zincblende structure, an interesting and useful feature of these materials is the ability to vary the mixture of elements on each of the two interpenetrating fcc sublattices of the zincblende structure. The ternary compounds such as AlGaAs and its alloys such as $Al_xGa_{1-x}As$ and other quaternary compounds can be made from these materials which are found to exhibit different electronic and optical properties [25]. The advancement in different epitaxial techniques such as Liquid Phase Epitaxy (LPE), Vapor Phase Epitaxy (VPE), Molecular Beam Epitaxy (MBE), Metal Organic Vapor Phase Epitaxy (MOVPE) etc have revolutionalised the growth and applications of these materials. Layered structures and heterostructures, which show many novel properties, are being fabricated using these techniques. In the present chapter, studies have been performed on compound semiconductor wafers, which are grown using LPE methods and layered GaAs structures grown using MBE method.

PART A

2.6 Photothermal deflection studies on intrinsic and doped InP.

2.6.1. Introduction

Thermal management in photonic devices is a major problem, which has attracted much attention in recent times, especially in the materials used for the fabrication of optoelectronic and thermoelectronic devices [26]. The III-V

semiconductors in general and InP in particular are prominent candidates which meet the requirements of photonics industry. Compound semiconductors have gained wide popularity in recent times due to their potential for higher speed of operation as compared to silicon semiconductors in electronics applications. Compound semiconductors also play a major role in the modern wireless communication systems and information technology. Optoelectronics technology has taken advantage of ternary and quartenary III-V semiconductors to generate the optical wavelengths and to device a variety of novel structures. These ternary and quartenary versions allow the bandgap tuning so that material can be tailored for a particular optical wavelength. In contrast to single component elemental semiconductors (for which the positioning of each atom on lattice site is not relevant), III-V semiconductors require good control of stoichiometry (i.e., the ration of two atomic species) during the crystal growth. However, the performance and reliability of devices based on these semiconductors depend greatly on their thermal parameters. InP is an important III-V semiconductor of technological importance in solid-state devices such as lasers, LEDs and solar cells. The subsequent sections given here focus on the evaluation of intrinsic InP as well as InP doped with Sn, S and Fe.

2.6.2. Experimental

A dual beam PTD technique has been employed here for the measurement of thermal diffusivity of samples under investigation. A schematic view of the experimental setup used for the present investigation is shown in figure 3. Optical radiation at 488 nm having a guassian profile with a diameter of 1.2mm, from argon ion laser (Liconix 5000) is used as the pump-beam. The pump-laser beam is mechanically chopped (Stanford Research Systems SR 540) and focused using a convex lens of focal length 20cm before it strickes on the samples. All the measurements are carried out at a laser power of 50 mW with a stability of ±0.5% and pump beam spot size at the sample

surface of 100 μm. The incident radiation is chopped at 15Hz so that $\omega\tau \ll 1$ where τ is the recombination time of photoexcited carriers. Under such experimental conditions, only pure thermal wave component dominates in the heat transport mechanism. All the specimens under investigation are opaque at the incident wavelength and the sample is placed at the bottom of a quartz cuvette having dimensions 10mm × 10mm × 40mm, containing CCl_4.
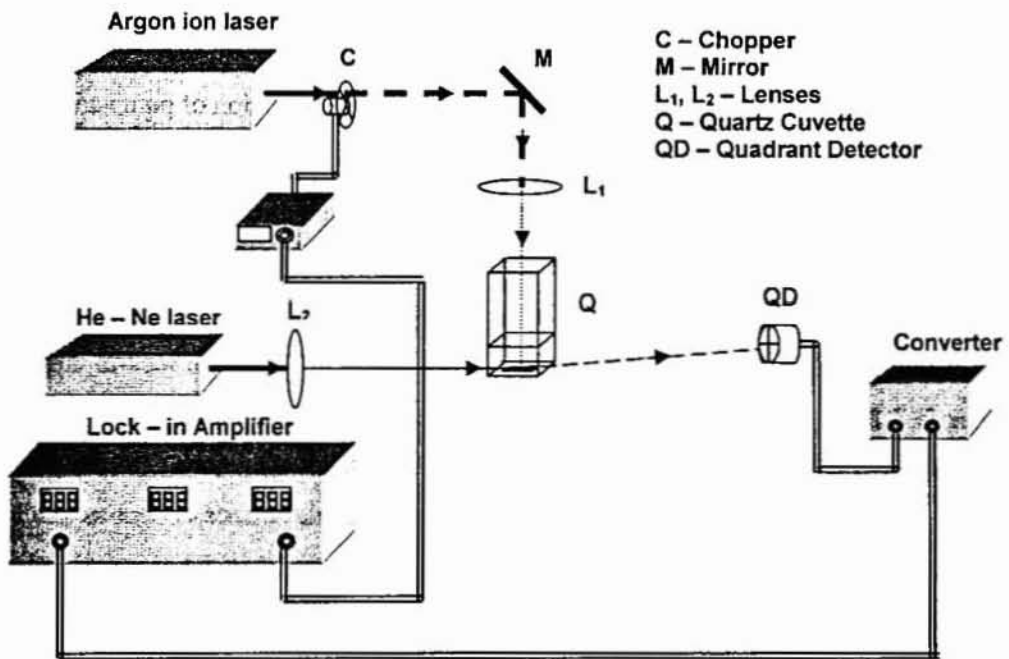

Figure 3. Schematical view of the dual beam photothermal deflection setup

The choice of CCl_4 as a coupling medium in most of the photothermal experiments is due to its low values of thermal conductivity, $k = 0.099 Wm^{-1}K^{-1}$, specific heat capacity, $C_p = 0.85 Jg^{-1}K^{-1}$, and thermal diffusivity, $\alpha = 7.31 \times 10^4 cm^2 s^{-1}$ [27-28]. Another important parameter, which favors CCl_4 as a coupling medium in photothermal studies is its high rate of change of refractive index with temperature, $\dfrac{dn}{dT} = 6.12 \times 10^4 cm^2 s^{-1}$. The probe laser beam used for the present studies is He-Ne laser (Uniphase) at 633 nm and having a power of 1mW. The probe laser beam has a guassian profile with a spot size of 700 μm and is focused to a spot size of 90 μm using a convex lens of radius 8cm at the interaction region of pump and probe. The probe beam is arranged such that it just skims along the sample surface, and it propagates along the y direction, which is orthogonal to the direction of propagation of pump beam (z axis). A position sensitive quadrant detector is used to measure the deflection of the probe beam. The output of the quadrant detector, is converted into electric signal using an I to V converter, and is fed to a dual phase lock-in amplifier (Stanford Research Systems SR 830). The entire experimental set up is laid out on a vibration-isolated table to protect the system from ambient vibrations. In the present arrangement, the distance between the probe and the sample surface is kept as small as possible so as to get a nondiffracted beam (from the sample edge) at the detector head.

The samples used for the present studies are intrinsic InP and InP doped with Sn, S and Fe. The intrinsic InP has a carrier concentration $10^{18} cm^{-3}$. InP doped with Sn and S have a doping concentration of $10^{18} cm^{-3}$ where as InP doped with Fe have a doping concentration of $10^{17} cm^{-3}$. Measurements are done on the doped samples cleaved along (111) plane as well as (100) plane and the intrinsic sample is cleaved along the (111) plane. All the samples have thickness $\sim 350 \mu m$ and they are grown by LPE method.

2.6.3. Results and Discussions

As explained earlier, various configurations of PTD technique are applicable for the thermal characterisation of solids. Among these, the skimming PTD technique is the simplest and the most popular approach for the thermal characterisation of materials. The unique advantage of taking the PTD signal as a function of pump-probe offset is that it allows point by point scanning over the sample surface. In order to achieve this experimental configuration, the probe beam, quadrant detector and the sample are firmly fixed at a particular position and the pump beam irradiation site is varied from one side of the probe-beam to the other side. Typical variations of the PTD signal phase as a function of pump-probe offset for intrinsic InP cleaved along (111) plane are shown in figure 4. Figure 4(a) represent the variation of PTD phase against pump-probe offset on the left side of the point of excitation where as figure 4 (b) represent the same on the right side of point of excitation. In the present study, only the lateral component of phase of PTD signal is taken into account as the semiconductor wafers have isotropic thermal properties along in-plane and the cross plane direction. The thermal diffusivity value of intrinsic InP is evaluated using the slope of these plots, the average value of which is measured as 0.438 ± 0.003 and it agrees well with the earlier reported thermal diffusivity value. Figures 5 to 10 shows the variation of phase of PTD signal as a function of pump-probe offset for the doped samples. In all these cases, figures labeled as (a) represent the variation of the PTD phase as a function of pump-probe offset on the left side of the point of excitation and figures labeled as (b) represent the variation on the right side of the pump beam.

Fig.4.a) Variation of PTD signal phase with pump-probe offset for intrinsic InP cleaved along (111) plane. Here probe is on the left side of the pump.

Fig. 4.b) Variation of PTD signal phase with pump-probe offset for intrinsic InP cleaved along (111) plane. Here probe is on the right side of the pump.

Fig. 5.a) Variation of PTD signal phase with pump-probe offset for InP doped with S cleaved along (111) plane. Here probe is on the left side of the pump.

Fig. 5.b) Variation of PTD signal phase with pump-probe offset for InP doped with S cleaved along (111) plane. Here probe is on the right side of the pump.
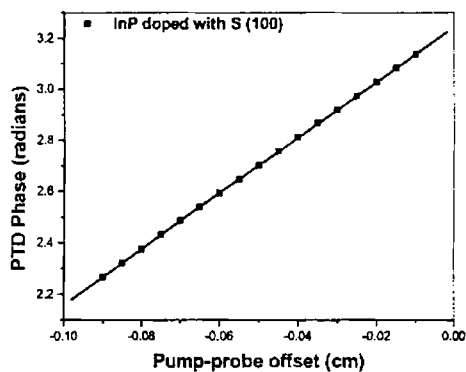
Fig. 6.a) Variation of PTD signal phase with pump-probe offset for InP doped with S cleaved along (100) plane. Here probe is on the left side of the pump.
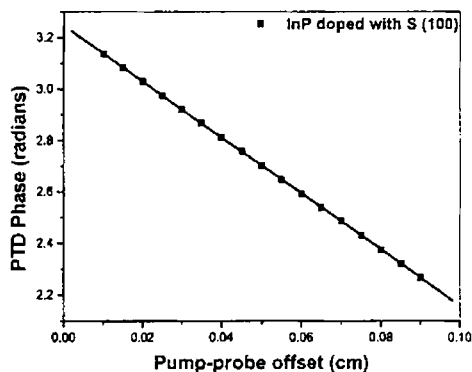
Fig. 6.b) Variation of PTD signal phase with pump-probe offset for InP doped with S cleaved along (100) plane. Here probe is on the right side of the pump.
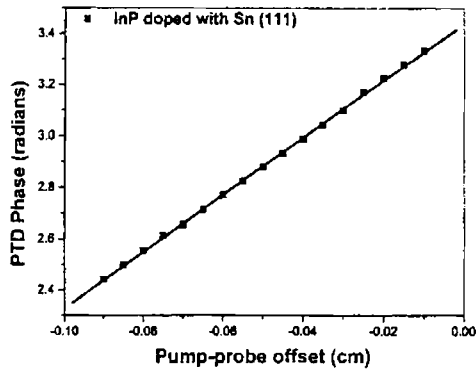
Fig. 7.a) Variation of PTD signal phase with pump-probe offset for InP doped with Sn cleaved along (111) plane. Here probe is on the left side of the pump.
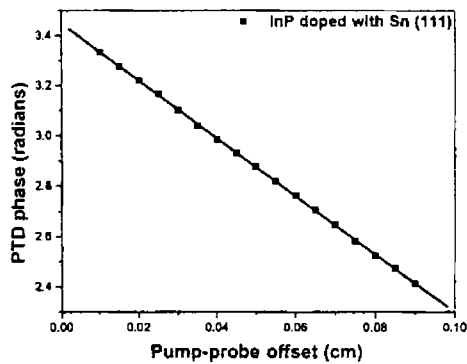
Fig. 7.b) Variation of PTD phase with pump-probe offset for InP doped with Sn cleaved along (111) plane. Here probe is on the right side of the pump.
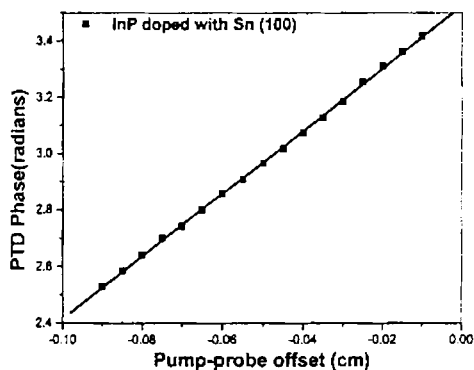
Fig. 8.a) Variation of PTD signal phase with pump-probe offset for InP doped with Sn cleaved along (100) plane. Here probe is on the left side of the pump.
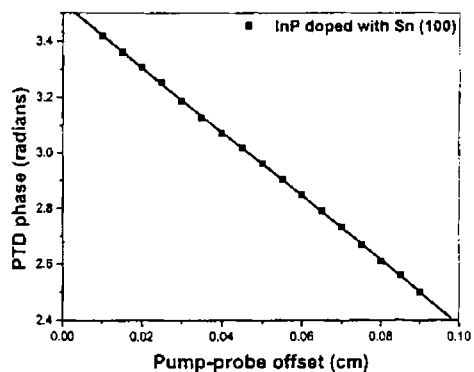
Fig. 8.b) Variation of PTD phase with pump probe offset for InP doped with Sn Sn cleaved along (100) plane. Here probe is on the right side of the pump.
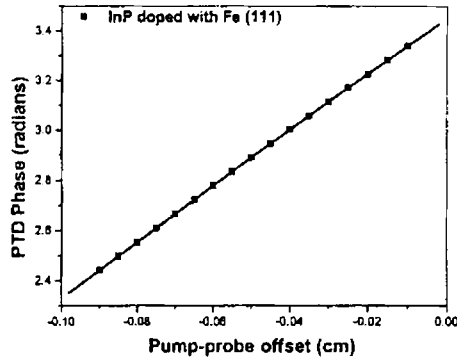
Fig. 9.a) Variation of PTD signal phase with pump-probe offset for InP doped with Fe cleaved along (111) plane. Here probe is on the left side of the pump.
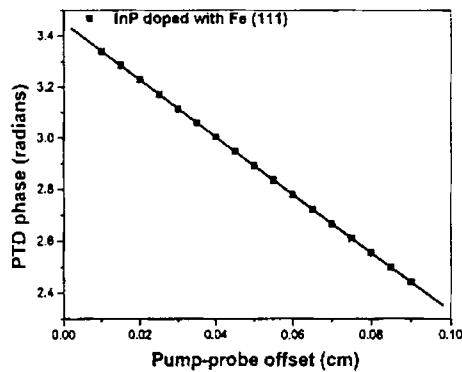
Fig. 9.b) Variation of PTD phase with pump-probe offset for InP doped with Fe cleaved along (111) plane. Here probe is on the right side of the pump.
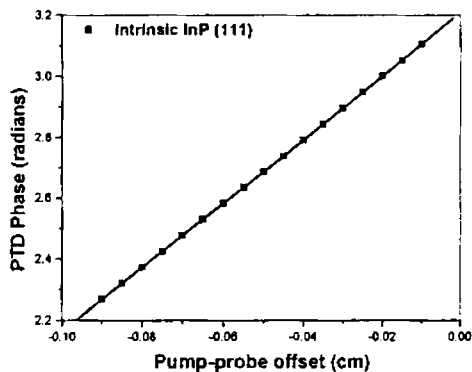
61
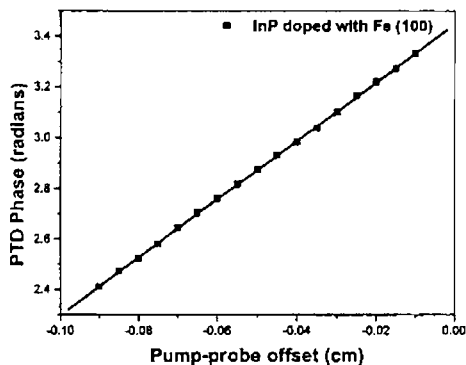
Fig. 10.a) Variation of PTD phase with pump-probe offset for InP doped with Fe cleaved along (100) plane. Here probe is on the left side of the pump.
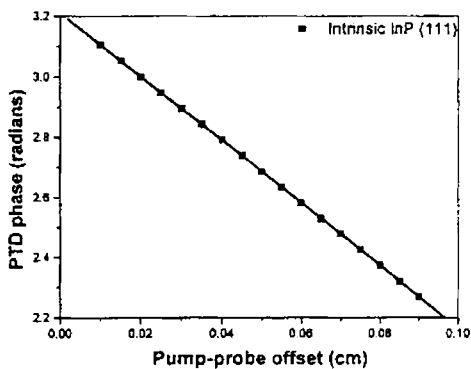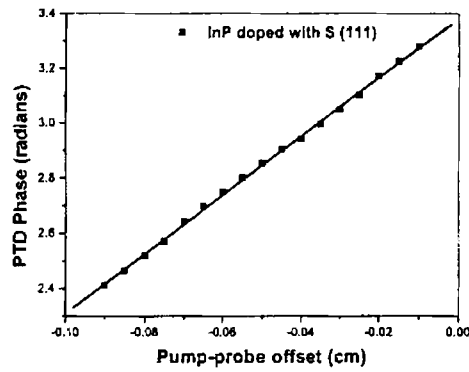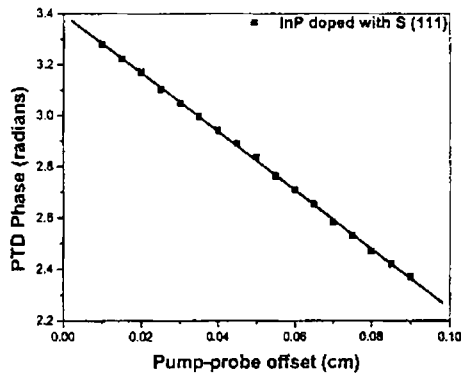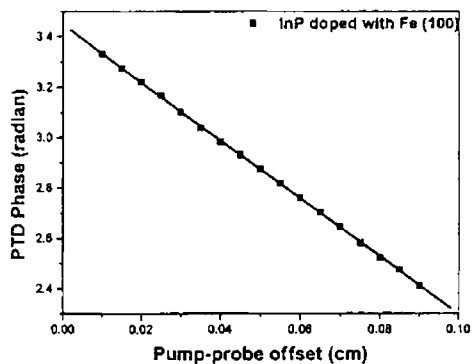

Fig. 10.b) Variation of PTD signal with pump-probe offset for InP doped with Fe cleaved along (100) plane. Here probe is on the right side of the pump

The thermal diffusivity values of all the specimens are evaluated using the same procedure. The measured thermal diffusivity values of intrinsic as well as doped samples are given in table I

Sample	Plane of cleavage	Doping concentration (cm^{-3})	Thermal diffusivity (cm^2s^{-1})
InP	111	-	0.438 ± 0.003
InP: S	111	10^{18}	0.403 ± 0.004
InP: S	100	10^{18}	0.394 ± 0.003
InP: Sn	111	10^{18}	0.389 ± 0.003
InP: Sn	100	10^{18}	0.382 ± 0.002
InP: Fe	111	10^{17}	0.379 ± 0.003
InP: Fe	100	10^{17}	0.360 ± 0.004

Table I. Thermal diffusivity of intrinsic and doped InP

It is seen from the table that all the doped samples have lower thermal diffusivity value in comparison with that of the intrinsic specimen. It can be understood in terms of phonon assisted heat transfer mechanism in semiconductors. In the case of semicondutors, heat is essentially carried away by both electrons and phonons. However, for semiconductors having carrier concentration less than $10^{20}cm^{-3}$, the contribution from electrons to thermal conductivity is negligibly small in comparison with that from phonons $\left({k_e}/{k_{ph}} = {1}/{3} \right)$ [29]. It means that for carrier concentration less than $10^{20}cm^{-3}$, the thermal energy transport in semiconductors is almost similar to that of dielectrics. In

the case of steady state photothermal experiments such as photothermal deflection effect, the detected signal depends on the thermal parameters (thermal diffusivity and thermal conductivity) of each quasi particle as well as on the distribution of momentum and energy among them (which are generated through the nonradiative deexcitations in the specimen) [30]. The electron gas is heated by surface and volume heat sources while the phonon gas is heated by surface sources. In the present investigation, all the specimens are opaque at the optical excitation wavelength and for the experimental frequency used here, thermal diffusion is the major process in heat transport. However, the transport of thermal energy is limited by various scattering processes suffered by phonons during its propagation through lattice. Phonon scattering is the key source that limits the performance of both electronic and optoelectronic devices. In the present studies, the incorporation of a dopant introduces more scattering centers in the host lattice, which effectively increases the scattering centers for phonons and consequently results in the reduction of phonon mean free path. It is well known that the lattice thermal conductivity

is directly proportional to the phonon mean free path through the relation $k_{ph} = \dfrac{1}{3}C_v v l$,

where C_v is the thermal capacity per unit volume, v is the sound velocity and l is the

phonon mean free path [15]. As the thermal diffusivity and thermal conductivity are

directly related through the relation $\alpha = \dfrac{k}{\rho c}$, the reduction in thermal conductivity due

to the reduction in phonon mean free path results in the reduction of thermal diffusivity values of the doped samples [31]. It is also reported [25] that lattice thermal conductivity

k is governed by lattice thermal resistivity (W) through the relation $k = \dfrac{1}{W} = AT^{-n}$,

where n is a constant at a particular temperature and A is a parameter which decreases with increase in doping concentration. The lattice thermal conductivity (thermal diffusivity) is essentially determined by the interaction of phonons and the scattering of

phonons with lattice. In addition to it, phonon-phonon scattering is the key source of scattering mechanism in semiconductors and is more important than electron-phonon interaction, especially at room temperature. All these processes together result in the reduction of phonon mean free path with doping which give a reduced thermal diffusivity value for doped samples as observed in the present measurements.

It is also seen from the table that the InP doped with Sn and S have higher thermal diffusivity value as compared to Fe doped semi insulating InP. The deep level impurities (which usually are metals), are deliberately incorporated into the compound semiconductors to alter the device characteristics. Addition of controlled amount of deep level impurities results in the reduction of switching time of bipolar devices. These deep level impurities create midgap energy levels, which can act as recombination centers when there are excess carriers in the semiconductor and as generation centers when the carrier concentration is below its equilibrium value as in the reverse-biased space charge region of p-n junctions or MOS capacitors [32]. Thus in effect, these midgap energy levels results in large relaxation around them and act as effective scattering centers for phonons. As noted above this increase in scattering centers reduces phonon mean free path and gives a reduced value for thermal diffusivity in Fe doped semi insulating InP. Among the InP doped with Sn and S, S doped InP shows a higher value for thermal diffusivity presumably due to the smaller size of dopant. Larger size of dopant results in larger variation in potential well and hence more effective scattering for phonons and consequently yields a lower value for thermal diffusivity [33].

From the table it is also obvious that the thermal diffusivity values of doped specimens cleaved in different planes are different. The plane of cleavage of compound semiconductors has great importance, especially in the fabrication of heterostructures. The difference in thermal diffusivity of the specimens cleaved along different planes can be understood in terms of variation in bond density with the plane of cleavage and

phonon assisted heat transport in semiconductors. In the case of InP, the sample cleaved along (111) plane has the average distance between the cation and anion as d whereas the samples cleaved along the (100) plane have a cation-anion distance of $d/\sqrt{3}$ [25]. Thus the bond density is high for the specimens cleaved in the (100) plane as compared to the samples cleaved in the (111) plane. In all the samples where the phonons are the major carriers of heat transport, the dynamical part of phonon temperature depends only on the characteristic features of phonons. As the bond density increases, the average phonon density also increases. The corresponding thermal diffusivity value $\alpha = k/\rho c$ from phonons also decreases. It has already been reported that, the average distance between the scattering centers essentially determines the resultant thermal diffusivity value of doped semiconductors. Besides that, the decrease in cation-anion distances effectively reduces the phonon mean free path and consequently thermal diffusivity value. The phonon relaxation time also increases with decrease in bond density resulting in a reduced value for thermal diffusivity for the specimens cleaved along the (100) plane. Such a variation in thermal diffusivity as a function of interparticle distances with doping has already been reported in the case compound semiconductors such as Bi_2Se_3 crystals, CdTe crystals [34-35]. The present studies have great importance both from device fabrication point of view as well from the growth of epitaxial layers. The plane of cleavage plays an important role on the lattice matching condition

2.6.4. Conclusion

This part of the present chapter deals with the measurements on the thermal diffusivity values of intrinsic and doped samples of compound semiconductor InP cleaved along different planes. From the analysis of data it is seen that the doping can influence the thermal diffusivity value through the scattering process of phonons. It is

also seen from the analysis that the semi insulating Fe doped InP have lower thermal diffusivity value as compared to Sn and S doped InP which in turn indicates that mid gap energy levels can influence the heat transport and hence thermal diffusivity value. Analysis of the data shows that thermal diffusivity value is sensitive to the direction of heat flow in semiconductor wafers. The present investigation clearly shows that in the case of semiconductors, which have carrier concentration less than 10^{20} cm^{-3}, the heat transport and hence thermal diffusivity value greatly depends on the propagation of phonons through the lattice. The inter particle distance is found to play a crucial role in the phonon distribution and hence the mean free path.

PART B

2.7. PTD investigation of anisotropic heat transport through layered structures.

2.7.1. Introduction

During the last decade, the fabrication and usage of layered materials have considerably increased in a variety of applications such as the utilization of semiconductor heterostructures and especially the double heterostructures, including quantum wells, quantum wires and quantum dots in electronics. Superlattices, anisotropic materials, different polymers and biological objects have required keen attention in modern science and technology [26]. Thermal characterisation of layered semiconductor structures has been a subject of great interest due to its anisotropy and its wide applicability in microelectronic and optoelectronic industry [13]. A number of recent review articles highlight the fact that the thermal conductivity and diffusivity of thin layers differ considerably from that of the corresponding bulk specimen [36-40]. This is due to the difference in microstructures such as grain size, amorphous nature and concentration of foreign atoms and defects, which strongly affect the scattering process of thermal carriers. In the case of layered structures, the interface thermal resistance and

scattering of heat carriers at the boundary also contribute to the reduction in thermal conductivity and thermal diffusivity. Besides that, thin layers of the specimen with same nominal composition as that of the bulk sample are reported to exhibit anisotropy and inhomogeneity. The effective thermal properties of layered structures are essentially determined by the properties of individual layers and the thickness of each layer. As the doping along with layer thickness can influence the thermal and transport properties of semiconductors in a substantial manner [41-42], a detailed study of anisotropic heat transport and hence the thermal diffusivity value of layered structures has great physical and practical significance.

2.7.2. Experimental

The experimental setup used for the present investigation is the same as that explained in the earlier part of the thesis with a difference that modulation frequency used in the present case is 10Hz. The samples used for the present study are n-type and *p*-type GaAs thin films grown upon semi-insulating GaAs substrates were used as samples in the investigation. The thin films are grown by the molecular beam epitaxial method (courtesy: Applied Physics Department, Technical University of Eindhoven, Eindhoven, The Netherlands). All the samples contained two epitaxial layers. A schematic of the sample structure with specific doping concentration are given in figure 11. For convenience we have labeled the samples arbitrarily as 1, 2, 3, and 4.The excitation photon energy used in the present case, viz., 2.54 eV, is much greater than the band gap energy of GaAs (1.43 eV) and the entire incident radiation is absorbed at the surface of the epitaxial layer itself. Consequently, all the specimens are considered to be opaque at the incident wavelength.

Sample 1

Si doped GaAs

Si doped GaAs

Semi-insulating GaAs
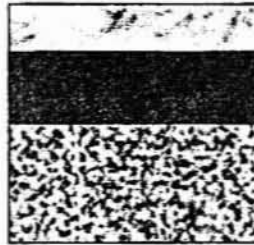
$l = 0.20 \mu m$ ✓ $n = 2 \times 10^{18} cm^{-3}$

$l = 1.80 \mu m$ ✓ $n = 2 \times 10^{18} cm^{-3}$

$l = 400.00 \mu m$ ✓

Sample 2

Si doped GaAs

Si doped GaAs

Semi-insulating GaAs
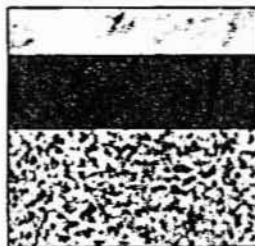
$l = 0.20 \mu m$ ✓ $n = 2 \times 10^{16} cm^{-3}$

$l = 2.80 \mu m$ ✓ $n = 2 \times 10^{16} cm^{-3}$

$l = 400.00 \mu m$ ✓

Sample 3

Si doped GaAs

Si doped GaAs

Semi-insulating GaAs

$l = 0.25 \mu m$ ✓ $n = 3.6 \times 10^{14} cm^{-}$

$l = 10.00 \mu m$ ✓ $n = 3.6 \times 10^{14} cm^{-}$

$l = 400.00 \mu m$ ✓

69

Sample 4

Be doped GaAs $l = 0.20\,\mu m$ $n = 2 \times 10^{18}\,cm^{-3}$

Be doped GaAs $l = 1.80\,\mu m$ $n = 2 \times 10^{18}\,cm^{-3}$

Semi-insulating GaAs $l = 400.00\,\mu m$
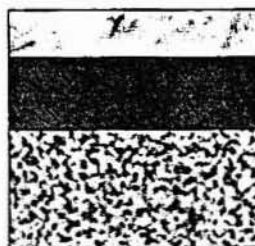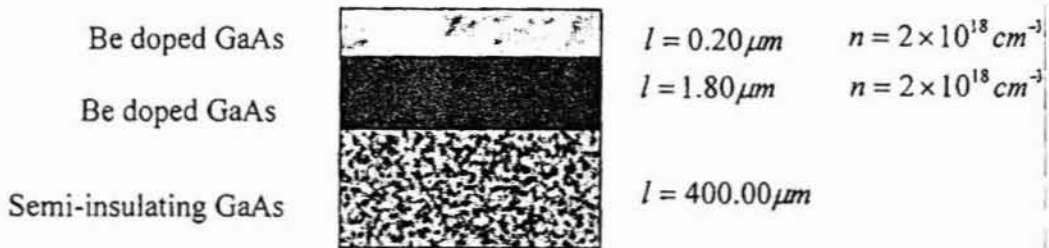
Figure 11. GaAs double epitaxial layers grown on GaAs substrate

The strength of mirage effect lies in the fact that, the two components (the tangential and normal components) of overall deflection of the probe beam depend essentially on the heat diffusion along the in plane and cross plane direction of specimen under investigation. Thus this technique is an effective tool to investigate the anisotropy in thermophysical properties of the specimen [43]. Eventhough, the mirage effect is well established for the thermal and optical characterisation for the materials, it is only recently that a group of researchers from National Institute of Standards and Technology (NIST), USA have utilized this technique for the investigation of the anisotropic thermal properties of multilayers such as Al/Ti [44]. The present work also follows the similar procedure, in which the phase of component of the deflection of probe beam in both tangential and normal direction is measured as a function of pump-probe offset. From the slope of phase of PTD signal as function of pump-probe offset, the tangential and normal component of thermal diffusivity values are evaluated.

2.7.3. Results and Discussions

Figure 12.a shows the variation in transverse component of phase of PTD signal as a function of pump-probe offset for the sample 1 whereas figure 12.b shows the variation of normal component for the same.
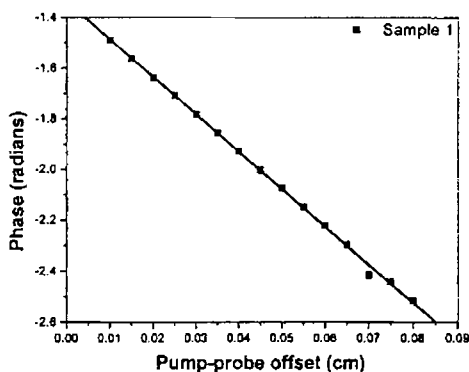
Fig.12.a) Variation of PTD phase with pump-probe offset for sample 1 in the transverse direction and the probe is on the right side of the pump beam.
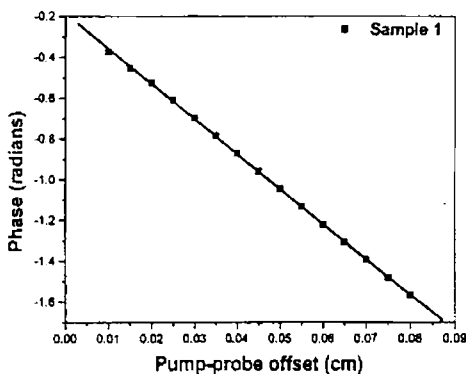
Fig. 12.b) Variation of PTD signal phase with pump-probe offset for sample 1 in the normal direction. Here the probe is on the right side of the pump beam.

Figures 13 to 15 show the respective normal and tangential component for samples 2, 3 and 4 respectively
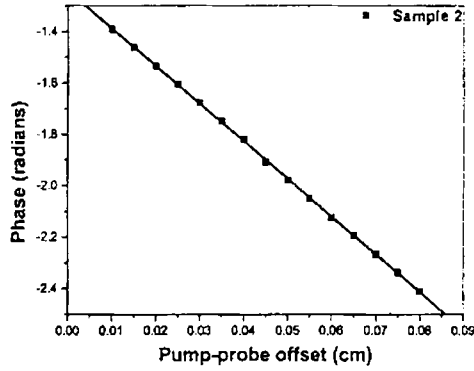
Fig. 13.a) Variation of PTD phase with pump-probe offset for sample 2 in the tangential direction. Here the probe is on the right side of the pump beam
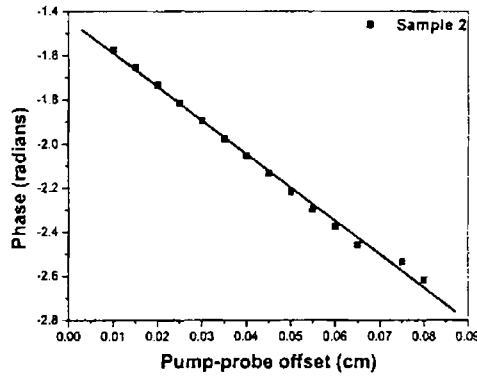
Fig. 13.b) Variation of PTD phase with pump-probe offset for sample 2 in the normal direction. Here the probe beam is on the right side of the pump beam
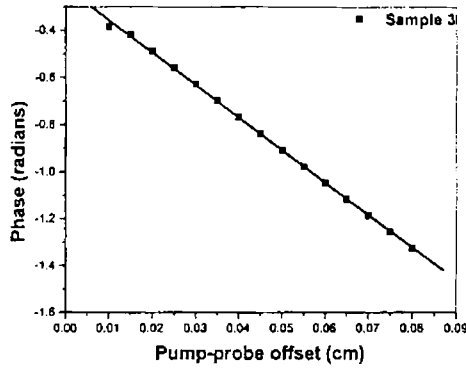
Fig. 14.a) Variation of PTD phase with pump-probe offset for sample 2 in the tangential direction. Here the probe is on the right side of the pump beam.
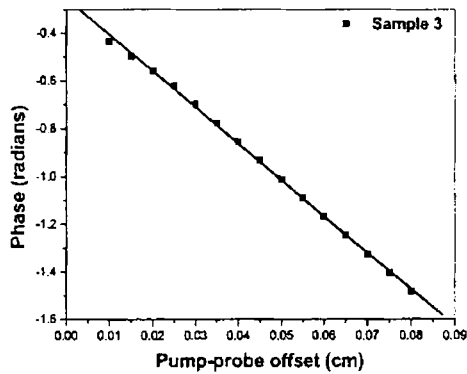
Fig. 14.b) Variation of PTD phase with pump-probe offset for sample 3 in the normal direction. Here the probe is on the right side of the pump beam.
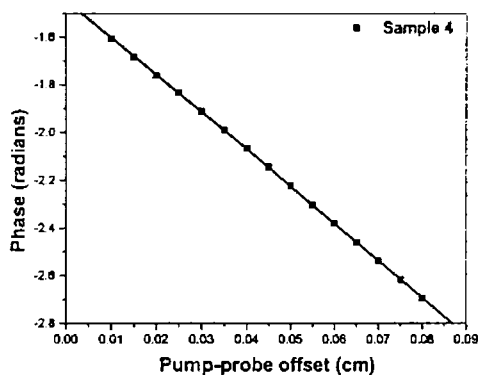
Fig. 15.a) Variation of PTD phase with pump-probe offset for sample 4 in the tangential direction. Here the probe is on the right side of the pump beam.
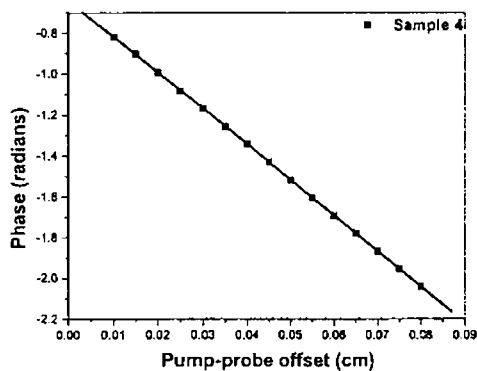
Fig. 15.b) Variation of PTD phase with pump-probe offset for sample 4 in the normal direction. Here the probe is on the right side of the pump beam.

74

The thermal diffusivity values evaluated from the slope of the plot of phase of PTD signal versus of pump-probe offset for all the specimens are tabulated in table II

Sample (please see the section 2.7.2 for description of samples)	Thermal diffusivity (cm^2s^{-1})	
	In plane	Cross plane
1	0.142 ± 0.0006	0.113 ± 0.0004
2	0.155 ± 0.0004	0.122 ± 0.0005
3	0.172 ± 0.0004	0.135 ± 0.0005
4	0.130 ± 0.0003	0.105 ± 0.0004

Table II. The in-plane and cross plane values of thermal diffusivity of different GaAs specimens under investigation.

It has been found that the magnitude of the thermal diffusivity value here is less than the value reported earlier for bulk GaAs [45-46]. The thermal diffusivity values measured along the in plane and the cross plane direction for all the specimens under investigation are shown in Table II, from which it is seen that the thermal diffusivity of samples vary with concentration of dopant and it is even sensitive to the nature of dopant. In the case of semiconductors, thermal energy is essentially carried away by electrons and phonons [47]. However, in the case of semiconductors with low or normal density of carriers, at all temperatures well below their melting point, heat conduction process is primarily due to phonons [48]. Thermal conductivity and hence thermal diffusivity are determined by the phonon mean free path, which in turn depends on phonon velocity and the relaxation time [2]. The propagation of phonons through the lattice suffers various scattering mechanisms such as phonon-phonon scattering, phonon-electron scattering and scattering of phonons by the crystal boundaries and defects. In

the case of semiconductors, at room temperature, the scattering of phonons is caused by the anharmonicity in the interatomic potential energy function. The electron-phonon scattering obviously depends on the carrier concentration and is important only at very high carrier density. In the present investigation, substrates of all the specimens are semiinsulating in nature so that the contribution from carriers is negligibly small. However, phonon scattering from crystal imperfections, point defects and impurities can be major contributing factors in determining the effective the thermal conductivity (thermal diffusivity) value. In the case of semiconductors, it is the propagation of acoustic phonons that is more effective in determining the thermal parameters as compared to the optical phonons [49].

The detected photothermal signal from a semiconductor is not solely dependent upon how heat is carried away by each quasiparticle system in the semiconductor and its thermal parameters (electron and phonon thermal diffusivity and thermal conductivity) but also on how energy and momentum are distributed between them i.e., the detected signal depends greatly on various scattering processes suffered by the heat carriers [47]. However, in the case of layered semiconductors the reduction in their effective thermal parameters [50] depends mainly on (a) the doping effect (b) the interface effect and (c) the quantum size effect. In the present investigation, the epitaxial layers have a thickness much greater than the mean free path of phonons in GaAs (~ 10-20 Å) so that quantum confinement has negligible influence in our investigations. Hence the phonon spectrum in each layer can be represented by its bulk form [49]. Since the epitaxial layer thickness is greater than the phonon mean free path, the normal and Umklapp scattering rates are identical to those for the bulk specimen [51]. The normal scattering processes are significant for longitudinal and low frequency transverse phonons, whereas Umklapp scattering is the dominating phenomena for high frequency transverse phonons. At room temperature, the high frequency transverse phonons are the effective carriers of heat [52].

In addition to these scattering mechanisms, phonons also suffer scattering from impurities present in the epitaxially grown layers, which in turn reduces the phonon mean free path, and hence the phonon group velocity. The reduction in phonon mean free path or phonon group velocity results in reduction of the lattice thermal conductivity [$k = \dfrac{Cv\Lambda}{3}$, where C is the volumetric specific heat, v is the phonon group velocity and Λ is the phonon mean free path] and hence the effective thermal diffusivity value. It has already been reported that lattice thermal conductivity k is governed by lattice thermal resistivity (W) through the relation $k = \dfrac{1}{W} = AT^{-n}$ (where n is a constant at a particular temperature and A is a parameter which decreases with increase in doping concentration) and it decreases with increase in doping concentration [25]. It is interesting to point out here that the thermal diffusivity value of p-type specimen is small as compared to n-type specimen. This is due to the fact that scattering rate of phonons due to impurities is proportional to the square of the mass difference between gallium and the dopant atom. In Be:GaAs, beryllium is much lighter than silicon, the mass difference between silicon and gallium is less in comparison to the mass difference between the beryllium and gallium. Thus the phonons in Be doped p-type specimen suffer large scattering rate and thus results in a reduced value for thermal diffusivity for the sample.

The interface effects also play a significant role in the reduction of thermal diffusivity of layered structures as compared to bulk specimen. As the thickness of epitaxial layers are relatively larger than the phonon mean free path, interface scattering cannot be either completely diffusive or specular in nature [53]. Specular interface scattering depends on the mismatch in acoustic impedance and phonon group velocity between the two layers. If the roughness of the interface is comparable to the wavelength of phonon, diffuse scattering at the interface will dominate in the interface scattering

mechanism. In the present case the layers are doped with impurities and they are grown by molecular beam epitaxial method so that interface scattering is both diffusive and specular in nature. A small increase in diffuse scattering due to increase in dangling bonds at the interface caused by the variation in doping levels can affect the thermal diffusivity value in a substantial manner [49]. When interface roughness is of the order of the phonon mean free path, it can act as an effective diffusive interface scattering center for phonons which results in the reduction of thermal diffusivity value [49]. The inelastic scattering caused by the anharmonic interatomic force due to doping and the phonon mode conversion at the interface can also results in the diffuse scattering mechanism. This thermal barrier resistance (TBR) due to interface roughness results in the reduction of thermal diffusivity value. However, the effect of interface roughness is relatively small as compared to the doping effects. In addition to these scattering mechanisms, dislocations in the epitaxially grown layers result in internal scattering which in turn causes a reduction in thermal diffusivity. In order to predict the exact contribution from each factor to the reduction in thermal diffusivity value, a more detailed investigation and theoretical modeling based on the propagation of various longitudinal and transverse acoustic phonons and its reflection and transmission at the interface, is needed. Nevertheless, the present measurement shows that the effective thermal diffusivity values in the in-plane and cross-plane show a considerable decrease as compared to the bulk specimen.

It is seen from the measurements that the thermal diffusivity values of the specimens under investigation follow a logarithmic dependence with doping concentration. It is reported [54] earlier that the phonon scattering rate is given by the expression $A\omega^4$, where ω is the phonon angular frequency. A is a constant related to the

doping concentration and is given by $A = \dfrac{nV^2}{4\pi\upsilon_s^3}\left(\dfrac{\Delta M}{M}\right)^2$, where n is the dopant

concentration, V is the volume of the host atom, υ_s is the average phonon group velocity,

M is the atomic mass of the host atom and ΔM is the difference between the host and

impurity atom. The above relation suggests a linear decrease in thermal diffusivity value

with doping concentration. However, the experimentally observed logarithmic

dependence could be due to the combined effect of both doping concentration and the

thickness of the epitaxial layers. An increase in the thermal conductivity value of layers

with specimens having thickness of the order of few μm range has already been reported

[49]. Our analysis of the results also leads to the same conclusion as sample 3 has a

relatively larger thermal diffusivity value as compared to other samples. It can be

attributed to the increase in spectral phonon heat capacity as well as to the reduction in

total relaxation time with size [55]. As mentioned earlier, at 300K only the high

frequency transverse phonons are the effective carriers of heat. The net effect of increase

in phonon heat capacity is the reduction of the amount of heat carried away by each

phonon. The typical relaxation time of the Umklapp process at 300K is about 10^{-9}s,

corresponding to a relaxation length of the order of micron. This indicates that even in

the specimens having thickness of the order of μm , as in the present investigation, size of

the epitaxial layer has pronounced effect on the effective thermal diffusivity value.

The cross plane thermal diffusivity is less as compared to in-plane thermal

diffusivity value. The phonons propagating parallel to the film have a greater phonon

mean free path as compared to those in perpendicular direction, resulting in a larger

thermal diffusivity value in the parallel direction [52]. In general, the measured thermal

resistance of the film in the cross plane consists of two parts viz., thermal resistance

within the film and the thermal boundary resistance at the interface [50]. The interface

and boundary scattering have larger effect on the mean free path of phonons propagating perpendicular to the point of excitation [49-50]. This is due to the temperature jump experienced by the phonons at the interface [50]. However, in the in-plane direction local thermal equilibrium is established over a length scale much smaller than the length of the specimen in that direction. The anisotropy in thermal properties of freestanding thin films have already been reported [52]. As the interface contains large number of dangling bonds it acts as effective scattering centers for phonons, which in turn results in reduced value for thermal diffusivity value along the perpendicular direction as compared to parallel direction. Thus physical anisotropy of the epitaxial layers results in the anisotropy of the measured effective thermal diffusivity value of all the samples under investigation [56].

2.7.4. Conclusion

This section of the present chapter the measurements of anisotropic thermal diffusivity on GaAs double epitaxial layers have been explained in detail. It is seen that the layered structures show a substantial reduction in effective thermal diffusivity value as compared to those reported earlier in bulk specimen. The in-plane thermal diffusivity is found to be larger as compared to its cross-plane value. Analysis of results shows that the nature of the dopant as well as the doping concentration has a pronounced effect on the propagation of thermal waves and hence on the thermal diffusivity value. The present study also suggests that in the case of layered structures, the mean free path of phonons in tangential direction is relatively large in comparison to the mean free path in the perpendicular direction. This can be ascribed to additional scattering of phonons in the normal direction due to the interface and thermal boundary resistance of the epitaxial layers.

2.8. *References*

1. Mandelis A (Edit) Progress in photothermal science and technology in semiconductors (Elsevier Science, New York) 1992.

2. Yu. G. Gurevich, G. Gonzalez de la Cruz, G. Logvinov and M. N. Kasyanchuk, Semiconductors, 32(11), 1179 (1998).

3. A. C. Boccara, D. C. Fournier and H. Badoz, Appl. Phys. Lett. 36, 130 (1979).

4. A. C. Boccara, D. Fournier, W. B. Jackson, and N. M. Amer, Appl. Opt. 20, 4580 (1981).

5. A. Salazar, A. Sa'nchez-Lavega, and J. Ferna'ndez, J. Appl. Phys. 65, 4150 (1989).

6. A. Salazar, A. Sa'nchez-Lavega and J. Ferna'ndez, J. Appl. Phys. 74, 1539(1993).

7. W. B Jackson and N. M. Amer, Phys. Rev. B, 25, 5559 (1982).

8. Casperson.L.W, Appl.Opt. 12, 2434 (1973).

9. Born.M and Wolf.E, Principle of Optics (Pergamon Press, Oxford) (1970).

10. A. Salazar and A. S. Lavega. Rev.Sci.Instrum. 65, 2896 (1994).

11. D. Fournier, J. P. Roger, C. Boue, H. Stamm, and F. Lakestani, Anal. Sci.17, S158 (2001).

12. B. Zimering and A. C. Boccarra, Rev. Sci. Instru. 67, 1819 (1996).

13. Li. B.C and Gupta. R, J. Appl. Phys. 89, 859 (2001).

14. A. Mandelis, Physics Today 29, August (2000).

15. Heinz K. Henisch (Edit), International series of monographs in semiconductors, Vol. 4 (Pergamon Press, Oxford) 1961.

16. A. Pinto Neto, H. Vargas, N. Leite and L. C. M. Miranda, Phys. Rev. B 40, 3924 (1989).

17. A. Pinto Neto, H. Vargas, N. Leite and L. C. M. Miranda, Phys. Rev. B, 41, 9971 (1990).

18. L. D. Favro and Xiaoyan Han Sensing for Materials Characterisation and Manufacturing , Vol 1 (The American Society for Nondestuctive Inc., Columbus) 1998.

19. H. S. Carslaw and J. C Jaeger, Conduction of Heat in Solids (Oxford Press) 1959.

20. H. S. Carslaw, Introduction to the mathematical theory of conduction of heat is solids (Mc Millan) 1921.

21. Shoucair, IEEE transactions on eduction, 32, 359 (1989).

22. Jasprit Singh, Semiconductor Optoelectronics, Physics and Technology (Mc-Graw Hill, Singapore) 1995.

23. Ben G Streetmann and Sanjay Banerjee, Solid State Electronic Devices, (Prentice Hall, India) 2001.

24. Charles M Wolfe, Nick Holonyak and Gregory E. Stillmann, Physical Properties of Semiconductors (Prentice – Hall, New York) 1989.

25. Sajan D George, P. Radhakrishnan, V. P. N. Nampoori and C. P. G. Vallabhan, Applied Physics B: Lasers and Optics (In print)

26. Mool. C. Gupta, Handbook of Photonics (CRC Press, New York) 1997.

27. J.D. Wienfordner (Edit) Photothermal spectroscopy method for chemical analysis (Wiley New York) 1996.

28. CRC Handbook of Chemistry and Physics (CRC Press, Boca Raton) 1999.

29. G. Gonzlez de la Cruz and Yu. G. Gurevic, Phys. Rev. B, 58 (12), 7766 (1998).

30. G. Gonzlez de la Cruz and Yu. G. Gurevic, Phys. Rev. B, 51, 2188 (1995).

31. S.D George, C.P.G.Vallabhan, M.Heck, P.Radhakrishnan and V. P. N. Nampoori Journal of Nondestructive Testing and Evaluation Vol.18 ,2, 75 (2002).

32. D. K. Schroder, Semiconductor material and device characterisation (Wiley Interscience, New York) 1998.

33. Sajan D George, P. Radhakrishnan, V. P. N. Nampoori and C. P. G. Vallabhan, J. of Phys. D: Appl. Phys. 36 (8), 990 (2003).

34. S. D George, S. Augustine, E. Mathai, P.Radhakrishnan, V. P. N. Nampoori and C. P. G. Vallabhan, Phys. Stat. Sol. (a) 196 (2) 384-389 (2003).

35. J. Ptruzzelo, J. Gaines, P. Van der Sluis, D. Olego and C. Ponzoni, Appl. Phys. Lett. 62, 1496 (1993).

36. Albert Feldman and Naira M Valzeretti, J. Res. Natl. Inst. Stand. Technol. 130, 107 (1998).

37. D. G. Chill, J. Vac. Sci. Technol. A 7, 1259 (1990).

38. L. Hatta, Int. J. Thermophysics 11, 293 (1990).

39. K. E Goodson and M. I. Flik, Appl. Mech. Rev. 47, 101 (1994).

40. C. L. Tien and G. Chen, J. Heat Transf. 116, 799 (1994).

41. I. Riech, P. Diaz and E. Marin Phys.status.solidi (b), 220, 305 (2000).

42. G. Chen and M. Naegu, Appl. Phys. Lett. 71 (19), 2761 (1997).

43. J. A. Sell (Edit), Photothermal investigations of solids and fluids, (Academic Press, Boston) 1989.

44. E. J. Gonzalez, J. E. Bonevich, G. R. Stafford, G. White and D. Jossel, J. Mater. Research 15(3), 764 (2000).

45. A. Mandelis Ed. Photoacoustic and Thermal Wave Phenomena in Semiconductors, Elsevier Scientific, North-Holland, New York (1987).

46. H. Vargas and L. C. M. Miranda Phys.Rep. 161(12), 43 (1988).

47. A. F. Carballo Sanchez, G. Gonzalez de la Cruz, Yu. G. Gurevich and G. N. Logvinov, Phys. Rev. B, 59 (16), 10630 (1999).

48. B.Yang and G. Chen, Phys. Low-Dim. Struct. 5/6, 37 (2000).

49. G. Chen Phys. Rev. B 57, 14958 (1998); Transactions of the ASME , 119, 220 (1997).

50. Ren .S.Y and Dow J. D. Phys. Rev. B, 25, 3750 (1982);T. Zeng and G. Chen, Journal of Heat Transfer 123 (2001).

51. M. G. Holland, Phys. Rev. 132, 2461 (1963).

52. C. Chen, C. L. Tien, X. Wu, J. S. Smith, Journal of Heat Transfer, 116, 325 (1994).

53. X. Wang, H. Hu, X. Xu, Transactions of the ASME 123, 138 (2001).

54. A. D. McConnell, Uma and Goodson, Journal of microelectromechanical systems, 10 (3), 360 (2001).

55. G. Chen and C. L. Tien, Journal of Thermophysics and Heat Transfer, 7(2), 311 (1993).

56. Sajan D George, P. Radhakrishnan, V. P. N. Nampoori and C. P. G. Vallabhan, Physical Review B, 68, 165319 (2003).

Thus, the task is, not so much to see what no one has yet seen; but to think what nobody has yet thought, about that which everybody sees

— *Erwin Schrodinger*

Chapter 3

Photoacoustic studies on transport properties of semiconductors

Abstract

In this chapter, results obtained from the photoacoustic studies on transport properties viz., thermal diffusivity, diffusion coefficient, surface recombination velocity and nonradiative recombination time of both direct and indirect bandgap semiconductors are described. The present chapter consists of three sections namely part A, part B and part C. In the part A, measurements made on thermal and transport properties of direct bandgap materials such as InP, GaAs and InSb are presented. The second part deals with the study of influence of nature of dopant on these transport properties in Si whereas latter part of this chapter describes the influence of doping concentration on thermal and transport properties of GaAs epitaxial layers.

3.1. Introduction

The last 25 years have witnessed the emergence of photoacoustic (PA) technique and related photothermal methods as extremely sensitive and effective techniques for the evaluation of thermal, transport and optical properties of matter in all its different states [1]. Depending on the specimen and the parameters to be measured, different versions of PA technique are being employed [2]. The microphone version of PA technique has gained wide popularity due to its simplicity and its capability for the simultaneous measurement of thermal and transport properties [3-7]. Semiconductors are the one class of photonic materials, where the versatility of PA technique to measure thermal and transport properties in a nondestructive way, can find very good practical appication [8-12]. This has extreme importance as the electrical and electrooptical properties of devices fabricated using these materials depend greatly on such transport properties.

Of the different configurations of the microphone version of PA technique, the one with the heat transmission configuration, which is the basis of minimal volume of Open Photoacoustic Cell (OPC), is the well accepted and widely used. Simultaneous measurements of thermal and transport properties of semiconductors and thin films can be carried out using this technique with good accuracy [13-15]. This technique also provides knowledge on the various material parameters of semiconductors, which are not easy to measure using conventional techniques. As the PA signal is produced by thermal waves that propagate through the specimen, the measured PA signal gives a clear picture about the microstructural variations arising due to doping [16]. The importance and practical significance of compound semiconductors and epitaxial layers for the photonics device fabrication are already mentioned in earlier chapters.

Eventhough, Si is a well-studied material, it is only very recently that a significant enhancement in internal quantum efficiency of pure Si was observed, and this is a major breakthrough in the field of microelectronics and optoelectronics [17]. In this context, a study of the measurement of thermal and transport properties via

thermal diffusivity, diffusion coefficient, surface recombination velocity and nonradiative recombination time of some compound semiconductors such as InP, GaAs and InSb, intrinsic and doped Si have great physical and practical significance. The same can be said of the GaAs epitaxial layers also.

3.2. PA signal generation in semiconductors

According to the thermal piston model of Rosencwaig and Gersho [18], modified by Pinto Neto etal for the evaluation of thermal and transport properties of semiconductors [19-20], the pressure fluctuations in the open PA cell due to the temperature fluctuations at the sample surface is given by

$$\delta P = \frac{P_0 \Theta}{T_0 l_g \sigma_g} e^{j\omega t} \tag{1}$$

where P_0 (T_0) is the ambient pressure (temperature), l_g is the length of the gas chamber, $\sigma_g = (1+j)a_g$, where $a_g = \left(\frac{\pi f}{\alpha_g}\right)^{\frac{1}{2}} = \left(\frac{1}{\mu_g}\right)$ with μ_g as the thermal diffusion length in the gas of thermal diffusivity α_g, and Θ is the sample temperature fluctuation at the sample-gas interface (x=0). Also $\omega = 2\pi f$ where f is the modulation frequency of the incident laser radiation. In the remaining section we consider the PA cell geometry for the heat transmission configuration shown schematically in figure 1. The temperature fluctuation Θ can be obtained from the solution of thermal diffusion equation given by

$$\frac{\partial^2 T}{\partial x^2} = \frac{1}{\alpha_s} \frac{\partial T}{\partial t} - \frac{Q(x,t)}{k_s} \tag{2}$$

where $\alpha_s (k_s)$ is the sample thermal diffusivity (conductivity), and Q(x,t) is the heat power density generated in the sample due to the absorption of intensity modulated laser radiation. In semiconductors, if the incident energy is greater than the band gap

of the semiconductor, then thermal power density Q(x,t) mainly arises due to three different processes.

(1) Thermalisation component, which arises due to fast nonradiative intraband transition in the conduction band of semiconductors. This occurs mainly due to the electron phonon interaction, which happens typically in the time scale of picoseconds. Hence this process can be assumed as an instantaneous process compared with the modulation frequencies usually used in the photoacoustic experiment. The heat power density due to this process is denoted by

$$Q_D = \frac{\beta(E - E_g)}{E} I_o e^{\beta(x+l_s)} e^{j\omega t} \tag{3}$$

where β is the optical absorption coefficient for photons having energy E, incident at $x = -l_s$ with an intensity I_0 (W/cm^2).

(2) The second component is due to the recombination of the photoexcited carriers in the bulk of the material after they travel a finite distance $(D\tau)^{1/2}$, where D is the carrier diffusion coefficient, and τ is the recombination time. The heat power density due to nonradiative bulk recombination is given by

$$Q_{NRR} = \frac{E_g}{\tau} n(x,t) \tag{4}$$

where n(x,t) is the density of the photoexcited carriers.

(3) The nonradiative recombination of the photoexcited carriers at the surface of the material also contributes to the total heat power density and it is given by

$$Q_{SR} = E_g \left[v\delta(x) + v_0\delta(x + l_s) \right] n(x,t) \tag{5}$$

where v_0 is the carrier recombination velocity at the heating surface and v is the surface recombination velocity at the sample-gas interface at x=0.

Gas   Sample   Gas

Incident Radiation

$$x = l_g \qquad x = 0 \quad x = -l_s$$
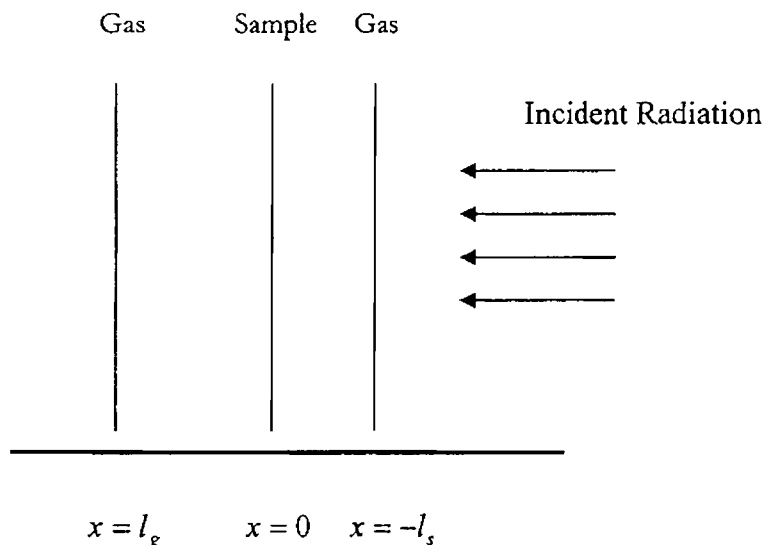
Figure 1. PA cell geometry for the heat transmission configuration.

From the above analysis, it is obvious that the solution to equation (2) depends on the density of photoexcited carriers which obeys the carrier diffusion equation, namely,

$$\frac{\partial n}{\partial t} = D\frac{\partial^2 n}{\partial x^2} - \frac{n}{\tau} + \frac{\beta I_0}{h\nu}e^{(x+l_s)}e^{j\omega t} - vn(x,t)\delta(x) - v_o n(-l_s,t)\delta(x+l_s) \quad (6)$$

For completely opaque samples, at the incident wavelength, it can be assumed that all the incident radiation is absorbed at the $x = -l_s$ surface so that we can replace $\beta I_0 e^{\beta(x+l_s)}$ in the equations (3) and (6) by $I_0(x+l_s)$. Since the thermal conductivity of surrounding air is very small, we neglect the diffusion of heat into the surrounding gas. Then the solution for the coupled equation (2) and (6), leads to the expression for pressure fluctuations for the thermally thick sample as

$$\delta P = \frac{2\varepsilon I_0 P_0}{T_0 l_g \sigma_g k_s \sigma_s}\left[\left[\frac{\varepsilon-1}{\varepsilon}\right]e^{-l_s\sigma_s} + \frac{F\sigma_s}{D\gamma\tau}\left[\frac{1}{\sigma_s^2 - \gamma^2} + \frac{v\tau}{\sigma_s}\right]\right] \quad (7)$$

90

where $\sigma_s = (1+j)a_s$, $a_s = \left(\dfrac{\pi f}{\alpha_s}\right)^{1/2} = \left(\dfrac{1}{\mu_s}\right)$ where μ_s is the thermal diffusion

length of the sample, $\gamma = \left(\dfrac{1+j\omega\tau}{D\tau}\right)^{1/2}$ is the carrier diffusion coefficient,

$\varepsilon = \dfrac{E_g}{h\nu}, r = \dfrac{\nu}{D\gamma}, r_0 = \dfrac{\nu_0}{D\gamma}$ and

$$F = \frac{1}{(1+r_o)(1+r)e^{\gamma l} - (1-r)(1-r_0)e^{-\gamma l}} \qquad (8)$$

The frequency range used in the present experiments satisfies the condition that $\omega\tau \ll 1$ so that F, r, r_0 becomes real constants independent of modulation frequency. It is reported by Pinto Neto etal [19] that the OPC signal for a semiconductor sample in the thermally thick region is essentially determined by the nonradiative recombination processes. Thus the expression for the pressure fluctuation in the experimental frequency range for which $\omega\tau \ll 1$ is given by

$$\delta P = \frac{2\varepsilon f_o P_o F}{T_o l_g k_s D\gamma\tau\sigma_g}\left[\frac{1}{\sigma_s^2 - \gamma^2} + \frac{\nu\tau}{\sigma_s}\right] \qquad (9)$$

and the phase of the OPC signal is given by

$$\Phi = \frac{\pi}{2} + \Delta\Phi \qquad (10)$$

where $\tan\Delta\Phi = \dfrac{\left(\dfrac{aD}{\nu}\right)(\omega\tau_{eff} + 1)}{\left(\dfrac{aD}{\nu}\right)(1 - \omega\tau_{eff}) - 1 - (\omega\tau_{eff})^2} \qquad (11)$

with $\tau_{eff} = \tau\left[\left(\dfrac{D}{\alpha_s}\right) - 1\right]$

By taking thermal diffusivity, diffusion coefficient, surface recombination velocity and relaxation time as adjustable parameters, the variable part of the equation (11) is fitted to the experimentally obtained phase angle versus frequency curve. The phase

of the photoacoustic signal is used for the evaluation of thermal and transport properties of semiconductors because the phase of the PA signal is a relative quantity so that no normalization procedure is required [21].

3.3. Importance of thermal and transport properties

The importance and physical significance of a transient thermophysical parameter, namely thermal diffusivity, have already been explained in the previous chapter. Diffusion coefficient is an important parameter for the semiconductors and at a particular temperature; the value of diffusion coefficient is essentially determined by the mobility of carriers [22]. The magnitude of diffusion coefficient depends on the impurity concentration and also on the nature of impurity. The value of diffusion coefficient along with the recombination time essentially determines the distance traveled by the photoexcited carriers before they recombine. Various scattering processes arising due to introduction of a dopant can affect the mean free path and the recombination time and hence the value of diffusion coefficient.

The surface recombination velocity of photoexcited carriers has a significant impact on the performance of devices used in electronic and optoelectronic industry. The surface recombination velocity has a profound effect on the spectral response of semiconductors, especially at high photon energies. Characterisation of the surface recombination velocity of semiconductors is of great importance for successful development of minority carrier devices such as heterojunction bipolar transistors, light emitting diodes, semiconductor laser and solar cells. In fact, the surface recombination velocity may strongly affect the "effective lifetime of minority carriers", which controls the principal electrical and electro-optical parameters of such devices. In addition, a possibility to distinguish between the surface and the bulk contribution, which detemine the effective lifetime of carriers is essential to optimize surface passivation procedures and epitaxial growth and re-growth conditions, during the fabrication of semiconductor devices.

The nonradiative recombination time is an important parameter, which determines the quantum efficiency of the semiconductor devices. In the case of indirect bandgap semiconductors such as Si, it is the nonradiative recombination mechanism that dominates, whereas in the case of direct bandgap semiconductors such as GaAs, InP etc, the dominating mechanism is the radiative recombination [23]. In addition to radiative recombination processes, the nonradiative recombination can take place mainly through two processes viz., Schokley Read Hall (SRH) recombination and multiphonon recombination mechanism or Auger recombination mechanism. In SRH mechanism electron-hole recombination takes place through the deep level impurities and this recombination mechanism is characterized by impurity density and its energy level in the bandgap as well as the capture cross section of electrons and holes. The energy liberated due to this event is dissipated by lattice vibrations or phonons. Another recombination mechanism which is dominant especially in intrinsic semiconductors is Auger recombination and the auger lifetime is inversely proportional to the carrier density. The energy released during this process is absorbed by another carrier.

3.4. Experimental Setup

Optical radiation from an argon ion laser at 2.54eV (Liconix 5300) is used as the source of excitation, which is intensity modulated using a mechanical chopper (Stanford Research Systems SR 540) before it reaches the sample. Detection of the PA signal in the cavity is made using a sensitive electret microphone (Knowles BT 1754). Details of the PA cell are explained in the following part. The cell has a flat response in the frequency range from 30 to 4000 Hz. The phase and amplitude of the PA cell is measured using a dual phase digital lock-in amplifier (Stanford Research Systems SR 830).
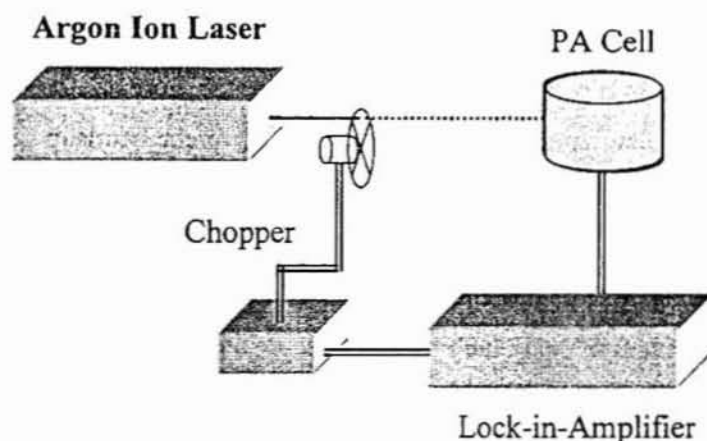
Figure 2. Experimental Setup used for the present investigation.

The cross sectional view of the homemade OPC is given in figure 3. OPC is fabricated on an acrylic (perspex) disc of thickness 1 cm and a diameter of 5.5 cm. The acoustic chamber is made by drilling a bore of diameter 3 mm, along the thickness direction, at the center of the disc. One end of this cylindrical hole is closed with an optical quality glass disc of thickness 1.4 mm and the other end is left open. Another fine bore of diameter 1.5 mm pierced at the middle of the chamber and perpendicular to it serves as the acoustic coupler between the chamber and the microphone. At a distance of 8 mm from the main chamber, the microphone is firmly glued to the orifice of the side tube. Shielded wires are used to take the electrical connections directly from the microphone. Entire system is then fixed inside a cylindrical hollow block of aluminium. Another identical acrylic disc with a 3 mm hole at the center serves as the top end of the cell and the sample under investigation is kept between the two to ensure airtight seal of the air chamber by the sample.
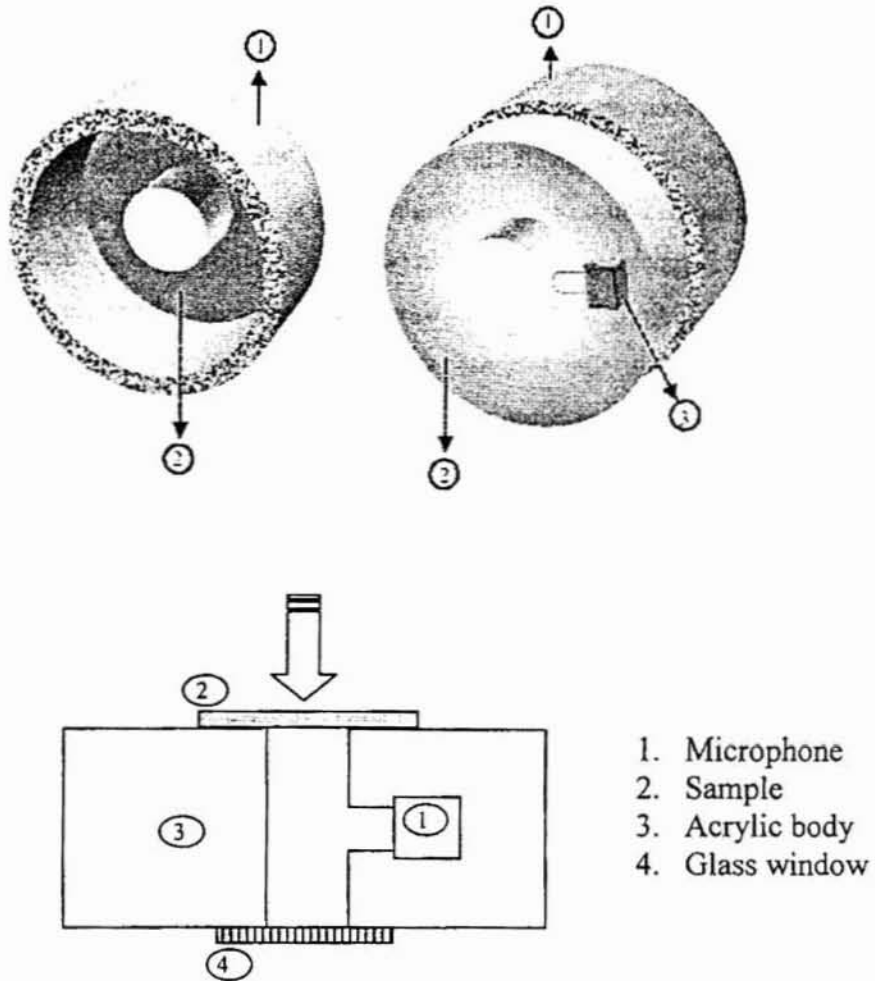
Figure 3. Cross-sectional view of Open Photoacoustic Cell.

1. Microphone
2. Sample
3. Acrylic body
4. Glass window

PART – A

3.5. Photoacoustic investigation on some intrinsic compound semiconductors

3.5.1. Introduction

The concept of waves is an integral part of our scientific culture and has nourished physicists, pure and applied alike, for centuries. The diffusion waves are a class of waves which lack wavefronts, cannot be beamed and do not travel far, yet

95

they form the basis of several new and revolutionary measurement technologies [24]. The thermal waves generated in the specimen after illumination with a chopped optical radiation is a particular class of diffusion with equal real and imaginary parts. The importance of equal real and imaginary parts of the wavenumber lies in the fact that it can be generated at all the frequencies [24]. However, depending on the method of excitation, the thermal waves generated in a specimen have different nature. For example, the thermal waves generated from a specimen due to the excitation with a focused beam are spherical in nature whereas plane thermal waves are generated due to the irradiation with a collimated optical radiation [25]. The major difference between thermal waves and the electromagnetic waves is that electromagnetic waves satisfy a hyperbolic equation, which is second order derivative in time whereas thermal waves satisfies a parabolic equation which satisfies a first order differential equation in time [26-27]. A variety of experimental techniques have exploited these thermal waves to measure the properties of materials.

This section of the present chapter deals with the simultaneous measurement of thermal and transport properties of some compound semiconductors, namely InP, GaAs and InSb using the simple and elegant open cell photoacoustic technique that utilizes the thermal waves generated in the sample. The experimental set up is same as that explained in the previous section. In all the measurements the phase of the PA signal is used for the simultaneous evaluation of thermal and transport properties because unlike the amplitude, phase is insensitive to beam intensity and it depends only on the surface temperature [28].

3.5.2. Results and Discussions

Figure 4, 5 and 6 shows the variation of the phase of PA signal as a function of modulation frequency obtained under heat transmission configuration. The continuous line represents the best theoretical fit to the equation (11). The fitting program follows essentially the least square method and the fitting procedure is done using MATLAB. The fitting procedure analysis resulted in the following accuracy of

the fitted parameters: thermal diffusivity ± 2%, diffusion coefficient ± 5%, nonradiative recombination time ± 3% and surface recombination velocity ± 8%. The values obtained for the best fitting parameters are given in table I. Such a simultaneous evaluation of thermal and transport properties of doped semiconductors using the phase of PA signal has already been reported [8-12]. However, the recent studies show that all these parameters are sensitive to doping concentration as well as to the nature of dopant. Hence the evaluation of thermal and transport properties of intrinsic samples has great physical and practical significance.
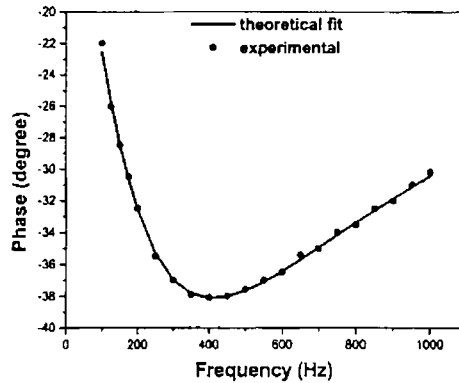
Figure 4. PA phase angle for intrinsic InP versus modulation frequency. The solid lines represents the best fit of the data using equation (11)
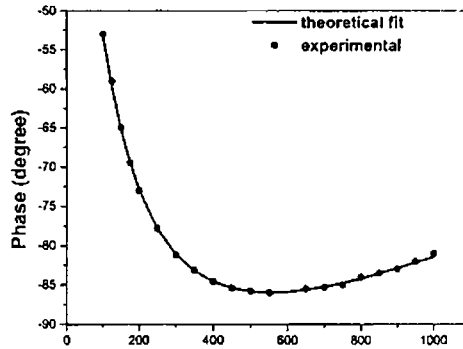
Figure 5. PA phase angle for intrinsic GaAs versus modulation frequency. The solid lines represents the best fit of the data fitting to equation (11)
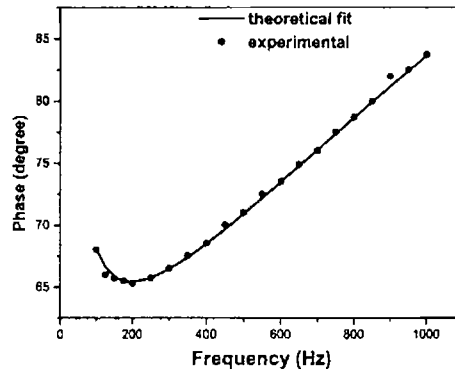
Figure 6. PA phase angle for intrinsic InSb versus modulation frequency. The solid lines represents the best fit of the data fitting to equation (11)

Sample	Thermal diffusivity (cm^2s^{-1})	Diffusion coefficient (cm^2s^{-1})	Surface recombination velocity (cms^{-1})	Nonradiative recombination time (μs)
InP	0.44	4.6	435	22.0
GaAs	0.26	7.4	456	3.0
InSb	0.16	22.0	498	0.7

Table I. Thermal and transport properties of compound semiconductors

As mentioned earlier, thermal diffusivity is an important thermophysical parameter and doping can affect the value of thermal diffusivity in a substantial manner. The measured thermal diffusivity values agree well with the earlier reported values of these compound semiconductors. Diffusion coefficient is an important thermophysical parameter for the semiconductors, and at a particular temperature, the value of diffusion coefficient is essentially determined by the mobility of carriers. Recent investigations show that the diffusion coefficient of semiconductors is sensitive to doping due to its mobility dependence [23]. The diffusion coefficient and mobility are related through Einstein's relation $D = \dfrac{\mu k_\mathrm{B} T}{e}$, where μ and e are the mobility and charge of the photoexcited carriers at a particular temperature T and k_B is the Boltzmann constant. The importance of the measurement of the diffusion coefficient of semiconductors using PA technique is that, PA signal generation depends on the nonradiative recombination of photoexcited carriers and hence the mobility of minority carrirs. The diffusion coefficient measured using the present technique gives the mobility of holes, which is, hard to measure using conventional methods. The values of mobility evaluated, viz., 177 cm^2/V-s for InP, 286 cm^2/V-s for GaAs and 850 cm^2/V-s for InSb, using the measured values of diffusion coefficient agree well with the earlier reported [29] mobilities of holes in the respective samples ($\leq$ 200 cm^2/V-s for InP, $\leq$ 400 cm^2/V-s for GaAs cm^2/V-s and $\leq$ 850 cm^2/V-s for InSb). Thus the present study shows that PA technique is an effective tool for the indirect measurement of mobility of minority carriers.

Surface recombination velocity has great significance in the fabrication of optoelectronic devices and the value of it depends on the growth technique employed for manufacturing of semiconductor wafer as well as on the quality of wafer. In general, surface contains large number of recombination centers due to the abrupt stop in the growth process. The present measurements are carried out on the rear surface recombination velocity, which have much significance when a semiconductor wafer is exposed to optical radiation as in many practical situations. The values of

G 8651

surface recombination velocity depicted in table I give a clear picture of surface recombination velocity of these intrinsic samples grown using Liquid Phase Epitaxial technique.

The applicability of compound semiconductors for the fabrication of optical sources used in optoelectronic industry is mainly due to the larger value of quantum efficiency. As these materials have direct bandgap, radiative transition dominates over the phonon assisted nonradiative recombination mechanism that results in higher value of quantum efficiency. The nonradiative lifetime (τ_{nr}) of these semiconductors are related to total lifetime (τ_T) of the carriers through its relation with radiative lifetime (τ_r), and is given by $\dfrac{1}{\tau_T} = \dfrac{1}{\tau_r} + \dfrac{1}{\tau_{nr}}$. In the case of undoped samples, auger recombination dominates over the impurity assisted SRH recombination mechanism. The nonradiative recombination time and carrier concentration are related through the expression $\tau_{nr} = \dfrac{1}{Cn_i^2}$, where C is the auger coefficient and n_i is the carrier concentration [29]. The auger coefficient are $\sim 0.9 \times 10^{-30}\, cm^6 s^{-1}$ for InP, $\sim 10^{-30}\, cm^6 s^{-1}$ for GaAs and $\sim 5 \times 10^{-26}\, cm^6 s^{-1}$ for InSb and the values of carrier concentration are $10^{17} cm^{-3}$ for InP, $10^{18} cm^{-3}$ for GaAs and $10^{16} cm^{-3}$ for InSb, respectively. The calculated value for nonradiative recombination time of the samples agrees well with the measured value given in table I. The present investigation shows that in the case of intrinsic samples auger recombination is the dominating nonradiative recombination mechanism in semiconductors.

3.5.3. Conclusion

In conclusion, the effectiveness of PA technique for the measurement of thermal and transport properties of semiconductors is demonstrated. It is seen that the PA technique under heat transmission configuration is an indirect tool for the measurement of mobility of minority carriers. It is seen from the analysis that in the

case of intrinsic samples, auger recombination is the dominating nonradiative recombination mechanism as compared to deep level assisted SRH recombination mechanism.

PART – B

3.6. Photoacoustic studies on intrinsic and doped Si

3.6.1. Introduction

Silicon is a key material that is used many microelectronic and microelectromechanical (MEMS) devices. In recent times, fabrication and characterisation of porous silicon has attracted much attention due to its enhanced photoluminescence property and its wide applications in the industry and even as a biomedical material [30]. Very recently, a study on the enhancement in internal quantum efficiency of pure crystalline silicon has been reported, which may revolutionalise the applications of silicon especially in the field of optoelectronics [17]. The conventional methods used for thermal analysis suffer from two problems such as need for relatively large size of the specimen and lenghty experimental procedures[31]. However, using the laser induced PA technique, the measurements can be carried out on a relatively shorter duration and on specimens having smaller size. Eventhough, a large number of studies have been reported on applications of PA technique for the measurement of thermal and transport properties of doped semiconductors, a systematic study of influence of nature of dopant on the thermal and transport properties of Silicon using PA technique under heat transmission configuration is yet to be reported.

The experimental technique and procedure is the same as that described in the earlier sections. The samples used for the present analysis are intrinsic Si and Si doped with B and P. Intrinsic Si has a carrier concentration of $10^{18} cm^{-3}$, whereas doped samples have a doping concentration of $10^{18} cm^{-3}$.

3.6.2. Results and Discussions

Figures 7, 8 and 9 show the variation of PA signal phase under heat transmission configuration as a function of modulation frequency for intrinsic Si and Si doped with B and P, respectively. The fitting procedure and errors involved in the analysis are the same as that mentioned earlier, in this chapter. The values obtained for the samples are given in table II.
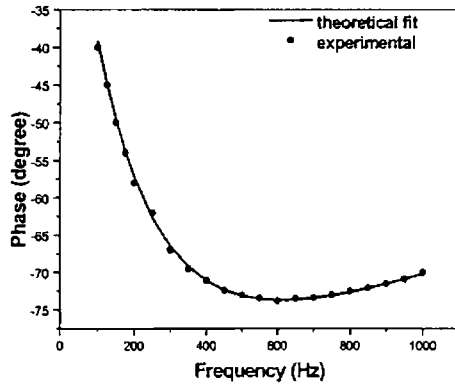
Figure 7. PA phase angle for intrinsic Si versus modulation frequency. The solid lines represents the best fit of the data o equation (11)
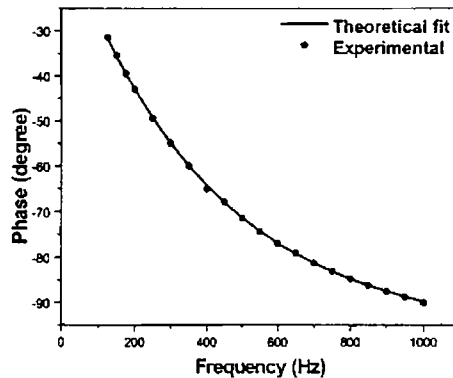
Figure 8. PA phase angle for B doped Si versus modulation frequency. The solid lines represents the best fit of the data to equation (11)
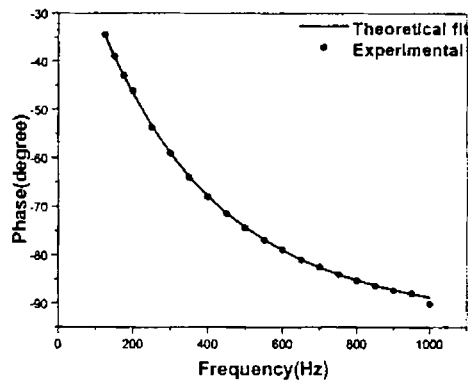
Figure 9. PA phase angle for P doped Si versus modulation frequency.
The solid lines represents the best fit of data to equation (11)

Sample	Thermal diffusivity (cm^2s^{-1})	Diffusion coefficient (cm^2s^{-1})	Surface recombination velocity (cms^{-1})	Nonradiative recombination time (μs)
Si	0.88	11.6	489	8.0
Si: B	0.81	10.6	632	0.9
Si: P	0.84	10.1	526	2.0

Table II. Thermal and transport properties of intrinsic and doped Si

As explained earlier, the thermal energy in semiconductors having carrier concentration less than $10^{20}cm^{-3}$ is essentially carried away by phonons. The various scattering mechanisms occurring during the propagation of phonon can affect the phonon mean free path in a substantial manner and can result in the reduction of phonon mean free path. The reduction in phonon mean free path results in the reduction of lattice thermal conductivity (thermal diffusivity). This phonon scattering

103

phenomena is a key source that limits the performance of many electronic and optoelectronic devices. The present investigation shows that doped samples have a reduced value for thermal diffusivity in comparison with intrinsic specimen, as a result of additional scattering centers arising due to doping, as noticed in the compound semiconductors (previous chapter). Nevertheless it is interesting to point out here that p-type sample shows a much reduced value for thermal diffusivity in comparison with n-type sample. The impurity scattering rate in the case of doped samples is proportional to the mass difference between the atom in the host lattice and the impurity atom [32]. In the present case, the mass difference between B and Si is greater than that between P and Si. Thus the increased scattering rate in B doped Si as compared to P doped Si results in a reduced value for thermal diffusivity for a given doping concentration. In addition to it, in case of p-type specimen, phonons suffer large scattering from holes having greater effective mass as compared to the electrons in the n-type sample [33]. Thus the p-type B doped Si shows a much reduced value for thermal diffusivity in comparison to P doped n-type Si.

Diffusion coefficient, the value of which is essentially determined by the mobility of photoexcited carriers is also sensitive to doping and even to the nature of dopant. Doping can result in the lowering of mobility of carriers and hence the value of diffusion coefficient. It is also reported that the diffusion coefficient has an inverse square root relation with effective mass of the photoexcited carriers. It is further seen from the table that the diffusion coefficient of n-type specimen is less than that of p-type sample. This owes to the fact that in the case of n-type sample, the minority carriers are holes, which have low mobility due to its greater effective mass as compared to electrons in the p-type specimen.

In general, the surface contains large number of recombination centers due to the presence of dangling bonds at the surface. In addition, the impurities can also act as recombination centers for the photoexcited carriers. It was reported earlier that the surface recombination velocity of the semiconductors increases with increase in doping concentration [34]. It is seen from the table I that the surface recombination

velocity of doped samples is greater than that of intrinsic one. It can be understood from the relation $v = \sigma v_{th} N_{st}$ (where σ is the capture cross section for the photoexcited carriers, v_{th} is the thermal velocity of the photoexcited carriers, and N_{st} is the number of trapping centers per unit area) that the surface recombination velocity is proportional to the density of surface trapping centers. Introduction of dopant results in the increase in number of trapping centers for photoexcited carriers and consequent increase in surface recombination velocity, which agrees well with the present experimental observation. However, for a given doping concentration, the surface recombination velocity is proportional to the thermal velocity of the photoexcited carriers and thus it has an inverse relation with the square of effective mass of photoexcited carriers. In the case of p-type specimen, the minority carriers are electrons with lower effective mass. Hence the surface recombination velocity of photoexcited carriers in p-type material is greater than that of n-type material.

The nonradiative recombination lifetime of Si is extremely important, as a recent investigation shows a considerable increase in the internal quantum efficiency of pure Si. Unlike compound semiconductors, it is phonon assisted recombination mechanism that is dominant in the case of Si. The nonradiative recombination time is inversely related to the thermal velocity of the photoexcited carriers as well as to the number of scattering centers through the expression $\tau_{nr} = \dfrac{1}{N_{st} v_{th} \sigma}$. The introduction of dopant increases the scattering centers in the specimen, which in turn results in the decrease of nonradiative recombination time as observed in the present investigation. However, for a given doping concentration, the nonradiative lifetime is inversely proportional to the thermal velocity of minority carriers. Hence in the case of n-type specimen, where the minority carriers are holes with lower thermal velocity due to its greater effective mass, a higher value for nonradiative recombination time occurs as compared to p-type specimen as observed in the present measurement.

3.6.3. Conclusion

The thermal and transport properties of intrinsic Si and Si doped with B and P has been measured using open cell photoacoustic technique. From the analysis of the data it is seen that doping can affect the thermal and transport properties viz., thermal diffusivity, diffusion coefficient, surface recombination velocity and nonradiative recombination time in a substantial manner. It is also seen that these parameters are sensitive even to the nature of dopant.

PART – C

3.7. Measurement of transport properties of GaAs epitaxial layers

3.7.1 Introduction

The perfection of various epitaxial growth techniques and composition dependent tailoring of lattice spacing have changed the scenario of application of semiconductors in the optoelectronic industry, especially for the fabrication of semiconductor lasers. In this context, thermal characterisation of semiconductor nanostructures and layered structures has recently attracted a lot of attention due to the increase in power dissipation per unit area with reducing the size of active devices. Also there exists a need to fabricate thermoelectric devices of low thermal conductivity. These two contrary demands can be approached with appropriate modification of phonon modes, which is the main concern of phonon engineers. The versatility of PA technique under heat transmission configuration extends to allow the simultaneous measurement of thermal and transport properties of epitaxial semiconductor layers grown on GaAs substrate. Recent investigations show that doping can affect the surface recombination velocity of epitaxial layers [34]. However, a detailed investigation on the influence of doping concentration on the thermal and transport properties of epitaxial layers is still in the initial stages.

This part of work is focused on the PA measurements on the epitaxial layer of GaAs doped with different concentration of Si, grown on a GaAs substrate by molecular beam epitaxy (MBE). The thermal and transport properties of epitaxial

layers are evaluated using the procedure explained in earlier sections. The epitaxial layers have thickness of 10.25, 3 and 2 μm, and the respective carrier concentrations are 2×10^{14}, 2×10^{16} and 2×10^{18} cm^{-3}.

3.7.2. Results and Discussions

All the measurements made on epitaxial layers are treated under monolayer approximation. The investigations on the influence of doping concentration on surface recombination velocity of Ge doped GaAs eptixial layers under monolayer approximation have already been reported [34]. The difference between two layer approximation and the monolayer method for photothermal experiments are apparent only at high frequencies, viz., in the range of hundreds of kilohertz [35]. As the epitaxial layers are grown using MBE technique, an isothermal contact can be assumed at the substrate/layer interface [36]. The fitting procedure and the errors involved are the same as explained earlier.

Figures 10, 11 and 12 show the variation in phase of PA signal as a function of modulation frequency. It is seen from the figures that there is a minimum in the phase plot of all the specimens under investigation. Many authors have attributed this shape of the curve arising from change in heat generation mechanism in semiconductors from bulk nonradiative recombination to surface recombination of photoexcited carriers [19-20, 36]. From the present studies, it is seen that the frequency at which the phase data show a minimum, changes with the concentration of dopant. This may be due to the increase in recombination centers with increase in doing concentration, which in turn enhances the heat generation due to bulk recombination. The values obtained for the specimens are tabulated in table III.
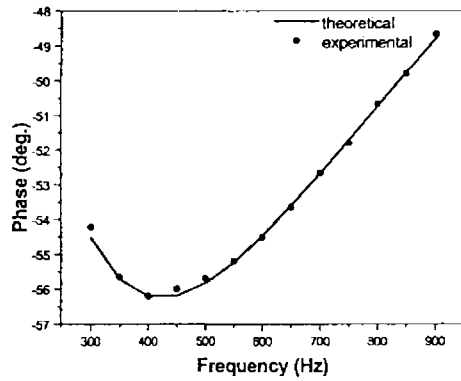
Figure 10. OPC phase angle for sample 1 versus modulation frequency.
The solid lines represents the best fit of the data to equation (11)
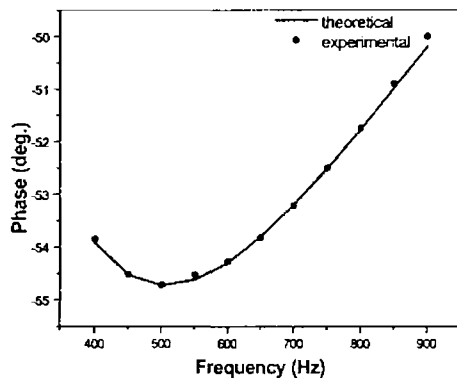
Figure 11. OPC phase angle for sample 2 versus modulation frequency.
The solid lines represents the best fit of the data to equation (11)
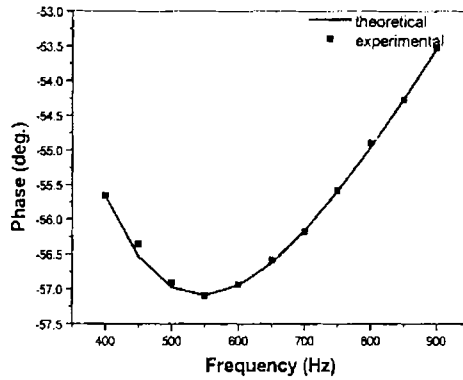
Figure 12. OPC phase angle for sample 3 versus modulation frequency. The solid lines represents the best fit of the data to equation (11)

Sample Number	1	2	3
Thickness of Epitaxial layer in μm	10.25	3	2
Thickness of Substrate in μm	400	400	400
Concentration of Silicon in cm^{-3}	2×10^{14}	2×10^{16}	2×10^{18}
Thermal diffusivity in cm^{2}s^{-1}	0.26	0.23	0.21
Diffusion Coefficient in cm^{2}s^{-1}	5.2	4.9	4.5
Surface recombination velocity in cms^{-1}	415	476	525
Nonradiative recombination time in μs	11.2	9.8	7

Table III. Thermal and transport properties of GaAs epitaxial layers

From table III it is seen that the thermal diffusivity value decreases with increase in doping concentration. This is because, as explained earlier, introduction

of dopant can act as point defects in the lattice and creates additional scattering centers for phonons which in turn reduces the phonon mean free path and hence the thermal conductivity value. As thermal conductivity and thermal diffusivity are directly related through the relation $\alpha = k/\rho C$, where k is the thermal conductivity, ρ is density and C is specific heat capacity, the reduction in thermal conductivity reduces the thermal diffusivity value with doping concentration. The relation between lattice thermal conductivity k and lattice thermal resistivity W through the equation $k = 1/W = AT^{-n}$ suggests such a concentration dependent decrease in thermal conductivity. In the present case i.e, T=300K and A is a parameter which decreases with increase in doping concentration. The value of n is reported as 1.25 for GaAs [37].

From the values of diffusion coefficient obtained here, it is seen that it is not the ambipolar transport but the diffusion coefficient of minority carriers that essentially determines the PA signal generation. This means that at the incident laser power, the photo induced carrier population is less than impurity concentration. The mobility dependence of diffusion coefficient through Einstein's relation explains the experimentally observed decrease in diffusion coefficient with doping.

Addition of dopants has a strong influence on surface topology. The dopants results in the deterioration in the transport properties of the photoexcited carriers. One of the effects of incorporation of dopants is the generation of macrosteps (terraces), and the bunched macrosteps give rise to striation. It was reported earlier that the surface recombination velocity of the photoexcited carriers increases with increase in doping concentration of Ge on an epitaxial layer of GaAs [38], which agrees with the results of the present investigation. It can be understood from the relation $v = \sigma v_{th} N_{st}$; that surface recombination velocity is directly proportional to density of surface trapping centers. The number of trapping centers for photoexcited

carriers at the surface of epitaxial layer increases with doping, leading to an increase in surface recombination velocity.

The present measurements suggest that doping can also affect the nonradiative recombination time of the photoexcited carriers. It is important to point out that the photoexcited signal is very sensitive to carrier lifetime, so that the proper choice of this parameter is a significant step in the simulation processes. In the case of doped semiconductors, especially for GaAs, the nonradiative recombination time due to both SRH and auger recombination time are of comparable magnitude. Introduction of dopants results in deep levels in the bandgap of GaAs and enhance deep level assisted SRH recombination mechanism [39]. The nonradiative recombination time is inversely related to the thermal velocity of the photoexcited carriers as well as to the number of scattering centers through the expression $\tau_{nr} = \frac{1}{N_{st} v_{th} \sigma}$. The introduction of dopant increases the scattering centers in the specimen, which in turn results in the decrease of nonradiative recombination time as observed in the present investigation.

3.7.3. Conclusion

This section of the present chapter clearly demonstrates the capability of PA technique in general and OPC detection in particular to study the thermal and transport properties of photoexcited carriers in layered structures. The influence of doping concentration on the thermal and transport properties of epitaxial layer of GaAs doped with Si of various concentrations is investigated using thermal wave transmission and detection technique. From the analysis of experimental data, it is obvious that the thermal diffusivity of epitaxial layers decreases with increase in doping concentration. It is likewise seen that the diffusion coefficient of minority carriers decreases with increase in doping concentration, which is evidently due to the reduction in mobility of carriers with doping. Doping also influences the surface recombination velocity and nonradiative recombination time. The surface

recombination velocity of the photoexcited carriers increases with increasing doping concentration, whereas the nonradiative recombination time decreases.

3.8. References

1. H. Vargas and L. C. M. Miranda, Review of Scientific Instruments, 74 (1), 794, (2003).
2. H. Vargas and L. C. M. Miranda, Phys. Rep. 161 (2), 43 (1988).
3. J A Balderas-Lopez and A. Mandelis, J. Appl Phys. 88 (11) 6815 (2000).
4. Ristovski Z D and M. D. Dramicanin, Appl. Opt. 36 (3) 648 (1997).
5. S. Sankara Raman, V. P. N. Nampoori , C. P. G. Vallabhan, G. Ambadas and S. Sugunan, Appl. Phys. Lett., 67, 2939 (1995).
6. Qing Shen and Taro Toyoda, Jpn. J. Appl. Phys., 39, 511 (2000).
7. Qing Shen and Taro Toyoda, Jpn. J. Appl. Phys., 39, 3164 (2000).
8. D. M. Todorovic, P. M.. Nikolic, M. D. Dramicanin, D. G. Vasiljevic and Z. D. Ristovski, J. Appl. Phys. 78(8), 5750 (1995).
9. D. M. Todorovic, P. M. Nikolic, D. G. Vasiljevic and M. D. Dramicanin, J. Appl. Phys. 76 (7), 4012 (1994).
10. P. M. Nikolic, D. M. Todorovic, A. I. Bojicic, K. T. Radulovic, D. Urosevic, J. Elzar, V. Balgojevic, P. Mihajlovic and M. Miletic, J. Phys. Condens. Matter. 8, 5673 (1996).
11. P. M. Nikolic, D. M. Todorovic, D. G. Vasiljevic, P. Mihajlovic, Z. D. Rsitovski, J. Elzar, V. Blagojevic and M. D. Dramicanin, J. Microelcton., 27, 459 (1996).
12. I. Delgadillo, M. Vargas, A. Cruz-Orea, J. J. Alvarado-Gil, R. Baquero, F. Sanchez Sinencio and H. Vargas, Appl. Phys. B, 64, 97 (1997).
13. D. M. Todorovic and P. M. Nikolic, Opt. Eng. 36 (2), 432- 445 (1997).
14. J. B. Alavrado, M. Vargas, J. J. Alavarado-Gil, I. Delgadillo, A. Cruz-Orea, H. Vargas, M. Tufino Velazquez, M. L. Albor-Aguilera and M. A. Gonzalez-Trujillo, J. Appl. Phys. 83 (7), 3807 (1998).
15. E. Marin, I. Riech, P. Diaz, J. J. Alvarado-Gil, R. Baquero, J. G. Mendoza-Alvarez, H. Vargas, A. Cruz-Orea and M. Vargas, J. Appl. Phys. 83 (5), 2604 (1998).
16. Sajan. D. George, Saji Augustine, Elizabeth Mathai, P. Radhakrishnan, V. P. N. Nampoori and C. P. G. Vallabhan, Phys.stat. sol. (a), 196 (2) 384 (2003).
17. T. Trupke, Appl Phys. Lett. 82, 2996 (2003).
18. A. Rosencwaig and A. Gersho, J. Appl. Phys., 47, 64 (1976).
19. A. Pinto Neto, H. Vargas, N. Leite and L. C. M. Miranda, Phys. Rev. B 40, 3924 (1989).
20. A. Pinto Pinto Neto, H. Vargas, N. Leite and L. C. M. Miranda, Phys. Rev. B, 41, 9971 (1990).
21. I. Riech, P. Diaz, T. Prutskij, J. Mendoza, H. Vargas and E. Marin, J.Appl.Phys. 86 (11), 6222(1999).
22. Jasprit Singh, Semiconductor Optoelectronics, Physics and Technology (Mc-Graw Hill, Singapore) 1995.
23. Sajan D George, Dilna. S, P. Radhakrishnan, V. P. N.Nampoori and C. P. G. Vallabhan, Phys. stat. Sol. 195 (2), 416 (2003).
24. A. Mandelis Physics Today, August, 29-34 (2000).
25. L. D. Favro and Xiaoyan Han, in Sensing for Materials Characterisation and Processing" (Edits. George Birnbaum and Bert. A. Auld) Vol 1, 399 (1998).

26.   G. Gonzlaez de la Cruz and Yu G Gurevich, Revista Mexicana De Fisica 45 (1) 41 (1999).

27.   Yu. G. Gurevich, G. Gonzalez de la Cruz, G. Logvinov and M. N. Kasyanchuk, Semiconductors, 32(11), 1179 (1998)

28.   F. Saadallah, N. Yacoubi and A. Hfaiedh, Optical Mateials, 6, 35-39 (1996).

29.   M Levinshtein, S. Rumyantsev and M. Shur (Edits.), Handbook on Semiconductor Parameters (World Scientific, Singapore) 1996.

30.   T. Kawahara, M. Mihara, J. Morimoto, k. Tahira, A. Motohashi, A. Kinoshita and T.Miyakawa, Jpn.J.App.Phys 39, 505 (2000).

31.   M. Reading, D. J. Hourston, Mo.Song, H. M. Pollock and A. Hanniche, American Laboratory, 13, Jan (1998).

32.   Angela. D. Mcconnell, Srinivasan Uma and K. E. Goodson, Journal of Microelectromechanical System, 10 (3), 360 (2001)

33.   Sajan D George, P. Radhakrishnan, V. P. N. Nampoori and C. P. G. Vallabhan, J. of Phys. D: Appl. Phys. 36 (8), 990 (2003).

34.   I. Riech, E. Marin, P. Diaz, J. J. Alvarado Gil, J. G. Mendoza Alvarez, H. Vargas, A. Cruz Oreas M. Caras J. Bernel Alvarado, Phys.stat.sol (a), 169, 275 (1998).

35.   C. Christofields, F. Diakonos, A. Seas, A. Christou, M. Nestoros and A. Mandelis, J. Appl.Phys, 80 (3), 1718 (1996).

36.   Sajan D George, Dilna.S, R. Prasanth, P. Radhakrishnan, C. P.G . Vallabhan and V. P. N. Nampoori, Opt, Eng., 42 (5) 1476 (2003).

37.   Sadao Adachi, Physical properties of III-V compound semiconductors (Wiley Intersicence, New York) (1992).

38.   I. Riech, E Marin, P. Diaz, J. J. Alavardo Gil, J. G. Mendoza-Alvarez, H. Vargas, A. Cruz-Orea, M. Vargas and J. Bernal Alvarado, Phys. Stat. Sol. (a), 169, 275 (1998).

39.   E. Marin, I. Riech, P. Diaz, J. J. Alvarado Gil, R. Baquero, H. Vargas, A Cuz-Orea and M. Vargas, J.Appl. Phys 83(3), 2604 (1998).

114

Chapter 4

Thermal characterisation of porous ceramics and conducting polymers

Abstract

Thermal characterization of two important classes of photonic materials is presented in this chapter, which consists of two sections. The first part deals with the measurements of thermal diffusivity of nano Ag metal dispersed ceramic Alumina matrix. Analysis of data shows that the pores in the lattice of the specimen sintered at different temperature can affect propagation of phonons in the lattice in a substantial manner and can result in the variation of thermal diffusivity value. In the second section measurements carried out on the thermal diffusivity of the conducting polymer namely, Polyaniline (PANI) doped with Camphor Sulphonic Acid (CSA) is described. Investigations on the heat transport on the composites of CSA doped PANI with CoPc are also carried out, details of which are given in this chapter.

PART – A

4.1. Thermal characterisation of porous nanometal dispersed ceramic alumina matrix

4.1. 1. Introduction

Ceramics are considered to be the one of the most suitable component for the fabrication of many of the devices used in electronic and optoelectronic industry. The wide applicability of these materials for the thermal, optical and structural applications is due to their special properties such as tunable electrical properties, toughness, high temperature tolerance, light weight and excellent resistance against corrosion and wear [1-2]. The thermal properties of these ceramics are basically determined by their composition and structure [3-4]. It is the rate of heat diffusion that essentially determines the thermal shock resistance of brittle solids such as ceramics. In the case of ceramics, thermal accumulation causes thermal induced stresses in the sample, which in turn causes catastrophic failure and deterioration in ceramic-based devices. The thermal shock resistance of ceramics can be improved by the incorporation of a nanometal with high thermal conductivity value into the ceramic matrix.

The functional nanocomposites involving a ceramic matrix and nanosized particles of transition metals, are known to exhibit multifunctional and attractive properties and are identified as potential candidates for structural [5], mechanical [6], catalytic [7-8], thermal [9-10], optical [11-12], magnetic [13-14] and electrical [15-18] applications. The mechanism behind such enhanced properties is found to be closely associated to the grain size distribution, grain morphology, the nature of grain boundaries and interfaces, the nature of intra-grain defects and interface purity [19]. Particularly, the thermal properties of nanometal dispersed ceramic matrix depend on porosity and grain size of these particles.

As has been demonstrated in the previous chapters, the laser induced photoacoustic (PA) and photothermal techniques are most suited for the

nondestructive and nonintrusive studies of the material parameters and structural defects of the materials including ceramics [20-21]. Thermal diffusivity is one of the importantthermophysical parameter, which has been studied effectively using the simple and elegant PA technique [22]. The dependence of PA signal on how heat diffuses through the specimen gives an indirect way to investigate the structural aspects of ceramics through the measurement of thermal diffusivity value. The importance of thermal diffusivity also lies in the fact that this unique thermophysical parameter determines the diffusion of heat through the specimen and it can be correlated with the hardness of the specimen. It has also been reported that local measurement of thermophysical parameters of the ceramics using photothermal techniques are an effective tool of measure some of the inherent properties of ceramics, which are hard to measure using conventional methods. A recent investigation shows the effectiveness of nondestructive photothermal technique for profiling the hardness of the material, which has tremendous applications in the industrial area, especially in the device fabrication [23]. The propagation of phonons and hence the value of thermal diffusivity are very much influenced by the structural variations arising due to variation in sintering temperature, incorporation of foreign atom etc. In the present section of thesis, a study of nanometal Ag dispersed on ceramic alumina sintered at 800^0C and 900^0C with various concentration of Ag atom (0%, 1% and 5%) is presented.

4.1.2. Preparation of the sample

The composite precursor was prepared from a mixture of boehmite (Al-O-OH) and silver nitrate. In a typical experiment, 1000 ml of boehmite (Al-O-OH) sol was prepared by hydrolyzing 250gm of $Al(NO_3)_3.9H_2O$ [S. D. Fine Chemicals, India] dissolved in 500ml of double distilled water followed by peptisation using nitric acid. Details of the method are reported elsewhere [24]. Silver nitrate [Glaxo Laboratories, India, Purity – 99%] in aqueous solution (5gm in 100ml) is added in different weight proportions (0%, 1% and 5 % with respect to aluminium oxide), to the boehmite sol

118

in separate batches and subjected to a mechanical stirring for a period of 4hours. The sol was first evaporated on a water bath and finally was dried at 90^0C. The precursor gel was further calcined at 450^0C for a period of 3hours. The nanocomposite samples were prepared by uniaxial consolidation to disc pellets of size 10mm diameter and 1mm thickness using a force of 4 tons for two minutes using hydraulic press. Care was taken to pelletise all the samples at identical experimental conditions. The pelletised samples are sintered at 800^0C and 900^0C with a soaking period of 3hours, to study the influence of sintering temperature on thermal diffusivity. The sintering temperature was limited due to the fact that the melting point of Ag is ~960^0C.

The Thermo Gravimetric (TG) studies undertaken by TGA-50H thermal analyzer (Shimadzu-50H, Japan) and the Differential Thermal Analysis (DTA) pattern taken confirms the Ag^+ ion formation. The XRDs of the specimens show that the samples are semicrystalline in nature. The microstructure of the sample is analyzed using Transmission Electron Microscopy (JEOL 3000 EX; JAPAN with an acceleration voltage of 300KV and a resolution of less than 0.2 nm) and it is seen that Ag particles are almost uniformly dispersed and the particle size in the dispersed phase ranges from 5 to 20 nm. All these samples are prepared at Ceramic Division of Regional Research Laboratory, CSIR, Trivandrum, India. The detailed explanations of preparation of these specific specimens are found elsewhere [25].

The density of the composite is determined by a water displacement method. The measured density is divided by a corresponding theoretical density, which gives the volume fraction or relative density (x) of the specimen. Then the porosity of the material is given by $p = 1 - x$ [26]. The values of porosities of specimen under study are incorporated into tables I. From the table it is obvious that both the sintering temperature and percentage of foreign atom have great influence on the porosity of the specimen. The porosity has great effect on determining the thermophysical parameters of ceramics.

Sintered Temperature (in ^{0}C)	Amount of Ag (in %)	Porosity
800	0	0.481
	1	0.418
	5	0.234
900	0	0.450
	1	0.410
	5	0.216

Table I. Porosity of the samples under investigation

4.1.3. R-G. Theory of thermal diffusivity measurements

According to Rosencwaig and Gersho theory [27] the pressure variation Q at the front surface of an optically thick sample $(l >> \frac{1}{\beta}$ where β is the optical absorption coefficient) depends on the thermal diffusivity of the sample and can be written as

$$Q = qe^{-j\phi} = BA \tag{1}$$

where $q = |Q|$, ϕ is the phase shift between Q and the excitation source, and B and A are given by

$$B = \frac{P_o \gamma W_a l \sqrt{\alpha^1}}{2l^1 T_0 K \sqrt{\alpha}} \tag{2}$$

and

$$A = \left[1 + \frac{g(d^+ + d^-)}{(d^+ - d^-)}\right]\left[g + \frac{(d^+ + d^-)}{(d^+ - d^-)}\right]\left(\frac{1}{\sigma l}\right)^2 \tag{3}$$

where $d^+ = e^{\sigma l}$; $d^- = e^{-\sigma l}$ and $\sigma = (1+j)\left(\frac{\pi f}{\alpha}\right)^{\frac{1}{2}}$ \tag{4}

120

and g is the ratio between the effusivities of the backing material (e") and the sample (e)

$$g = \frac{e''}{e} = \left(K''/K \right) \left(\alpha/\alpha'' \right)^{1/2} \qquad (5)$$

In the above expressions l, K and α are thickness, thermal conductivity and thermal diffusivity of the specimen, respectively. T_o and P_o are the ambient temperature and pressure, γ is the ratio of specific heats, W_a is the amount of light absorbed and l' and α' are the thickness and thermal diffusivity of the gas. The thermal effusivity of the gas can be neglected compared to the effusivity of the sample, the ratio being less than 1%. The term A depends on the modulation frequency through the product σl where

$$\sigma = (1 + j) \left(\pi f/f_c \right) \qquad (6)$$

f_c is the characteristic frequency, which can be obtained from (4) and (6) as

$$f_c = \alpha/l^2 \qquad (7)$$

The thermal diffusivity α can be determined by measuring the amplitude of PA signal as function of chopping frequency. One of the factors that determines the amplitude of the PA signal is the thermal diffusion length (μ) given by

$$\mu = \left(\alpha/\pi f \right)^{1/2} \qquad (8)$$

where f is the chopping frequency. When the sample is thermally thin ($\mu > l$), the PA signal gets modified by the thermal properties of the backing material. In the thermally thick regime the PA signal is independent of the thermal properties of the backing material. For a given sample thickness, one can have a transition from thermally thin regime to thermally thick regime by increasing the chopping frequency, Hence in the log(amplitude) versus log(frequency) plot a slope change

occurs at the characteristic frequency $\left(f_c\right)$. Knowing the characteristic frequency and the sample thickness, we can calculate thermal diffusivity as

$$\alpha = l_s^2 f_c \tag{9}$$

4.1.4. Experimental Setup

The source used for the present investigation and the experimental conditions are the same as that explained in previous chapters. However, the major difference between the present measurements and the earlier studies is that in the present case, the reflection configuration is employed so that in the thermally thin region, the properties of the backing material determines the PA signal generation. The cell is designed in such a way that the its walls have good acoustic impedance and the cell is acoustically isolated. The material used for making the cell window, glass, is completely transparent at the incident wavelength, which is important to avoid the influence of window in PA signal generation. In order to minimize the PA signal from the walls due to the absorption of incident radiation, the thermal mass materials used for the fabrication of PA cell should be quite large. In the present studies, perspex having large thermal mass is used for the fabrication of cell. The cylindrical geometry is chosen for the cell cavity with an orifice opening to microphone cavity so as to avoid the scattered light reaching the microphone. The volume of the acoustic cavity is so chosen such that it is minimum and the cell is nonresonant under the present experimental condition. At the same time care also be taken while choosing the volume of the cell so as to avoid the complete damping of acoustic signal before reaching the microphone. The microphone used (Knowles BT 1754) has a flat response over the frequency range between 30-4000 Hz.

4.1.5. Results and Discussion

Initially the experimental setup used for the present investigation is calibrated by the evaluation of thermal diffusivity of Cu. Figure 1 shows the variation of

log(PA amplitude) as a function of log (frequency). By knowing the transition frequency at which the sample changes from thermally thin to thermally thick region from the graph, the thermal diffusivity value $(1.18 \pm 0.003 \ cm^2s^{-1})$ is evaluated, which is found to be in good agreement with earlier reported value [21].
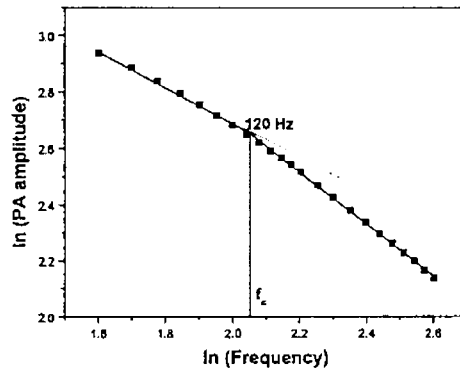
Figure 1. Variation of PA amplitude with modulation frequency

Figures 2 to 4 represents variation in amplitude of PA signal as function of modulation frequency for samples sintered at 800^0C and having Ag concentration 0%, 1% and 5% respectively.

Figure 2. Amplitude spectrum of intrinsic alumina sintered at 800ºC

Figure 3. Variation of PA amplitude with modulation frequency of alumina containing 1% Ag nanometal sintered at 800°C

Figure 4. Variation of PA amplitude with modulation frequency of alumina containing 5% Ag nanometal sintered at 800°C

Figure 5 to 7 represent the PA amplitude spectrum for samples sintered at 900°C having Ag concentratons o%, 1% and 5 %

124
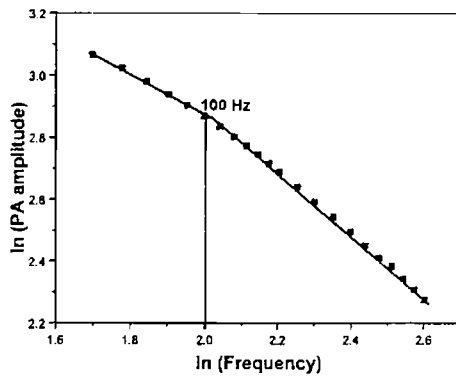
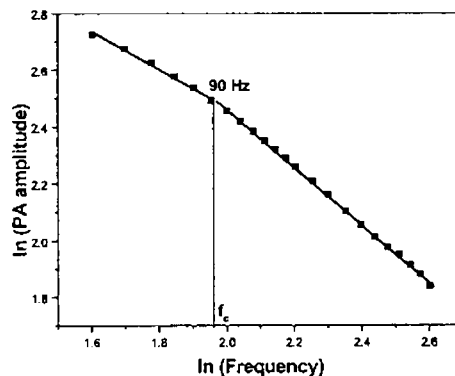Figure 5. Variation of PA amplitude with modulation frequency of intrinsic alumina sintered at 900°C
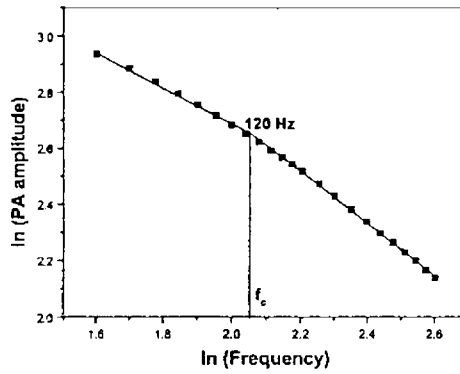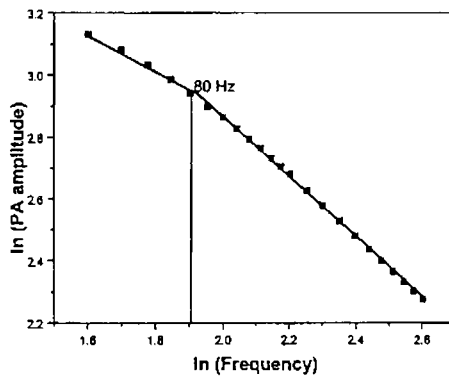

Figure 6. Variation of PA amplitude with modulation frequency of alumina containing 1% Ag nanometal sintered at 800°C
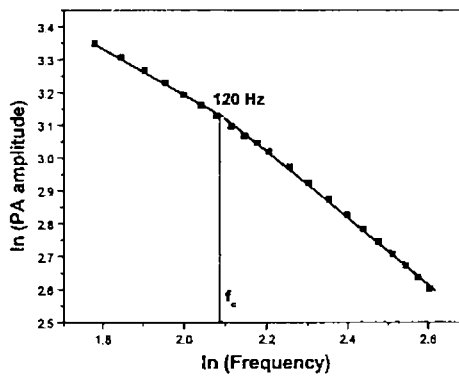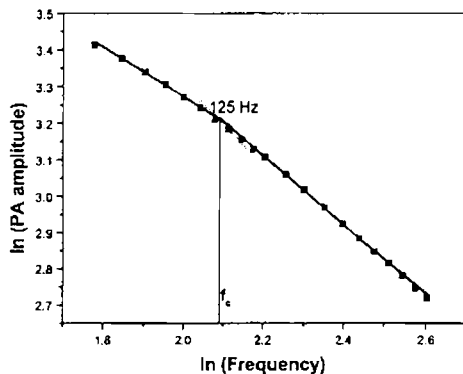
Figure 7. Variation of PA amplitude with modulation frequency of
alumina containing 5% Ag nanometal sintered at 900°C

The measured values of thermal diffusivities and thickness of all the
specimens under investigation are tabulated in table II.

Sintered Temperature (°C)	Amount of Ag (in %)	Sample thickness (in μm)	Transition frequency (in Hz)	Measured thermal diffusivity $(cm^2 s^{-1})$	Calculated value of thermal diffusivity $(cm^2 s^{-1})$
800	0	520	90	0.243 ± 0.003	0.240
	1	480	120	0.276 ± 0.006	0.280
	5	550	120	0.363 ± 0.005	0.362
900	0	530	100	0.280 ± 0.004	0.279
	1	630	80	0.316 ± 0.004	0.311
	5	560	125	0.392 ± 0.005	0.400

Table II. Thermal diffusivity values of specimen under investigation

It is obvious from table II that, for specimens sintered at a particular
temperature, the thermal diffusivity value increases with Ag concentration. This
variation in thermal diffusivity can be understood in terms of variation in porosity

126

with the inclusion of nanometal and carrier assisted heat transfer mechanism in these samples. From table I it is also clear that the porosity of the specimen decreases with increase in concentration of nanometal in the ceramic bulk. This is due to the fact that the inclusion of metal increases the relative density of the composite resulting in higher mechanical strength. This fact has wide applicability in the device fabrication based on these materials. The observed variation in thermal diffusivity with porosity can be understood by considering the specimen as a two-phase mixture in which regular shaped particles are embedded in a continuous matrix. The corresponding thermal conductivity of the specimen is given by the Leob equation $K_c(p) = K_0(1 - p)$ where K_0 is the thermal conductivity of the specimen having zero porosity. Correspondingly, the thermal diffusivity value of the specimen having porosity 'p' is given by the expression $k_c(p) = k_0 \dfrac{(1 - p)}{(1 - p)}$ resulting in thermal diffusivity values, which are independent of porosity. However, all the measurements on thermal diffusivity under present investigation exhibit a strong dependence on the porosity of the specimen. In order to incorporate the influence of pores in the propagation of thermal waves and hence the thermal diffusivity value A. Sanchez etal. [26] modified the Leob equation for the evaluation of thermal diffusivity value

as $$k_c(p) = k_0 \frac{(1 - \gamma p)}{(1 - p)}$$ ·(10)

where γ is an empirical constant which essentially determines the significance of pores on thermal diffusion processes. The evaluated values of γ are 1.472 and 1.450 for the specimens sintered at 800^0C and 900^0C. The value of $\gamma > 1$ also implies the fact that the effect of porosity on heat conduction processes is not a mere density effect (air holes in the bulk volume) but it is also related to the structure of the material. Thus enhancement in relative density with the inclusion of metal into the ceramic matrix and consequent lowering of porosity of the specimen result in the efficient heat transfer in the metal dispersed ceramics, which in turn results in higher

value for thermal diffusivity. Besides that, in the case of metal dispersed ceramics, the interconnected metal network provides an efficient way to heat transport processes across the composite by electrons and therefore enhances the heat diffusion mechanism. Thus, in the case of metal dispersed ceramic matrix, heat is essentially carried by both phonons and electrons. Such an increase in thermal diffusivity with the inclusion of Ag doped Zirconia composites have already been reported [28]. An increased thermal diffusivity (thermal conductivity) reduces thermal accumulation in the specimen and a consequent increase in the resistance against thermally induced fracture enhances the applicability of these materials in the industry.

It is also seen from the tables that the sintering temperature also influences the thermal diffusivity value. Calcination of the specimen during its preparation results in the expulsion of organic material, volatile impurities and moisture content in the sample. The treatment of gel at higher temperature (sintering) substantially reduces the number of pores in the lattice and enhances the connectivity. This is obvious from the fact that the relative density increases with sintering temperature which in turn results in the lowering of porosity with sintering temperature. The reduction of pores in the lattice reduces the scattering centers for heat carriers and increases its mean free path. This increase in the mean free path of heat carrier results in an increased value for thermal diffusivity [29] of the specimens sintered at higher temperature. An extrapolation of equation (10) yields the thermal diffusivity of the specimens having zero porosity as $0.240 cm^2 s^{-1}$ and $0.279\ cm^2 s^{-1}$ suggesting that increase in concentration of nanometal into ceramic host can results composites for higher thermal diffusivity value. From the present analysis it is obvious that the porosity decreases with sintering temperature and this suggests that samples of different thermal diffusivity value can be obtained by changing the sintering temperature.

128

4.1.6. Conclusion

In the present study, we have measured the important thermophysical parameter namely thermal diffusivity of pure alumina and nano Ag metal dispersed alumina ceramic matrix prepared by gel route. The present investigation throws light into the dynamics of heat diffusion process in the two-phase network. The present study also shows that the heat diffusion processes which is essentially characterized by the thermal diffusivity value, is sensitive to porosity of the specimen as well as to the inclusion of foreign atom into the host lattice. Also it can be seen that that thermal diffusivity value increases with decrease in porosity as well as with increase in metal content in a ceramic host. The sintering temperature has also great influence on the structural properties and hence on the thermal diffusivity value of the ceramics.

PART – B

4.2. Thermal characterisation of Camphor Sulphonic Acid doped Polyanilne and its composites with Cobalt Phthalocyanine

4.2.1. Introduction

The discovery of most recent generation of polymers, viz., conducting polymers, and the possibility to dope these polymers to obtain a full range of materials from insulator to metal have created a new field of research on the border line between chemistry and condensed matter physics [30]. The invention of this fourth generation of polymetric materials, offered the promise of achieving a new class of substances which can exhibit the electrical and optical properties of metal or semiconductors and while retaining the attractive mechanical properties and processing advantages of polymers [31-33]. The flexibility in electrical, structural and optical properties of these polymers can be achieved by various doping techniques such as chemical doping, electrochemical doping, photodoping, doping by acid base chemistry etc [30]. The electrochemical doping and related electrochemistry of conducting polymers have developed into a field of its own with

129

applications that range from polymer batteries and elctrochromic windows to ligh-emitting electrochemical cells. The chemistry and physics of non doped semiconducting state are of great interest because they provide a route to "plastic electronic" devices such polymer based light emitting diodes, plastic lasers, plastic photodiodes, photovoltaic cells, ultrafast image processors (optical computers), thin film transistors and all-polymer integrated circuits [34-36]. Conducting polymers also exhibit many novel properties that are not typically available in other materials such as availability of semiconducting and metallic polymers which are soluble in and processable from common solvents, availability of transparent conductors, and semiconductors in which the Fermi energy can be controlled and shifted over a wide range. Recent experimental studies have established that, for conducting polymers, the electrical properties and the mechanical properties improve together, in a correlated manner, as the degree of chain extension and chain alignment is improved [30]. The research works at the present time on conducting polymers are focused on the observation of superconductivity in doped conducting polymers [37-38]. The reason for such an optimistic approach is that they are metallic in nature and the coupling of the electronic structure to the molecular structure is well known. Upon doping, the bond lengths change such that charge is stored in solitons, polarons and bipolarons. Thus, the electron-phonon interaction that is responsible for superconductivity in conventional metal, leads to important effects in metallic polymers. In this context, doubly charge bipolarons can be thought of as analogous to real-space Cooper pairs.

Although the discovery of conducting polymers has been made in 1976, these materials are processed in metallic form only in early 1990s using polyaniline (PANI). PANI has been investigated over 100 years and attracted interest as a conducting polymer for several reasons: the monomer is inexpensive, the polymerization reaction is straight forward and proceeds with high yield, and PANI has excellent stability. The highly electrically conducting emeraldine salt (ES) form can be processed by post doping of a protonic acid with emeraldine base (EB) form or

using acid solution processing routes. In spite of the large number of experimental and theoretical studies devoted to the characterisation of physical properties of doped polyaniline, the thermal characteristics of these materials are not given sufficient attention. However, the thermal characteristics of these materials are extremely important, especially from the device fabrication point of view. In this section, for the first time, a study on the measurement of thermal diffusivity of Camphor Sulphonic Acid (CSA) doped PANI and its composites with Cobalt Pthalocyanine (CoPc) using open cell photoacoustic technique is presented. As the proper choice of volume fraction of composites allows the tunability in the thermophysical properties of materials, the present investigation has great importance in the context of modern optoelectronic industry.

4.2.2. Preparation of the sample

Polyaniline was prepared by the direct oxidation of aniline using a chemical oxidant. The monomer aniline and aqueous percholoric acid were kept at 4^0C to which ammonium per sulphate was added drop by drop. The mixture was then stirred for two hours followed by filtering and then washing with water and methanol. Subsequently, the polyaniline doped with percholorate was converted to insulating polyaniline emeraldine base (PANIEB) base using hydrazine hydrate. The PANIEB is doped with 0.5m CSA in nitrogen atmosphere to produce the emeraldine salt (ES) form of these specimens and the product is purified and dried in vacuum oven. The tetramer CoPc was prepared, purified and characterized by solution method. In this technique, CoPc, pyrometallic diahydride, excess urea, ammonium chloride and ammonium molybdate were grounded well and heated at 180^0C in nitorbenzene media for 12 hours. The reaction mixture was then cooled, washed with methanol several times to remove nitrobenzene. The crude product was further boiled with 2N sodium hydroxide contained sodium chloride and filtered. The residue was acidified with hydrochloric acid and washed several times and dried finally to obtain phthalocyanine tetramer. The composites of these materials were made as follows.

The powdered PANI doped with CSA was blended with tetrameric CoPc by mixing them homogenously in agate motor. Blends of CSA doped PANI and tetrameric CoPc corresponding to the specific volume fractions (90% PANI:CSA – 10% CoPc, 50% PANI:CSA – 50% CoPc and 10% PANI:CSA – 90% CoPc) were prepared. All these samples are black in colour.

4.2.3. Theoretical background

According to Rosencwaig and Gersho (RG) theory [29], with gas-microphone detection of PA effect, the signal depends upon the acoustic pressure disturbance at the sample-gas interface, which in turn depends on the periodic temperature variations at the sample-gas interface. Exact expressions for the temperature variations at the interface are derived on the basis of RG theory. However, the propagation of acoustic waves through the gas volume is treated in an approximate heuristic manner. For an optically opaque sample, all the incident radiation is absorbed at the surface of the sample. When a sinusoidally modulated light beam of intensity I_0 is incident on a sample surface with an absorption coefficient β, the heat density generated at any point x due to the light absorbed at this point can be represented by

$$\frac{1}{2}\beta I_0 e^{\beta x}\left(1+\cos\omega t\right) \tag{11}$$

According to R G theory, the pressure variations in the acoustic chamber for an OPC detection configuration is given by

$$Q_{th}=\frac{\gamma P_0 I_0\left(\alpha_g\alpha_s\right)^{1/2}}{2\pi T_0 l_g k_s f}\frac{e^{j\left(\omega t-\pi/2\right)}}{\sinh\left(l_s\sigma_s\right)} \tag{12}$$

where γ is the ration of specific heat capacities of air, $P_0\left(T_0\right)$ is the ambient pressure (temperature), f is the modulation frequency, l_i, k_i and α_i are the thickness, thermal

conductivity and thermal diffusivity of the medium i, where $i = g$ refers to the gas

and $i = s$ refers to the sample under investigation. Also $\sigma_i = (1 + i)a_i$, where

$a_i = \left(\dfrac{\pi f}{\alpha_i}\right)^{1/2}$ is the thermal diffusion coefficient of the medium i.

For a thermally thin sample, $(l_s a_s \ll 1)$, the above equation reduces to

$$Q_{th} \cong \frac{\gamma P_0 \alpha_g^{1/2} \alpha_s}{(2\pi)^{1/2} T_0 l_g l_s k_s} \frac{e^{j(\omega t - 3\pi/4)}}{f^{3/2}} \qquad (13)$$

In this case the amplitude of PA signal varies as $f^{-1.5}$

At higher modulation frequencies, the sample becomes thermally thick,

$(l_s a_s \gg 1)$, so that PA signal becomes

$$Q_{th} \cong \frac{\gamma P_o I_o (\alpha_g \alpha_s)^{1/2}}{\pi T_0 l_g k_s} \frac{e^{-l_s \sqrt{\pi f/\alpha_s}}}{f} e^{j(\omega t - \pi/2 - l_s a_s)} \qquad (14)$$

From the last equation it is obvious that for thermally thick sample, the amplitude of

PA signal varies as $\left(\dfrac{1}{f}\right) \exp(-b\sqrt{f})$, where $b = l_s \sqrt{\pi/\alpha_s}$, whereas phase

decreases linearly with $\sqrt{f}$, namely, $\Phi_{th} = -\pi/2 - b\sqrt{f}$. Hence the thermal

diffusivity can be evaluated either from the amplitude or phase of the PA signal

obtained under heat transmission configuration. A necessary condition that should be

satisfied for employing OPC configuration is that the specimen under investigation

should be opaque at the incident wavelength. Though the phase and amplitude of the

PA signal contains clear signature of the thermal transport properties of the specimen,

phase data is more reliable for open cell configuration since the amplitude data

depends on many external parameters such as sample surface quality and detector

response at different wavelengths.

However, in the case of plate shaped specimens, the contribution to the PA signal from the thermoelastic bending due to the temperature gradient existing in the specimen cannot be neglected, especially when the sample is in the thermally thick region. The existence of temperature gradient causes an expansion of the sample parallel to the sample surface, thereby inducing bending along the thickness direction. Such a vibrating sample acts as a mechanical piston; this is otherwise known as drum effect. In the thermally thick regime the pressure fluctuation in the air chamber of the OPC detector from the thermoelastic displacement, for optically opaque sample is given by [39],

$$Q_{el} \cong \frac{3\alpha_T R^4 \gamma P_0 I_0 \alpha_s}{4\pi R_c^2 l_s^2 l_g k_s f} \left[\left(1 - \frac{1}{z}\right)^2 + \frac{1}{z^2} \right]^{1/2} e^{j\left(\omega t + \pi/2 + \Phi\right)} \tag{15}$$

where $z = b\sqrt{f}$, $\Phi = \tan^{-1}\left(\frac{1}{z-1}\right)$ and α_T is the sample thermal expansion coefficient. R is the radius of the front hole of the microphone and R_c is the radius of the OPC air chamber. The above equation mean that the thermoeleastic contribution, at high frequencies varies as f^{-1} and the phase Φ follows the expression

$$\Phi_{el} \cong \Phi_0 + \tan^{-1}\left(\frac{1}{(z-1)}\right) \tag{16}$$

Thus, for thermally thick sample, if thermoelastic contribution is dominant, the thermal diffusivity value can be evaluated from the modulation frequency dependence of the signal phase.

4.2.4. Experimental Setup

A detailed description of the experimental setup is given in chapter 3. Briefly, an optical radiation at 488 nm operating at a power level of 50 mW with a stability of 5% from an Argon ion laser is mechanically chopped (Stanford Research Systems SR 540) before it impinges on the sample surface. The rear surface of the

specimen is glued to the PA cell cavity using vacuum grease. The output amplitude and phase of the PA signal generated in the cavity are detected using a sensitive microphone (Knowles BT 1754) and the output of which is connected to a dual phase lock-in amplifier (Stanford Research Systems SR 830). All the samples under investigation have an average thickness ~ 600 μm.

4.2.5. Results and Discussions

The transition frequency, (f_c), at which sample changes from the thermally thin to thermally thick region for the CSA doped PANI is shown in figure 8. Measurements of all the specimens are taken in the thermally thick region so that thermoelastic bending also contributes to the PA signal generation. Figure 9 to 13 shows the variation of phase of PA signal, by taking account of the thermoelastic contribution, as a function of modulation frequency. The thermal diffusivity values used for the best fit between theoretical model suggested by equation (16) and experimental phase spectrum for CSA doped PANI and its composites with CoPc as well as for intrinsic CoPc are tabulated in table III.
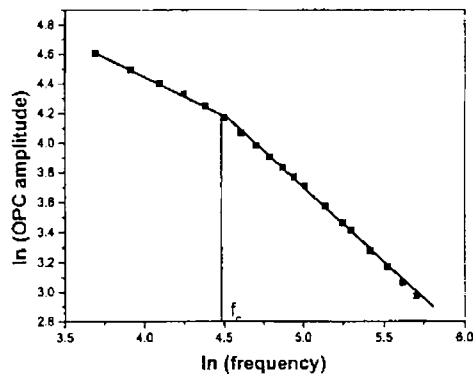

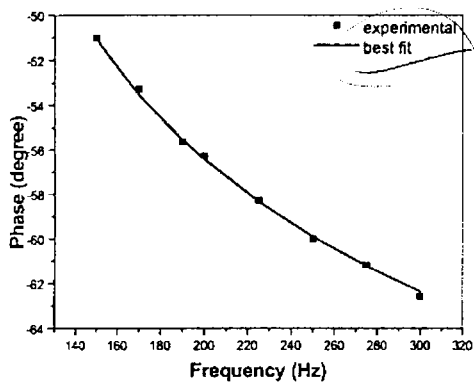Figure 8. PA amplitude spectrum of CSA doped PANI

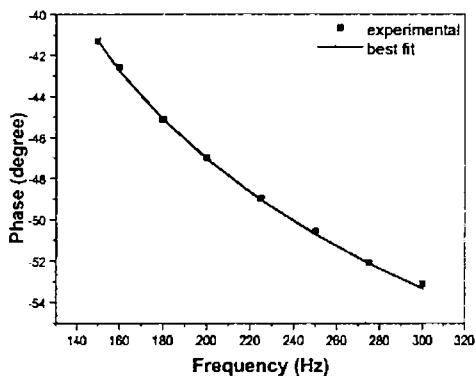Figure 9. PA phase spectrum of CSA doped PANI

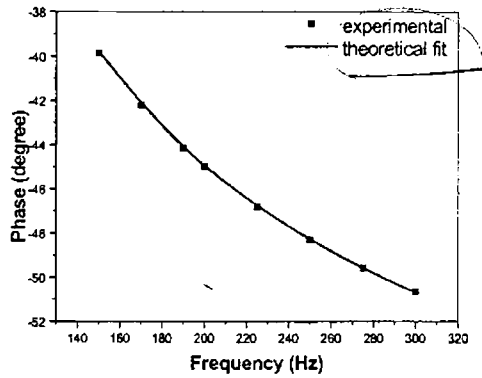Figure 10. PA spectrum of 90% CSA doped PANI:10% CoPc composites

Figure 11. PA spectrum of 50% CSA doped PANI:50% CoPc composites
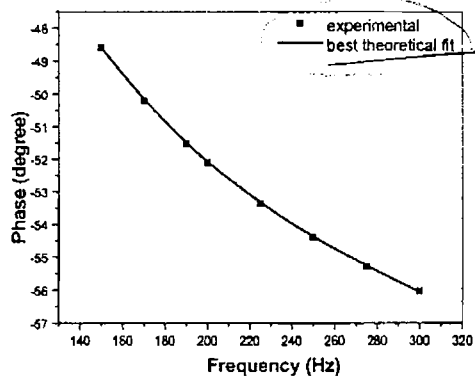

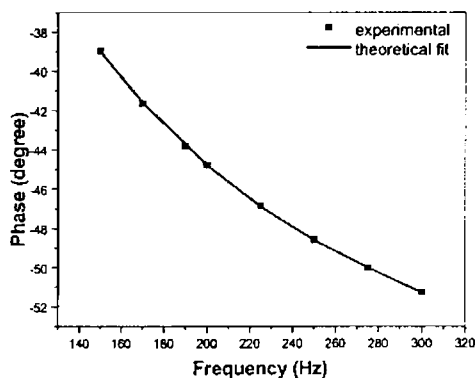Figure 12. PA spectrum of 10% CSA doped PANI:90% CoPc composites

Figure 13. PA phase spectrum of CoPc

It may be said that even though thermal conductivity is a well-known parameter, the role played by thermal diffusivity is usually undervalued and misunderstood, especially in heterogeneous materials such as composites [40]. Although in most of the condensed matter materials there exists direct relation between thermal conductivity and thermal diffusivity, composites of polymers not follow such a relation due to its heterogeneity. In the real sense, all the thermal properties of the heterogeneous materials are discontinuous functions of the position coordinates and consequently neither Fourier's law, nor the heat conduction equation can be applied. However, the concept of "effective" thermal properties i.e., the properties of equivalent homogenous material that produces the same physical effects appears to be useful [40]. In the case of composites, the heat capacity follows the mixture rule i.e, it depends only on the volume fraction of the composites. The effective thermal conductivity value depends on the thermal conductivity of constituents where as effective thermal diffusivity depends on both the thermal diffusivity and thermal conductivity of the components. Thus with the proper choice of volume fraction of constituents of the composites, it is possible to manufacture materials with thermal properties that are never found in natural materials. It is seen from the table III that, in the present case also the effective thermal diffusivity varies

with volume fraction of the composites, which have wide applications in the modern industry.

Sample	Thermal diffusivity (cm^2s^{-1})
CSA doped PANI	$0.760 \pm .0004$
CSA doped PANI (90%) and CoPc (10%)	$0.404 \pm .0003$
CSA doped PANI (50%) and CoPc (50%)	$0.356 \pm .0002$
CSA doped PANI (10%) and CoPc (90%)	$0.289 \pm .0003$
CSA doped PANI (0%) and CoPc (100%)	$0.241 \pm .0002$

Table III. Thermal diffusivity values of the composites ~

From table III it is obvious that CSA doped PANI exhibits maximum value for thermal diffusivity. This can be understood in terms of carrier (electrons and phonons) assisted heat transfer mechanism in CSA doped PANI. In this case, for which the sample is protonated with 50% of CSA, the density of charge carriers in the sample is approximately equal to the density of protonated chain sites. At this doping concentration, phenomenological percolation theory has been used to explain increased carrier density in these specimens. Protonation may occur in such a way that favours repeated doping of polymer chains or conglomeration of doped chains rather than an unbiased distribution, such that metallic islands are present in the material. As the level of doping of CSA is increased in this system, the number and/or size of metallic regions would be expected to increase. Hence an increase in effective charge transport occurs due to increased 'metallic' content of the specimen and a consequent reduction in the tunneling/hopping distance between the metallic regions as well as an increase in charge carrier density. In the case of bulk material, doping above the threshold level could result in the overlap of the metallic islands, which could permit an easier path of charge transport via percolation [41]. In the case of bulk polymers as in the present case, due to strong electron-phonon

interaction, the charge transport mechanism is dominated by phonon assisted quantum mechanical tunneling called hopping [42-43]. In the case of crystalline samples, a precise phase order exists between the adjacent polymer chains and this is expected to allow coherent charge transport along and between the individual chains so that the systems have a regular polaron structure [41]. Therefore the mean free path of carriers is limited not by scattering at interchain events, by phonon scattering due to thermal motion of crystal lattice or by molecular vibrations. In the case of PANI doped with 50% CSA, the average separation between the conduction band states is so small that the effective charge carrier density and the strength of interaction between carrier states is large and consequently the conductivity and carrier mobility is increased. Thus in the present case, polarons (due to strong electron-phonon interaction) are effective carriers in heat transport mechanism and the increase in electron density and a consequent increase in effective polaron density due to post doping with protonic acid results in higher value for thermal diffusivity in CSA doped PANI.

It is also clear from table III that the composites of CSA doped PANI with CoPc decreases with increase in volume fraction of CoPc. This is due to the existence of interfacial thermal contact resistance (ITCR) between the different constituent phases in a composite as well as from the thermal expansion mismatch [44]. The existence of such thermal barriers lead to a lowering of the effective thermal diffusivity of the composite. The present analysis shows that the combination of good thermal diffuser with a bad diffuser can result in composites of intermediate thermal diffusivity value. The measured values of CoPc fall in the typical range of thermal diffusivity of phthalocyanines. The d.c and a.c. electrical conductivity measurements on these materials also observed such a variation in their conductivity value, as reported by other researchers. These authors attributed it to the decrease in effective carriers for the charge transport [45]. Such a decrease in effective carriers results in the reduction in interaction between electrons and phonons and consequently a reduction in polaron assisted heat transfer mechanism in the

140

constituents of these composites. A reduction in ability of thermal energy transport of the constituents can result in a reduction in effective thermal diffusivity value of the composites.

In order to investigate the correlation between thermal diffusivity and physical properties of the composites, hardness measurements of all these specimens are carried out. Hardness is measure of the ability of material to resist a permanent deformation. The values obtained for hardness using indentation (Shore D measurements based on American Society of Testing and Materials standards) technique are tabulated in table IV

Sample	Shore D Hardness
CSA doped PANI	10
CSA doped PANI (90%) and CoPc (10%)	15
CSA doped PANI (50%) and CoPc (50%)	18
CSA doped PANI (10%) and CoPc (90%)	22
CSA doped PANI (0%) and CoPc (100%)	25

Table IV. Shore D Hardness values of samples

It is seen from the table that there exists an inverse relation between the thermal diffusivity value evaluated here and hardness of the specimen. The shore D scleroscope, which is commonly employed for the measurement of hardness of polymers and polymer composites, measures the hardness in terms of elasticity of the material and the hardness value is a measure of the resistance of the material to indentation. The greater this value, the greater is the resistance. It is seen from table III and IV that hardness of the specimens exhibits an inverse relation with thermal diffusivity of the specimen. This may be because a higher value of hardness for the composite is due to the compact arrangement of constituents . i.e, the increase in average number of contacts for each constituent. The increase in number of contacts result in interfacial thermal resistance and consequently the thermal barrier resistance.

141

This increase in ITCR and TBR results in a decreased value for effective thermal diffusivity value [46].

4.2.6. Conclusion

In conclusion, a study on the measurement of the thermal diffusivity value of CSA doped PANI and its composites with different relative volume fraction of CoPc using open cell photoacoustic technique is presented. From the present investigation it is clear that, with the proper choice of the volume fraction of specimen having different thermal diffusivity, we can modify the effective thermal parameters of the composites. The present analysis shows that the combination of a good thermal diffuser such as CSA doped PANI with a bad diffuser CoPc results in composites having intermediate thermal diffusivity value. It is also seen from the results that a correlation between the effective thermal parameters of the composites and physical properties such as hardness of the specimen is possible.

4.3. References

1. W. H. Taun, WB Chou, Journal of European Ceramic Society, 583 (1996)
2. T . Sekino, A Nakahira, M Nawa, A Nilhara, Journal of Japan Soc. of Powder and Powder Metal, 38, 326 (1991)
3. D. M Liu and WH Taun. Acta mater. 44(2), 813 (1996)
4. J Wang, CB Ponton, P. M. Marquis British Ceramic Transaction, 92, 67, (1993)
5. T. Sekino and K. Niihara, Nanostruct. Mater. 6, 663 (1995)
6. Y. Ji and J A Ueomans. Journal of Euorpen Ceramic Society 22, 1927 (2002)
7. R. Roy, S. Komameni, D. M. Roy, Material Research Symposium Proce. 32, 347 (1992)
8. S. Komameni, J. Mat. Chem. 2, 1219 (1992)
9. H. Hirano, K. Niihara, Mat. Lett. 26, 285 (1996)
10. R. Birringer. Mat. Sci. and Engg. A 117, 33 (1989)
11. M. C. Cheung, H. L Chan, Q. F. Zhou, C. L. Choy Nanostruct. Mater. 7, 837 (1997)
12. B. Prevel, B. Palpant, J. Lerme, M. Dellarin, M. Treilleux, L. Savoit, E. Duval and M. Broyer Nonostruct. Mater. 12, 307 (1999)
13. R. D. Shull, L. H. Bennet, Nanostruct. Mater. 1, 83, (1992)
14. R. D. Shull, R. D. McMichael, J. J. Ritter, Nanostruct. Mater. 2, 205 (1993)
15. J. Jose and M. Abdul Kadar, Acta Mater. 49, 729 (2001)
16. F. Capel, C. Moure, P. Duran, A. R. Gouzalez-Elipe and A. Caballero, Appl Phys. A., 68, 41 (1999)
17. M. Aoki, Y. M. Chiang, I. Kosacki, H. Tuller, Y. Liu, J. Am. Ceram. Soc. 79, 1169 (1996)
18. Y. M. Chiang, E. B. Lavik, D. A. Bloom Nanostruct. Mater. 9, 663 (1997)
19. S. Bhaduri and S. B. Bhaduri JOM, 1, 44 (1998)
20. R. Castaneda-Guzman, M. Villagran-Muniz, J. M. Sangier-Bleas, S. J. Perez Ruiz and O. Perez- Martinez, Appl. Phys. Lett. 77(19), 3087 (2000)
21. S. Sankararaman, V. P. N. Nampoori, C. P. G. Vallabhan. G. Ambadas and S. Sugunan, Appl. Phys. Lett. 67 (20), 2939 (1995)
22. Castro Rodriguez, M. Zapata Torres, V, Rejon Moo, P. Bartolo Perex and J. L. Pena, J. Phys. D. Appl. Phys. 32, 1194 (1999)
23. D. Fournier, J. P. Roger, A. Bellouati, C. Boue, H. Stamm and F. Lakestani, Anal. Sci., s 158 (2001)
24. T. V. Mani, P. Krishna Pillai, A. D. Damodaran and K. G. K Warrier, Mat. Lett. 9, 237 (1994)
25. A. A. Anappara, S. K. Ghosh, P. R. S. Warrier, K. G. K .Warrier and W. Wunderlich, Acta. Mater. (in print)
26. A. Sanchez Lavenga, A. Salzar, A. Ocariz, L. Pottier, W. Gomez, L. M. Villar and E. Macho, Appl. Phys. A., 68, 15 (1997)
27. Rosencwaig and Gersho, J. Appl. Phys. 47 (1), 64 (1976)
28. D. M. Liu and W. H. Taun, Mat. Chem. and Physics, 48, 258 (1997)
29. Sajan D George, Aji. A, Anapara, K. G. K. Warrier. P. Radhakrishnan, V. P. N. Nampoori and C. P. G. Vallabhan, Proc. SPIE, 5118, 207 (2003)
30. Alan J Heeger, Current Applied Physics I, 247-267 (2001)

31. H. Shirakawa, E. J. Louis, A. G. MacDiarmid, C. K. Chiang and A. J. Hegger, Chem. Commun. 578 (1977)

32. C. K. Chiang, C. R. Fincher, Jr. Y. W. Park, A. J. Hegger, H. Shriakawa and E. J. Louis, Phys. Rev. Lett. 39, 1098 (1977)

33. R. Ranby in W. R. Salaneck, I. Lundstrom and B. Ranby (Eds) Conjugated Polymers and Related Materials: The Interconnection of Chemical and Electronic structures (Oxford University Press) 1993

34. H. Tomozawa, D. Braun, S. Philips, A. J. Hegger and H. Kroemer, Synth. Mat. 22, 63 (1987)

35. H. Tomozawa, D. Braun, S. Philips, A. J. Hegger and H. Kroemer, Synth. Mat. 28,C 687 (1989)

36. J. H. Burroughnes, D. D. C. Bardley, A. R. Brown, R. N. Marks. R. H. Friend, P. L. Burns and A. B. Homles, Nature, 347, 599 (1990)

37. T. Wang, K. M. Beauchamp. D. D. Berkelye, B. R. Johnson, J. X. Liu, J. Zhang and A. M. Goldman, Phys. Rev. B 43, 8623 (1991)

38. G. Yu, C. H. Lee, A. j. Hegger, N. Herron, E. M. McCarron, L. Cong, G. C. Spalding, C. A. Nordman and A. M. Goldman, Phys. Rev. B. 45, 4964 (1992)

39. L. F. Perondi and L. C. M. Miranda, J. Appl. Phys. 62(7), 2955 (1987)

40. A. Salzar. Euro. J. Phys. 24, 1 (2003)

41. E. R. Holland, S. J. Pomfret, P. N. Adams and A. P. Monkman, J. Phys.C. 8, 2991 (1996)

42. D. Moses, A. Daogariu and A. J. Hegger, Synth. Mater.116, 19 (2001)

43. M. Koehler, J. R. De Lima, M. G. E. Da Luz and I. A. Hummelgen, Phys. Stat. Sol. (a), 173, 29 (1999)

44. P. J. Mendoza, A. Mandlies, L. Nicolaides, J. Huerata and E. M. Rodriguez, Anal. Sci. 17, s 29 (2001)

45. Saravanan and M. R. Anatharaman (Revised version is communicated to Journal of Applied Physics)

46. D. Forunier, J. P. Roger, A. Bellouati, C. Boue, H. Stamm and F. Lekstani, Anal. Sci., 17, s 158 (2001)

144

Chapter 5

Photoacoustic measurement of thermal

conductivity of liquid crystal mixtures

Abstract

Thermal characterization of liquid crystal mixtures of cholesterol and 1 hexadecanol with various relative fractions of constituents have been carried out using laser induced photoacoustic technique. The phase of liquid crystal mixtures are identified using Polarising microscope as Smectic A. Thermal diffusivity measurements of liquid crystal mixtures are done using open cell photoacoustic technique whereas thermal effusivity is measured using conventional photoacoustic technique. From the measured values of thermal diffusivity and thermal effusivity, the calculation of thermal conductivity and thermal capacity has been made. Analysis of data shows that hydrogen bonding has a significant effect on thermal properties of liquid crystal mixtures.

5.1. Introduction

The term liquid crystal signifies a state of aggregation that is intermediate between the crystalline solid and the amorphous liquid. As a rule, a substance in this mesophase or liquid crystalline state is strongly anisotropic in some of its properties and yet exhibits a certain degree of fluidity. Differences in orientational and spatial ordering of the molecules define the mesophases. Depending on the detailed molecular structure, the system can pass through one of more mesophases before the transformation to completely isotropic liquid. Transitions to these intermediate states may be brought about by purely thermal processes (thermotropic mesomorphism) or by the influence of solvents (lyotropic mesomorphism). The thermotropic liquid crystal composed of rod like molecules can be broadly classified into three groups; nematic, cholestric and smectic. The nematic liquid crystal has a high degree of long-range orientational order of molecules, but no long-range transnational order. The cholestric mesophase is also a nematic type of liquid crystal except that it is composed of optically active molecules. Smectic liquid crystals have stratified structures but a variety of molecular arrangements are possible within each stratification. Thermotropic liquid crystal can be further classified into two groups: enantiotropic or monotropic. The former type can be changed into liquid crystal state by lowering the temperature of the liquid or by raising the temperature of a solid. However, the monotropic liquid crystals can only be changed into a liquid crystal state by either an increase in temperature of a solid or by a decrease in temperature of a liquid, but not both. Thermotropic liquid crystals are usually made of discotic shape or rod shaped molecules. Discotics are flat disc-like molecules consisting of a core of adjacent aromatic rings. This allows for two-dimensional columnar ordering of liquid crystal. Rod-shaped molecules have an elongated and anisotropic geometry, which allows for preferential alignment along any spatial direction. Structurally, most of the rod shaped molecules fall into two categories, the columnar and the nematic. Polymer liquid crystals have a basic monomer unit mass of low molar mass mesogens

having rod-like or disc like shapes, which are attached to the polymer backbone in the main chain itself, or as a side groups [1-2].

Lyotropic mesophases occur as a result of solvent induced aggregation of the constituents into micellar structures. Lyotropic mesogens are typically amphiphilic, which means that they are composed of both lyophilic (solvent-attracting) and lyophobic (solvent-repelling) parts. This causes them to form into micellar structures in the presence of a solvent, since the lyophobic ends will stay together as the lyophilic ends extend outwards towards the solution. As the concentration of the solution is increased and the solution is cooled, the micelles increase in size and eventually coalesce. This separates the newly formed liquid crystalline state from the solvent. In the lamellar or neat phase of the lyotropic liquid crystals, water is sandwiched between the polar heads of adjacent layers, while the hydrocarbon tails, which are disordered or in a liquid like configuration are in a non-polar environment [2].

Thermal measurements play an important role in locating and characterizing the different phases and phase transitions in liquid crystals. Differential scanning calorimetry (DSC) is extensively used to locate transition temperatures and to determine the important thermal properties of the specimen [3]. High resolution calorimetric measurements, in particular near phase transitions, are usually carried out by adiabatic scanning calorimetry or a.c. calorimetric techniques [4-6]. These methods give information only on the static quantities such as enthalpy, heat capacity etc [7-9]. A more complete characterisation of these specimens, however, also requires determination of the thermal transport properties such as thermal diffusivity, thermal effusivity and thermal conductivity. Conventional steady state gradient and transient techniques have mainly been used to determine the thermal conductivity which rather demands larger size specimens [6-8]. Some high-resolution a.c. techniques [10], such as forced Rayleigh light scattering, have been used in a number of cases to measure the thermal diffusivity and thermal conductivity [11-15]. However, since 1970s, the multitude ways of generating photothermal effects using

all kinds of radiation, from laser to particle beams and the diversity in detection schemes of the thermal or acoustical waves have revolutionalised the field of nondestructive characterisation of liquid crystals. Photoacoustic (PA) and related photothermal methods are the well established technique for the characterisation of liquid crystals, especially for the evaluation of dynamic thermal parameters as well as for the phase transition studies because the temperature rise during these experiments is only ~ mK so that photothermal experiments do not result any phase transitions in the liquid crystals. These thermal methods are particularly useful in studying the polymer and polymer containing samples. Modern polymeric materials are usually blends or composites with complex morphologies that are crucial in determining their material properties [16-22].

Although thermal diffusivity and thermal conductivity are extensively investigated using various techniques, thermal effusivity is one of the important and unique thermophysical parameter which is least explored in applied physics [22]. Thermal effusivity is a rather abstract physical quantity that characterizes the material from the standpoint of its heat storage capacity. The thermal effusivity, e_s, defined by $(k\rho C)^{1/2}$, has the dimensions of $Ws^{1/2}cm^{-2}K^{-1}$, where k is the thermal conductivity, ρ is the density and C is the specific heat capacity. Though the thermal effusivity is a relevant thermophysical parameter for surface heating or cooling processes, as well as for quenching processes, a direct measurement of this quantity using conventional heat flow methods is not easy. The thermal effusivity measures essentially the thermal impedance of the sample, or effectively, the sample's ability to exchange heat with the environment. Hence, its value is very significant in the case of liquids and in liquid crystals, especially when these are used as temperature sensors or in temperature sensing devices.

As the mixtures of liquid crystals are extremely important since they provide thermophysical parameters that are not available in nature. Such a tunability in the thermophysical parameters of the mixtures has wide applicability, especially from

industrial point of view. In this context, a nondestructive evaluation of thermal diffusivity and thermal effusivity of liquid crystal mixture manufactured from cholesterol and 1 hexadecanol with various relative mass fractions has great physical significance and practical applications. Measurement of these two dynamic thermophysical parameters allows the evaluation of thermal conductivity and specific heat capacity of the samples under investigation.

5.2. Sample Preparation

The two substances (Cholesterol and 1 hexadecanol) comprising the mixture were carefully weighed in different mass proportion (70%:30%, 60%:40%, 50%:50%, 40%:60%). The mixture was then heated to a temperature well above the melting point with continuous stirring to ensure thorough and complete mixing. The homogeneous mixture was then quickly cooled and solidified by quenching in ice. This process was repeated until constant melting and transition temperatures were obtained.

Although cholesterol is non-mesomorphic, it must be considered to be potentially mesomorphic since even cholesteryl chloride gives a monotropic cholesteric phase, and it is possible that the hydrogen bonding in pure cholesterol increases the intermolecular cohesion and is responsible for its high melting point. The presence of hexadecanol may present alternate sites to which the cholesterol hydroxyl groups can hydrogen bond without resulting in a high melting crystal lattice, yet giving sufficiently strong intermolecular attractions to make possible the existence of an anisotropic melt.

The presence of a liquid crystalline phase is usually quiet easy to identify but the identification of the phase type is often very difficult. Optical polarizing microscopy is the most common method used to identify liquid crystal phases. A small sample of the liquid crystal is placed on a microscope slide with a cover slip. The slide is placed in a hot stage of variable temperature which is placed under a microscope between crossed polarizers. When viewed between cross polarizers an

isotropic liquid will appear black because the polarized light will be extinguished by the second, crossed polarizer. Liquid crystals have certain ordering of their constituent molecules and are birefringent. Accordingly, plane polarized light are affected by the liquid crystal material, and does not, in all cases, get extinguished by the second or crossed polarizer and this generates a colored texture pattern. It is easy to identify some of the more simple, common liquid crystalline phases (Nematic, Smectic A, Smectic C etc) eventhough some of the others are quiet difficult to identify and a great deal of experience is required. If the sample with an unknown liquid crystalline phase is mixed with a known and fully characterized liquid crystal then the complete miscibility across the phase diagram indicates that two phases are identical. Such miscibility studies are frequently employed in the identification of liquid crystal phase. In the present case, an Olympus Polarizing microscope in conjunction with a Linkam [TMS 94] heating stage is used for the microscopic textural observations. The polarized thermal microscopic observations revealed that all the mixtures exhibit Smectic A (SmA) phase. In the present case, for the convenience, mixtures containing 70% Cholestrol: 30% 1 Hexadeconal is called as sample 1 whereas 60% Cholestrol: 40% 1-Hexadecanol, 50% Cholesterol: 50% Hexadecanol and 40% Cholestrol and 60% 1-Hexadecanol are called samples 2, 3 and 4, respectively. Figure 1 to 4 shows the phase of mixtures under investigation. This method provides a simple and quick method for exploring the textures of liquid crystal mixtures.
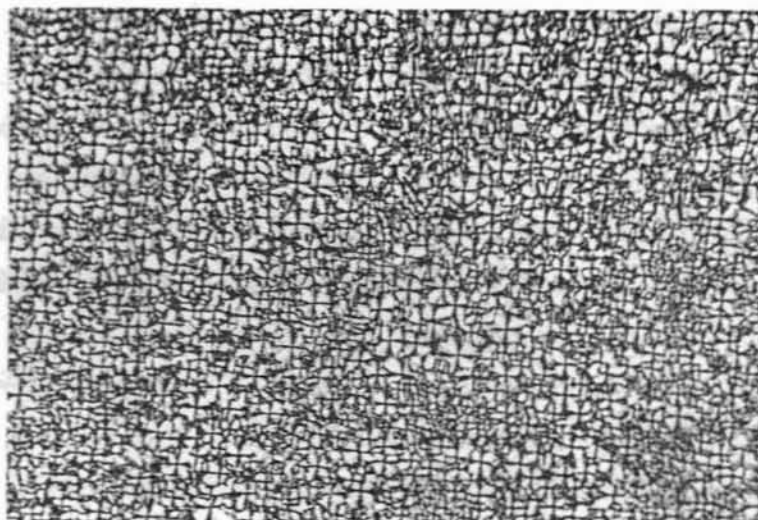
Figure 1. Textural observation of sample containing Cholesterol:
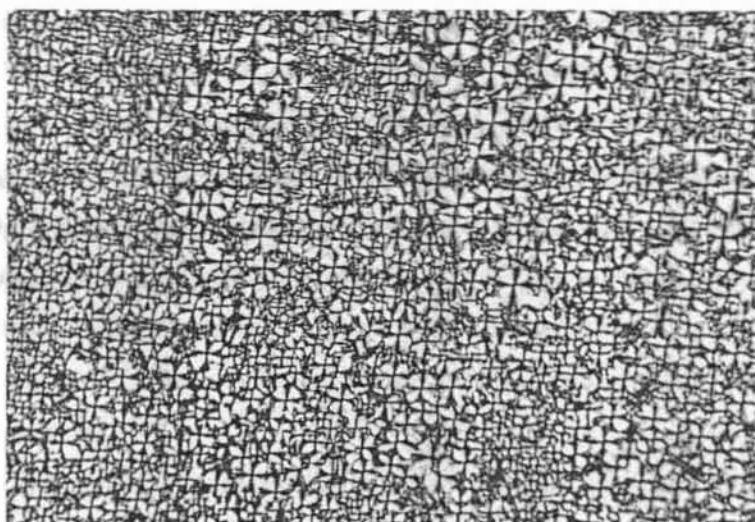1 Hexadecanol (70:30)

Figure 2. Textural observation of sample containing Cholesterol:
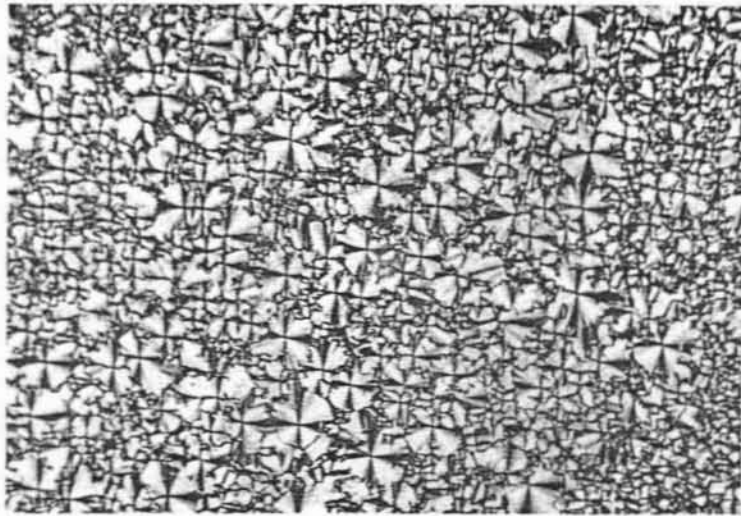1 Hexadecanol (60:40)

Figure 3. Textural observation of sample containing Cholesterol:
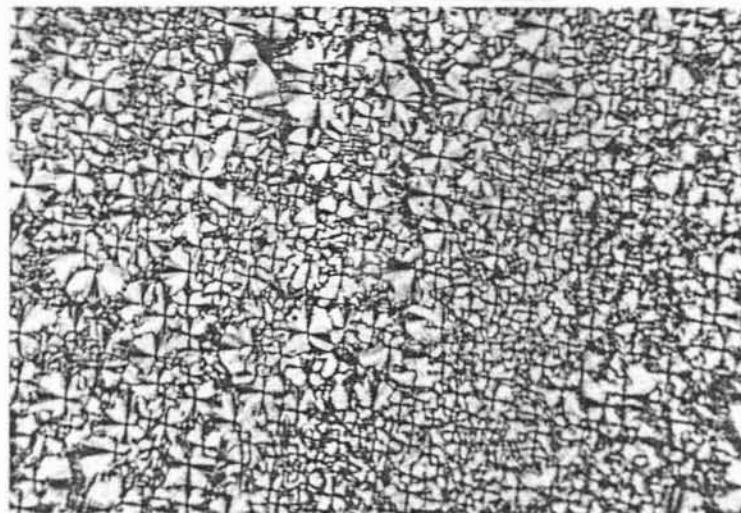1 Hexadecanol (50:50)

Figure 4. Textural observation of sample containing Cholesterol:
1 Hexadecanol (40:60)

5.3 Thermal diffusivity measurements

The necessary theoretical background for the evaluation of the thermal diffusivity of the specimen under heat transmission configuration by taking into account the effect of thermoelastic bending due to temperature gradient existing within the specimen is given in the latter part of the previous chapter. The same procedure is followed here also. However, in this case the exposed portion of the specimen is covered with a thin aluminium foil so as to attain complete opaque condition as shown in figure 5. The thickness of the aluminium foil is so small $(5\mu m)$ that it becomes thermally thick only in the MHz frequency range. Hence the Al foil does not affect the thermal diffusivity value of the specimen under investigation.
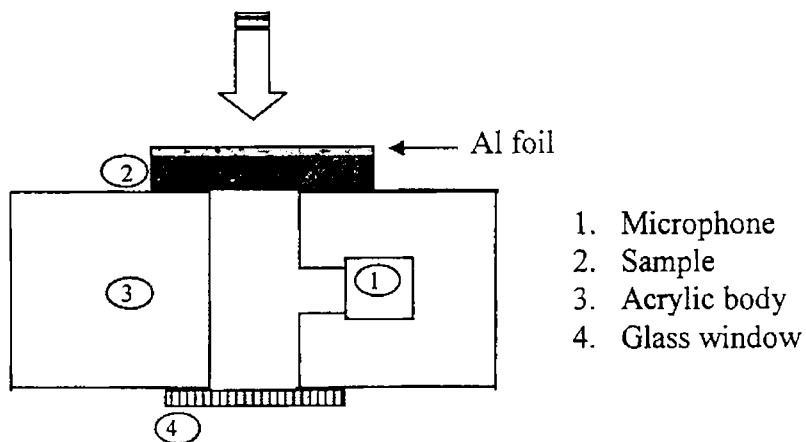

Al foil

1. Microphone
2. Sample
3. Acrylic body
4. Glass window

Figure 5. Cross sectional view of OPC for the measurement of thermal diffusivity

5.4. Thermal effusivity measurements

For the thermal effusivity measurements, the same liquid crystal mixtures those used for thermal diffusivity measurements are used. By using the PA configuration and the procedure described by Velva et.al [23] is possible to measure the thermal effusivity of the specimen under investigation. The cross sectional view

of the PA cell for thermal effusivity measurements is schematically shown in figure 6. In this case the modulated (Stanford Research Systems SR 540) optical radiation is focused to the aluminium foil (thickness ~ 60 μm) and the opposite side of which the specimen is attached using a thermal paste. Here also, the aluminium foil allows the optical opaqueness condition of the specimen at the incident wavelength (488 nm from an argon laser at 50 ± 0.05 mW).

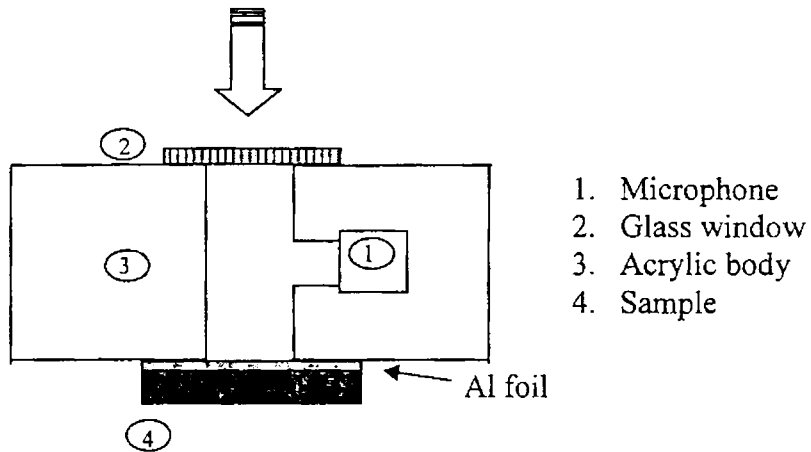1. Microphone
2. Glass window
3. Acrylic body
4. Sample

Figure 6. Cross sectional view of PA cell for the measurement of thermal effusivity

From the Rosencwaig and Gersho theory the detected PA signal (Knowles BT 1834), and the consequently measured (dual phase lock in amplifer – Standford Research Systems SR 830) signal, is given [23] by ,

$$T(x,t) = \theta_g(x)\exp(j\omega t) = \theta\exp(-\sigma_0 x)\exp(j\omega t) \qquad (1)$$

with $\quad \theta = \dfrac{\beta I_0}{k_0\sigma_0}\left\{\dfrac{(1+\bar{b})\exp(l_0\sigma_0)+(1-\bar{b})\exp(-l_0\sigma_0)}{(1+\bar{b})\exp(l_0\sigma_0)-(1-\bar{b})\exp(-l_0\sigma_0)}\right\} \qquad (2)$

where β is the optical absorption coefficient and I_0 is the intensity of incident radiation and also $\bar{b} = b\tanh(l_s\sigma_s) \qquad (3)$

with $b = \dfrac{k_s \sigma_s}{k_0 \sigma_0} = \dfrac{\sqrt{k_s \rho_s c_s}}{\sqrt{k_0 \rho_0 c_0}} = \dfrac{\varepsilon_s}{\varepsilon_0}$ (4)

Here $\sigma_i = (1 + i)a_i$ is the complex thermal diffusion coefficient. Here the index i denotes the sample $(i = s)$, air $(i = g)$ and the aluminium foil $(i = 0)$. $a_i = \sqrt{\dfrac{\pi f}{\alpha_i}}$ and $\alpha_i, k_i, \rho_i, c_i$ and e_i are the thermal diffusivity, conductivity, density , specific heat capacity and effusivity of the specimen 'i'.

In the modulation frequency (f) range forwhich the sample is thermally thick, the equation (3) can be written as

$$\theta = \frac{\beta I_0}{k_0 l_0 \sigma_0^2} \left(\frac{1}{1 + \left(\dfrac{b}{l_0 \sigma_0} \right)} \right)$$ (5)

For the case in which only the aluminium foil close to the PA cell, then the PA signal is reduced to

$$\theta_0 = \frac{\beta I_0}{k_0 l_0 \sigma_0^2}$$ (6)

From the ratio between equations (5) and (6), the equation becomes

$$R = \frac{\theta}{\theta_o} = \frac{1}{1 + \left(\dfrac{b}{l_0 \sigma_0} \right)}$$ (7)

Then the thermal effusivity value of each sample is obtained by fitting the experimentally obtained ratio of the signal as a function of chopping frequency to that of equation (7)

5.5. Results and Discussions

The variation of PA phase spectrum under heat transmission configuration for the samples under investigation is shown in figures 7 to 10. In all the cases, the

thermal diffusivity of the specimen is used as the fitting parameter. The best values obtained as fitting parameter for thermal diffusivity by taking into account of the thermoelastic bending of the specimen are given in table I
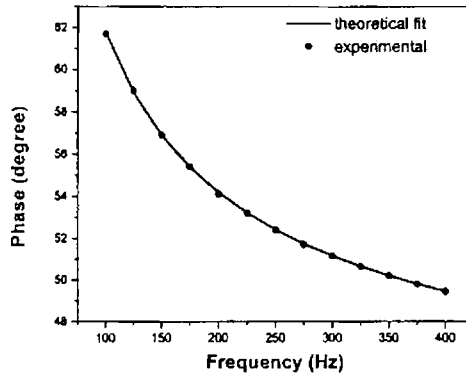

Figure 7. Variation of phase of PA signal as a function of modulation frequency for sample 1
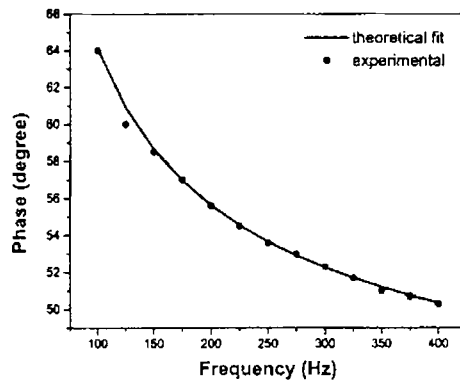

Figure 8. Variation of phase of PA signal as a function of modulation frequency for sample 2

Figure 9. Variation of phase of PA signal as a function of modulation
frequency for sample 3

Figure 10. Variation of phase of PA signal as a function of modulation
frequency for sample 4
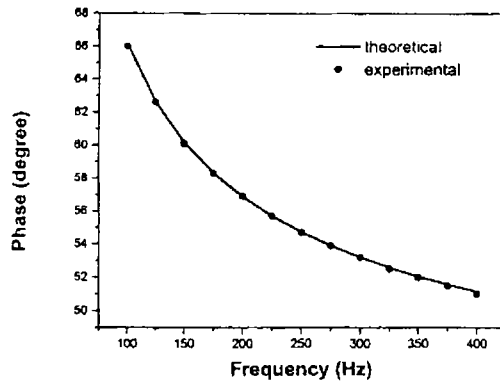
Figure 11 to 14 shows the variation of ratio of PA amplitude between sample attached to Al foil and Al foil alone as a function of modulation frequency. In all the cases, the unknown thermal effusivity of the specimen is taken as the fitting

parameter. The values obtained for the thermal effusivity of all the specimen are given in table I.

Figure 11. Variation of ratio of PA amplitude as a function of modulation
frequency for sample 1

Figure 12. Variation of ratio of PA amplitude as a function of modulation
frequency for sample 2

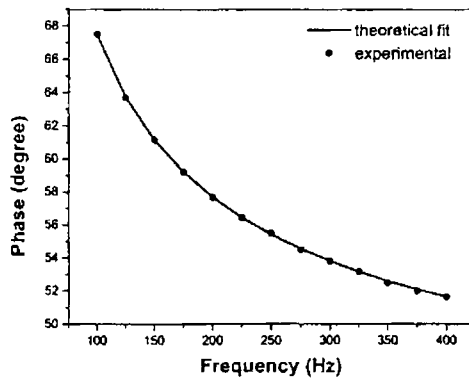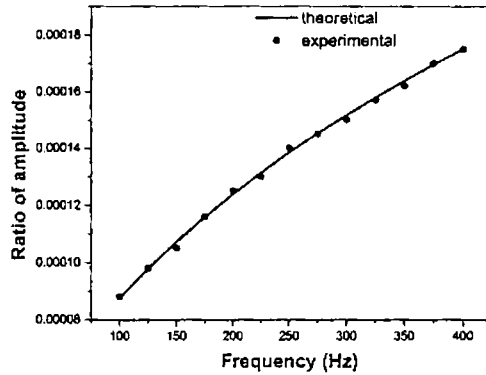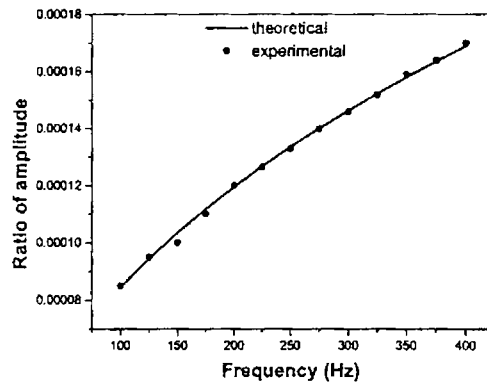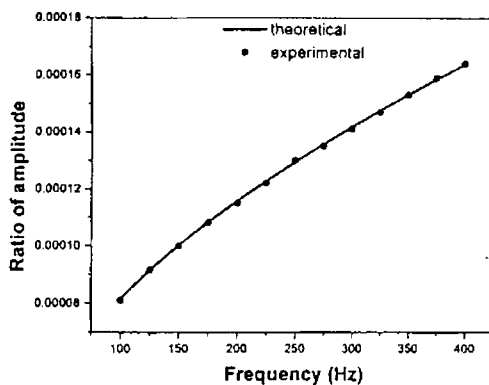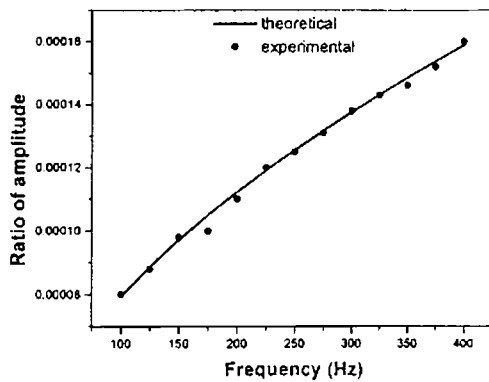Figure 13. Variation of ratio of PA amplitude as a function of modulation frequency for sample 3

Figure 14. Variation of ratio of PA amplitude as a function of modulation frequency for sample 4

Sample	Thermal diffusivity $(\times 10^{-6} m^2 s^{-1})$	Thermal effusivity $\left(Ws^{\frac{1}{2}} / m^2 K \right)$	Thermal conductivity (W/mK)	Heat Capacity $\left(\times 10^6 J / m^3 K \right)$
1	2.304 ± 0.003	17.1 ± 0.2	0.260 ± 0.004	0.1130 ± 0.004
2	2.770 ± 0.005	16.5 ± 0.2	0.271 ± 0.003	0.0991 ± 0.003
3	3.061 ± 0.003	16.0 ± 0.2	0.281 ± 0.004	0.0915 ± 0.004
4	3.602 ± 0.004	15.5 ± 0.1	0.294 ± 0.003	0.0820 ± 0.003

Table I. Thermal parameters of liquid crystal mixtures under investigation

It is seen from table that the thermal diffusivity value increases with increase in relative fraction of 1 hexadecanol whereas thermal effusivity, measure of thermal impedence decreases with increase in relative fraction of 1 hexadecanol. The increase in thermal conductivity with increase in relative fraction of 1 hexadecanol can be understood in terms of increase in effective hydrogen bonding (H-bonding) and the subsequent effective transport of thermal energy through the mixture. H-bonding is one of the key interactions for chemical and biological processes in nature due to its e stability, directionality and dynamics [24-26]. For molecular aggregates, hydrogen bonding plays an important role in the association of molecules. In the case of mixture of two different substances, as in the present case, liquid crystal formation will depend on two factors: first, the ability of the molecules to pack into a single liquid crystal "lattice" and secondly, the mean orientational cohesive energy. The OPM studies on the specimen under investigation shows that all the specimens are in the Smectic A phase which is considered as the more crystalline liquid crystal phase. Although pure cholesterol is non-mesogenic, it can be considered to be potentially

mesomorphic because even cholesteryl chloride gives monotropic cholesteric mesophase. An increase in intermolecular cohesion is possible through hydrogen bonding in the case of pure cholesterol which in turn causes the high melting point of cholesterol. Introduction of hexadecanol molecules may present alternate sites to which cholesterol hydroxyl group can hydrogen bond without resulting in the high melting point of the crystal lattice, yet giving sufficiently strong intermolecular attractions to make possible the existence of an anisotropic melt. The increase in relative volume fraction of the 1 hexadecanol increases the number sites available for the H- bonding and consequently more intermolecular attraction. With the increase in intermolecular attraction and consequent cohesive structure, the liquid crystal mixture provides easier path for heat transport and result in an increased value for thermal conductivity with increase in relative fraction of 1 hexadecanol. The unification of components of the mixture through H-bonding causes the reduction in heterogeneity of the liquid crystal mixture. As the heterogeneity of the specimen decreases, the factors which causes in the reduction in thermal parameters of the heterogeneous materials, namely interface thermal resistance and lattice expansion mismatch also decreases [27]. This may also cause the increased value for thermal conductivity with the increase in relative fraction of 1 hexadecanol.

5.6. Conclusion

In conclusion, in this chapter, investigations on the dependence of effective thermal parameters on the volume fraction of constituents in a liquid crystal mixture consisting of cholesterol and 1 hexadecanol have been presented. It is seen that thermal conductivity (thermal diffusivity) of the specimen increases with increase in volume fraction of 1 hexadecanol whereas thermal diffusivity decreases. Analysis of results shows that H-bonding play a key role in determining the effective thermal parameters of a liquid crystal mixture. The present study also suggests that tunability in effective thermal parameters is possible by varying the volume fraction of the constituents.

5.7 *References*

1. S. Chandrasekhar "Liquid Crystals" Cambridge University Press, New York (1992)
2. Satyen Kumar (Edit), "Liquid Crystals I the Nineties and Beyond" World Scientific, Singapore (1995)
3. Jan Thoen (Chapter 6) in Physical Properties of Liquid Crystals, Wiley – VCH, Singapore (1999)
4. C. W Garland in Geometry and Thermodyanmics (Ed, J. C. Toledano) NATO ASI Ser.B 229m, 221 Plennum New York (1990)
5. M. A. Anisimov Critical Phenomena in Liquids and Liquid Crystals, Gordon and Breach, Philadelphia (1990)
6. J. Thoen in Phase Transitions in Liquid Crystals (Eds: S. Martellucci and A. N. Chester) NATO ASI Ser.B 229m, 290, Plennum New York (1992)
7. C. W Garland in Phase Transitions in Liquid Crystals Eds: S. Martellucci and A. N. Chester) NATO ASI Ser.B 229m, 290, Plennum New York (1992)
8. J. Thoen, Int. J. Mod. Phys. B, 9, 2157 (1995)
9. C. W. Garland in Liquid Cystals: Physical Properties and Phase Transitions (Eds: S. Kumar), Oxford University Press (1997)
10. T. Akhahane, M. Kondok, K. Hashimoto and N. Nagakawa, Jpn. J. APpl. Phys, 26, L100, (1987)
11. M. Marinelli, U. Zammit, F. Mercuri and R. Pizzaferrato, J. Appl. Phys, 72, 1096 (1992)
12. C. Glorieux, E. Schoubs, ang J. Thoen, Mater. Sci. Eng., A122, 87 (1989).
13. J. Thoen, C. Glorieux, E. Schoubs and W. Lauriks, Mol. Cryst. Liq. Cryst., 191, 29 (1990).
14. U. Zammit, M. Marinelli, R. Pizzoferrato, F. Scudieri and S. Martellucci, Phys. Rev. A, 41, 1153 (1990).
15. J. Thoen, E. Schoubs, V. Fagard in O. Leroy and M.A. Breazeale (Eds.), Physical Acoustics: Fundamentals and Applications, (Plenum Press, New York), 1992.
16. M. Marinelli, U. Zammit, F. Scudieri and S. Martellucci, High Temperature – High Pressures, 18, 1 (1986).
17. F. Scudieri, M. Marinelli, U. Zammit and S. Martellucci, J. Phys. D: Appl. Phys., 20, 1045 (1987).
18. G. Pucceti and R. M. Leblanc, J. Chem. Phys., 108 (17), 7258 (1998).
19. J. Thoen, Intl. J. Mod. Phys. B, 9 (18 & 19), 2157 (1995).
20. N.A. George, C.P.G. Vallabhan, V.P.N. Nampoori, A.K.George and P. Radhakrishnan, Appl. Phys. B 73, 145 (2001).
21. N.A. George, Smart Mater. Struct. 11, 561 (2002).
22. N.A. George, C.P.G. Vallabhan, V.P.N. Nampoori, A.K.George and P. Radhakrishnan, Opt. Eng., 40(7) 1343, (2001).
23. L. Veleva, S. A. Tomas, E. Marin, A. Cruz-Orea, I. Delgadillo, J. J. Alvarado Gil, P. Quintana, R. Pomes, F. Sanchez, H. Vargas and L. C. M. Miranda, Corrosion Science, 39 (9), 1641 (1997)
24. Yoon-Sok Kang and Wang-Cheol Zin, Liquid Crystals, 29, 3, 369 (2002)

25. J. Borg, M. H. Jansen, K. Sneepman and G. Tiana, Phys. Rev. Lett. 86, 1031 (2001)
26. S. I Torgova and A. Strigazzi, Mol. Crys.Liq. Cryst., 336, 229(1999)
27. P. J. Mendoza, A. Mandelis, L. Nicolaides, J. Huerta, and M. E. Rodriguez, Anal.Sci.,17, s 269 (2001)

———-

Prediction is difficult, especially about the future

- *Neils Bohr*

Chapter 6

Summary and Future challenges

Abstract

A summary of the work presented in this thesis as well as the concluding remarks based on the analysis of results has been made. Suggestions for the further work along this direction are also outlined.

6.1. Summary and Conclusions

A detailed account of the measurements done on the thermal and transport properties of certain class of important photonic materials of current interest such as semiconductors, layered structures, nanometal dispersed ceramics, composites of conducting polymer and liquid crystal mixtures are made in this thesis. Investigations have been carried out using the two most important nondestructive laser induced photothermal methods namely photothermal deflection and photoacoustic technique. Measurements presented on this thesis reveal the versatility and applicability of these photothermal techniques for the characterization of a range of photonic materials, in addition to providing a better understanding of the physics of heat transport through these materials, which is essential for the progress of photonic industry. A brief review given on the introductory part of this thesis about the various photothermal techniques and on the applicability of the techniques which are employed here on the class of materials so as to reveal the potential of these methods.

Thermal wave physics has been an active area of research as it has created basis for several new and revolutionary measurement technologies. All the photothermal techniques are based on the detection of the thermal waves generated in the specimen following illumination with pulsed or chopped optical radiation. Photothermal deflection and photoacoustic technique, which are based on the generation and propagation of thermal waves and subsequent effects in the specimen as well as in the coupling medium allow the evaluation of many of the material parameters which are hard to measure using conventional techniques.

In recent years, many researchers all around the world have paid much attention for the thermal characterization of compound semiconductors both in intrinsic and extrinsic state with a special emphasis on the influence of doping on the fundamental properties of these materials. These investigations are extremely important as a thorough understanding of the fundamental properties such as thermal diffusivity and its variation with doping are essential for getting a better insight into the physical processes tacking place in these materials. In this context, the

photothermal deflection technique, which have several advantages over other photothermal methods is a good tool for the evaluation of thermal diffusivity of compound semiconductors namely InP and InP doped with Sn, S and Fe cleaved along (111) and (100) plane. When a solid sample is irradiated with a focused laser beam, thermal waves generated from this point source will propagate in all directions, the characteristics of which are determined by the thermal properties of the sample. The profile of refractive index gradient generated in a coupling fluid in contact with the heated surface of the solid sample is ultimately decided by these thermal waves. A weak probe-beam propagating through this gradient gets deflected. The phase of the deflection signal as a function of the distance between the point source and the probe-beam holds a linear relationship and the slope of the plot determines the thermal diffusivity of the solid sample. The present investigation shows that both the doping and plane of cleavage have significant influence on propagation of phonons through the lattice and hence on the thermal diffusivity value.

Thermal characterization of layered structures is a challenging area of research. Photothermal deflection technique along with its unique features such as noncontact and nondestructive nature allows the measurement of anisotropy in effective thermal parameters of layered structures. Measurement of effective thermal parameters such as thermal diffusivity along the in-plane and cross plane directions of layered semiconductors is extremely important, especially for the device design and fabrication. The investigations carried out on the in-plane and cross plane thermal diffusivity value of the GaAs double epitaxial layers grown on GaAs substrate with various doping concentration of Si and a particular concentration of Be show that these materials exhibits great anisotropy in effective thermal diffusivity value. In addition to that, both doping concentration and nature of dopant have great influence on effective thermal diffusivity value. Analysis of the results reveals that in addition to impurity scattering, the interface scattering and thermal barrier resistance are playing a major role in determining the effective thermal diffusivity of layered semiconductors.

In spite of the existence of several photothermal techniques, photoacoustic technique has gained wide popularity due to simplicity in experimental setup as well as the capability of simultaneous measurement of thermal and transport properties with good accuracy. Photoacoustic phase measurements are an excellent approach to investigate the heat transport mechanism in materials. It also enables one to measure the thermal and transport properties viz., thermal diffusivity, diffusion coefficient, surface recombination velocity and nonradiative recombination time of both direct and indirect bandgap semiconductors. In the present work, measurements done on some compound semiconductors such as InP, GaAs and InSb reveal the effectiveness of open cell photoacoustic technique to monitor the minority carriers in the semiconductors. Analysis also show that PA technique offers an indirect way to measure the mobility of minority carriers in semiconductors as well as the auger recombination mechanism, which is the dominating nonradiative recombination mechanism in undoped semiconductors. Experiments carried on intrinsic Si and Si doped with B and P reveal that the nature of dopant has great influence on the thermal and transport properties of semiconductors. Studies done on the Si doped GaAs epitaxial layers using photoacoustic under heat transmission configuration reveals that thermal and transport properties of epitaxial layers vary significantly with doping concentration.

Ceramics are considered to be an ideal material for many of the electronic and optoelectronic applications. However, the thermophysical parameters of these materials are greatly affected by various factors such as sintering temperature, incorporation of foreign atom etc. In the present work focus has been made on the nano Ag metal dispersed ceramic alumina matrix with various concentrations of Ag and sintered at different temperature. The reflection detection configuration have been employed and by knowing the transition frequency from the amplitude spectrum of the photoacoustic signal, at which the sample changes over from thermally thin to thermally thick regime, the thermal diffusivity is evaluated. Analysis shows that thermal diffusivity value is sensitive to both Ag concentration and

porosity. It is also seen from the analysis that sintering temperature also affects the thermal diffusivity value in a significant manner.

The fourth generation of polymers viz., conducting polymers, have created an active research area on the border line of condensed matter physics and chemistry. However, the thermal characterization of these materials has not been investigated in detail so far. Fabrication of composites with various consitutents is attaining much importance due to its tunability in effective thermophysical parameters. Here focus was made on the measurement of thermal diffusivity of Polyaniline (PANI) doped with Camphor Sulphonic Acid (CSA) and its composites with Cobalt Phthalocyanine (CoPc). Analysis of results show that CSA doped PANI exhibits maximum value for thermal diffusivity and the effective thermal diffusivity value decreases with increase in relative fraction of CoPc. The interface thermal resistance and thermal expansion mismatch play a major role in the effective thermal parameters of heterogeneous systems such as composites.

Various configurations photoacoustic technique have been employed for the evaluation of different thermal properties of materials and are utilized to measure the relative composition dependence of liquid crystal mixtures. Heterogenous materials consisting of liquid crystals and polymers have wide range of applications, ranging from bistable displays to photonic bandgap materials. As the liquid crystallanity and themophysical parameters depend greatly on the relative fraction of constituents, the complete thermal characterization of liquid crystal mixture consisting of various relative fraction of Cholestrol and 1 Hexadecanol have great physical significance and practical applications. The thermal diffusivity of liquid crystal mixtures is evaluated using photoacoustic technique under heat transmission configuration whereas conventional photoacoustic technique is employed for the measurement of thermal effusivity of the materials. Evaluation of these two dynamic thermophysical parameters using simple, elegant and nondestructive photoacoustic technique is very relevant as these parameters allow the complete thermal characterization of the

specimen under investigation. Analysis of data shows that the Hydrogen bonding play a key role in determining the thermal properties of liquid crystal mixtures.

In general, the versatility and applicability of two important photothermal techniques, namely photothermal deflection technique and photoacoustic technique for the evaluation of fundamental properties of photonic materials are highlighted in this thesis.

6.2. Challenges for the future

Some of the outstanding issues that requires serious consideration are listed below:

1) Theoretical and experimental investigations are required on the exact contribution of various scattering mechanism during the propagation of thermal carriers especially in layered semiconductors and multiple layer structures.

2) Application of probe beam deflection technique to measure the surface and bulk acoustic wave velocity and consequent determination of elastic constants of the materials need further investigations. The dependence of these properties on doping also needed to be studied.

3) There is exist a need for research both from theoretical as well as experimental point of view to investigate the influence of electric field on the thermal and transport properties of materials, especially semiconductors.

4) Investigation of influence of more than single nano metal into a ceramic host on the thermophysical properties can be made.

5) As the thermal characterization of conducting polymers is in the initial stages, the photothermal techniques can play a major role in this area.

6) The application of open cell photoacoustic technique in the presence of electric field has not been made yet. The variation in thermal parameters with electric field and its variation with across the phase transition of liquid crystals is a really interesting and challenging field.

7) Applications of open cell photoacoustic technique to evaluate the thermal parameters of binary mixtures as well to investigate the chemical reactions are not exploited till now

8) and more...................

G8651